Vehicle Safety Institute

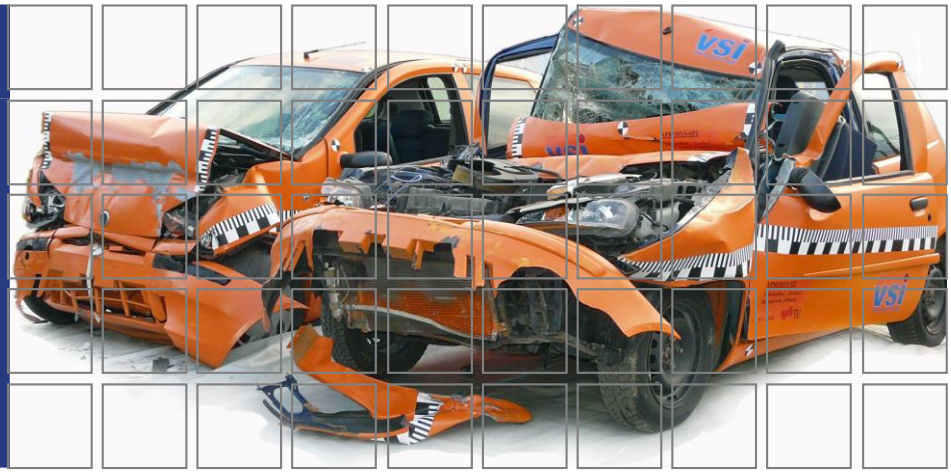

Mario Popijac, BSc

Creation and validation of a FE-Model of a volunteer sled testbed

MASTER'S THESIS to achieve the university degree of

Master of Science

Master's Degree Program:

Submitted to

Graz University of Technology

Supervisor: Univ.-Prof. Dipl.-Ing. Dr.techn. Hermann Steffan

Vehicle Safety Institute

Graz, December, 2022

AFFIDATIV

I declare that I have authored this thesis independently, that I have not used other than the declared sources/resources, and that I have explicitly marked all material which has been quoted either literally or by content from the used sources. The text document uploaded to TUGRAZonline is identical to the present master's thesis.

Graz, _____ _____

Signature

ACKNOWLEDGMENT

I would first like to thank my thesis advisor Dipl.-Ing. Dr.techn. Gregor Gstrein of the Vehicle Safety Institute at Technical University of Graz. The door to Dipl.-Ing. Dr.techn. Gstrein office was always open whenever I ran into a trouble spot or had a question about my research or writing. He consistently allowed this paper to be my own work, but steered me in the right the direction whenever he thought I needed it.

I would also like to thank the experts who were involved in the validation survey for this research project: Dipl.-Ing. BSc Desiree Kofler, and Dipl.-Ing. BSc Nico Erlinger. Without their passionate participation and input, the validation survey could not have been successfully conducted.

ABSTRACT

The aim of this study was to create a detailed and validated Finite Element Model of the volunteer sled testbed LowG, for the usage with numerical Human Body Models (HBM). The combination of the FE model LowG and an active HBM will enable to simulate and analyse the human reaction and kinematics in case of an emergency braking manoeuvre with the active muscle reaction and possible the influence of the equipment on the experiment.

The workflow for the creation of the FE-model contains three phases: model creation, verification and validation.

In the first phase, a detailed FE mesh was created based on an existing CAD model of the testbed. Thereby geometrical simplifications had to be done first, before meshing the single components with different element types, according their topology. For a straightforward usage, the model was also parameterized, to enable the setting of the experimental parameters (e.g. seat position and orientation, angles of cushion and seatback, etc). in the same way also in the FE model.

The meshing was followed by the verification, in which a range quality criteria was chosen for the model plausibilisation.

The validation process contains two experiments, one with quasi-static loading condition of the seat and seatback foam with ballast plate, and another one with dynamic loading of the seat and seatback with the different head impactors.

The outputs of the experiment with the quasi-static loading condition are the reaction forces on the six support rods between two hexapod plates during the ballast. The outputs of the experiment with the dynamic loading condition are following metrics: Compression of the seat foam on the cushion and seatback, impactor acceleration and calculated velocity, and again the reaction forces on the six support rods.

The validations of the model response in static loading condition as well in dynamic loading condition proofs a good correlation with the experiments. The overall goal of this study, to create a well validated, stable running simulation model, as basis for further research that includes combination of the detailed FE-model of the LowG testbed and numerical HBMs (e.g. THUMS v6 or THUMS v4) was accomplished. Some possible improvements of the model and it`s validation were identified in the course of the work and are suggested as follow up items: Examples of the latter are to involve different possible configuration scenarios (e.g. other seat orientation, angle setting, …) in experiments as basis for further model validation or to further analyse found deviations in the oscillation behaviour of the test rig and the model.

TABLE OF CONTENTS

LIST OF FIGURES

LIST OF TABLES

1 INTRODUCTION

1.1 Overview – Human body models in the development of occupant systems

In order to protect occupants in case of an accident, vehicles are equipped with a number of so-called restraint systems, as for example the seat belt or the airbags. The latter ensure an early coupling of the occupant with the vehicle motion, distribute the load to body regions to minimize the injury risk and prevent an ejection of the occupant.

The development of these systems is based on the application of human body models, that provide the relation between a certain loading (e.g. acceleration, force) of a defined body region and a thereof resulting injury risk for the car occupant. Such human body models are the main assessment tools used in research and the development of the vehicle safety technology [1].

Since the beginning, crash test dummies (ATD – anthropometric test device) have been used in physical crash tests to derive the loading and the resulting injury risk of car occupants [1] as base for improving occupant safety. They were first developed in mid-20th century and in the 1970s the first Hybrid 1 crash test dummy was developed. Since then the development still continuous with regular new updates and new dummies [1].

Examples of recent dummies for front impact are THOR, Q Dummies, WorldSID for side impact BioRID II for rear impact [1].

The development of restraint systems is widely based on finite element simulation in order to reduce the number of cost-intensive crash-tests. Therefore, all physical ATD`s have a digital twin, typically available as commercial model.

In the last decade, the computational power and resources significantly increased, which led to the further detailing of either the car models but also the dummy models. This progress enabled development of so-called numerical Human Body Model (HBM), which are a highly detailed finite element models of the human body.

The application of such models promises additional potential to evaluate injury risks and to be part of the development and improvement of passive and active safety systems [1]. With HBM typically feature detailed anatomical geometry and biomechanical properties of the human body.

Some of the examples of properties are skeletal structure, joints, stiffness, and mass distribution [1]. The purpose of numerical HBM is to investigate the kinematics of the human body, stress and strain evaluations in bones and joints, but also deeper analysis of organ injuries or more general injury mechanisms [1].

Numerical human body models are being developed since the 1990s and their development is still ongoing (see figure 1-1) [1]. In 2000 the first HBM in the world that could simulate the entire body, the “Total Human Model for Safety” (THUMS) was launched [2].

Today is the THUMS one of the most advanced virtual model in the world. Its characteristics are representing the structures of the body, including bones, organs, muscles, and more as well their durability in response to force and impact [1].

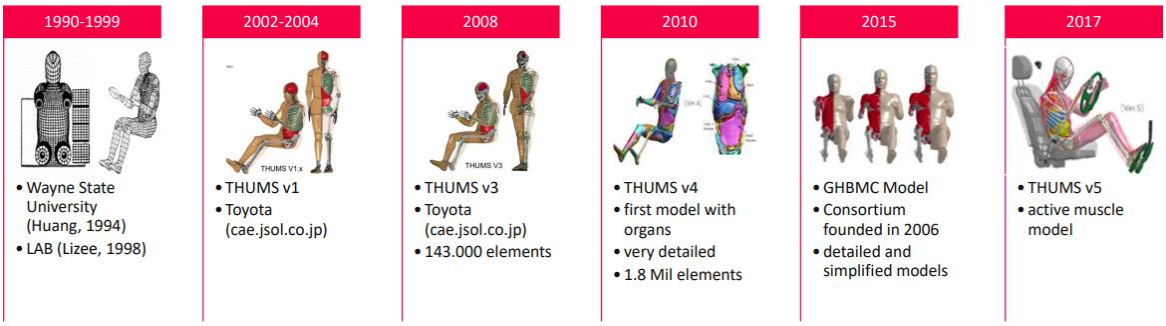

Figure 1-1: Human body model development through decades [1]

Comparing the applicability of both, ATDs and HBMs, there are benefits as well limitations for each. Following exemplary points account as benefits for ATDs:

A lot of experience and knowledge was gained up to present in the usage of crashtest-dummies and in the application of the metrics and injury criteria, that can be assessed [3]. This approves, as the number of road traffic fatalities is steadily decreasing, whereas the number of accidents is increasing. Further the results of crash-tests are typically not doubted, in comparison to simulation results [1]. At the end of a development process comes always the approval in a physical test, employing a crashtest-dummy. Same is true for legislation, where only physical tests are valid [3].

In contrast, there are significant benefits considering the application of (passive) numerical human body models in particular in future development – in the following a selection is briefly described.

For a numerical HBM, there is typically no specified directions of loading (e.g. front, side, rear) as for an ATD, what is particularly relevant for novel seating positions. Another advantage is the high biofidelity, or rather the possibility to analyse multiple anthropometries-, even (deviating from 50th or 5th percentile occupants).

By the simulation of the numerical HBM, direct biomechanic analysis is possible (e.g. rib fracture vs. thorax compression) [1], because the general advantage of the simulation is the derivation of difficulty measurable quantities [4].

One common limitation of crashtest-dummies as well as passive numerical human body models is the bad biofidelity in low load scenarios, e.g. emergency braking. Consequently, both are not representative for low load levels. The requirement, that a crashtest-dummy is designed very robust in order to withstand high acceleration crash tests [1], it is too stiff in low load scenarios. On the other hand, the passive numerical HBM has no muscular activation option, muscular tissue is only implemented with correct mechanical properties and mass [5].

In the near future it is assumed that, commercial vehicles worldwide will be more and more equipped with advanced vehicle safety technologies, such as autonomous emergency brakes that reduce the risk of injury due to collisions [6]. However, for evaluating occupant injury risks in frontal collision after AEB operation, it is critical to know the position of the occupant which is influence by the effect of muscle activity. Crash dummies are effective and biofidelic for high speed impact, however a crashtest-dummy cannot imitate the human reaction prior to collision and accident [1].

To get accurate data for the initial conditions of the occupant at the crash as basis for the development of seat belts, airbags and other important parts that are relevant for occupant safety, the human body model with active muscles proved to be most effective [7].

The active HBMs (THUMS v5, THUMS v6) have a muscle – activation controller for representing the muscle conditions of sleeping, relaxed, and braced [6]. At relaxed muscle condition the HBM has only reflex reactions, and at braced the HBM has active muscles.

With the muscle activation, the kinematics of occupants under different conditions of muscle activation can be investigated, as well for example the effects of muscle activity during deceleration before a crash on injury risks. Such as any other finite element model, HBM require a wide range of validation test to be a useful predictive assessment tool. In the following, different validation stages are summarized.

1.2 Validation of numerical human body models

The validation is the process for assessing the reliability of FE model [8]. For HBM, validation aims to show that the model is biofidelic and one applied method is comparing HBM results with the available PMHS-tests. This method involves the comparison of component test (e.g. fracture ribs) to full body tests and comparison of simulation results with PMHS. However, this method is limited to the load cases that are available from PMHS tests [1].

Tests with focus on pre-crash forward head excursions of passive HBMs gave the conclusion that, a HBM is more comparable to PHMS rather than to volunteers, because the muscle activation plays relevant role for acceleration levels in braking manoeuvres scenario [7]. This gives the indication, that also the validation of the muscular activity for active numerical HBMs plays a crucial role for a good overall biofidelty, in particular for low loads.

In the following, current research that deals with the validation of active HBMs and the conduction of volunteer tests, as basis for the latter are summarized:

Tests with volunteers are used for the validation of active HBMs [6]. The validation of the HBMs with volunteers is proceeded in passenger cars and on seats mounted on sled systems in a laboratory [7]. Volunteer tests of braking in passenger cars have the possibility to be performed in the realistic environment, when the volunteer is situated in unaware state. The related disadvantages lies in lack of measuring possibilities for example. Three types of testing with volunteers in passenger cars have generally been done: the volunteer applying the brake pedal by themselves, full braking events with initial relaxed muscle conditions (1.0 – 1.1 g) [7] and at multiple deceleration levels [7].

On the other hand, in numerous experiments with a sled testbed investigated the differences in the response of relaxed and braced muscle states of volunteers at various acceleration levels, from 0.2 up to 5.0 g was analysed [7].

In the research conducted by Erlinger, Kofler, Heider, Klug [7] experimental volunteer test with sled tests with the sled testbed representing brake events were carried out, with the goal to serve as basis for the HBM simulations. The objective of the research was to identify the parameters that are influencing the kinematics of the HBM with the background question, how unknown boundary conditions and the posture affect the HBM results. The condition of each volunteer was relaxed state and unawareness of the exact acceleration onset. The volunteer responses showed to be very subject – specific, for example the peak forward head excursions caused by acceleration pulse. On the other hand, the output data between attempts of the same volunteer had no bigger deviations [7]. In this research, different HBM models were used in different scenarios such as THUMS Version 4.02, THUMS Version 5.03 and THUMS Version 6.02 [7]. However, the sled testbed was not represented as detailed FE model, but the seat FE model was developed. For the seat model creation, the geometry data was scanned by laser. For the calibration of the material parameters, material tests of the foam material

were conducted and applied. Mounting structures between the seat and the sled were represented with translational springs [7].

In the research of Kato, Nakahira, Atsumi, Iwamoto [6] the validation goal was to develop the THUMS V6, the detailed HBM with a muscle-activation controller for predicting occupant injury risks in frontal collisions with deceleration before the crash. Firstly, cadaver test data was used for the validation of the model in direct impact and compression conditions. In addition, the kinematic response characteristics considering the muscle activation were validated with the experiment with volunteers and the sled testbed [6]. The research suggested the importance of considering the muscle activity for predicting injuries. The simulations setup with the THUMS V6 consisted of one of each occupant model types AF05, AM50, AM95, and a simplified interpretations of a FE sled model. The sled was interpreted as model of footplates, rigid seat, steering wheel, three-point seatbelt and the other version was the vehicular sled model that includes a Ford Taurus vehicle body, an automotive seat, a 3-point seatbelt, pedals, and a steering wheel with an airbag for drivers [6].

The research of Ejima, Zama, Satou, Holcombe, Ono, Kaneoka and Shiina [5] studied the physical motion of the human body under pre-crash conditions in low speed front impact tests. The validation experiment was performed with a linear – motor sled with rigid seat, steering wheel and seat-belt. The characteristic of the validation is the front impact test on human volunteers, where the subject muscles were initially relaxed and at approximately 130ms, muscle responses were observed to start activation after the onset of acceleration. The conclusion of the research was that the effects of muscular activity on each motion of the body part have been approved, where the body motion is divided into four phases in the pre-crash condition [5]. The goal of the research was to investigate the influence of the human body posture changes on the injuries in a traffic accident, and to develop the approach for the injury prediction [5].

The focus of previous studies was on the development of the HBM with validation test with sled testbed and vehicles with volunteers [6] [5] [7]. Thereby it was shown, that validation tests in cars have the drawback that the required data for parameterizing the muscle models is difficult to gain. The main studies used as base for the calibration of active muscle models (e.g. THUMS v6) was conducted in lab, using a volunteer sled.

At VSI, such a sled system was developed for the same purpose, addressing also shortcomings of the equipment used in the studies described. This testbed is described in the following chapter.

1.2.1 Sled testbed LowG

The sled testbed LowG is a new equipment in the laboratory of the Vehicle Safety Institute that is being used in experiments for the analysis of human reaction and kinematics in case of an emergency braking manoeuvre [9]. It's basic specifics are stated in Table 1-1:

Table 1-1: basic specifics of LowG [9]

maximal travel distance	3.75m
maximal velocity	4.3 m/s
maximal acceleration	10m/s²

The LowG is built for tests with volunteer participation, ensuring on high safety standards. It is designed highly adaptable to enable testing in a wide range of occupant postures and loading conditions:

The movable footrest can be adapted for passenger anthropometry or to a specific vehicle type and the belt is adaptable for both passengers and drivers. The seat foam has simple geometry the measurement of the local deformation and an optional force measurement system installed in the seat back and seat cushion. A further measurement system is located on hexapod rods for recording seat interaction forces [9].

Figure 1- 2: Sled testbed LowG

The LowG testbed features several outstanding capabilities during the experiment:

- It makes reproducible boundary conditions and individual acceleration profiles.
- It allows different seating positions by individual rotation of the backrest and seat compression around the Y-axis and upright position ↔ Zero-G Position [10].
- There are different loading directions by rotation of the seat around the Z-axis such as static rotation of the seat about 360° for front and rear loading scenarios.

A planned further upgrade of the test-bench will be an upgrading testbed for dynamic rotation of the seatback during pulse application [11].

Generating data of volunteer tests for HBM validation in different seat positions and different anthropometries is the main goal of testing with the LowG. The featured measurement systems shown in the figure 1-3 are 3D motion capture systems with Qualisys software, electromyography measurement to record the activity of volunteers. In order to create realistic data of human reactions to a kinematic input, it has to be made sure, that the environment (Crashlab) is not influencing the reaction. Therefore, the application of distraction methods tasks was analysed and tested.

Figure 1-3: (left) Qualysis motion capture system [9]; (middle) EMG measurement [9]; (right) Application of distraction methods [9];

1.3 Motivation

The test-rig is in operation since spring 2022 and a limited number of volunteer test studies was already conducted. However, for the planned application, as base for the parameterisation of active human body models, there is an open gap, that is the actual scope of this work:

In order to be able to apply the measured data (3D Kinematics, muscular activity) of the volunteer to the active HBM, it has to be made sure, that the boundary conditions – particularly the kinematic input – is the same.

With detailed FE model of the sled testbed the goal is to ensure that boundary conditions of the test bed are correctly mapped in the simulation model, for example the deformation of the test bench during the tests. As mentioned [7], it is unknown how such unknown boundary conditions are affecting the occupant motion and thereby the output data. Therefore, using the FE model of the sled it should be possible to find the cause of the occurrence, for example when the experiment and simulation results are deviating from each other.

In addition for the demonstration of the applicability of the model, also the implementation of numerical HBMs is the result of this research, more specifically the THUMS v4 (passive), and THUMS v6 (active), is cope of this work. That implementation of the HBM together with the FE model of the

sled testbed is the basis for further research studies focusing on the validation of the simulation of the occupant kinematics during a braking manoeuver.

The goal is to create the FE model of the LowG test-rig capable to create different simulation scenarios, more specifically to imitate the setting possibilities of hardware sled testbed.

With the possibility to create and validate complex and detailed finite element (FE) models of sled testbed and assembling with HBM, a deeper understanding of the behaviour of passengers and drivers in passenger cars under different conditions should be more reachable.

1.4 Objective

This study aims to create an FE-Model of the LowG volunteer sled testbed and validate it against the experiment tests reported in the following chapters. The thesis thereby focuses on the creation and validation of a detailed finite element (FE) model of the sled testbed, but not further the effects of boundary conditions and postures in simulations with human body models (HBMs) when replicating volunteer tests in an occupant environment.

Following objectives are thereby in focus:

- The simulation model has to be created in enough detail to represent the boundary conditions for the HBM realistically
- The simulation models must be reasonably simplified to prevent significant additional simulation effort
- The model has to be compatible with current HBM in terms of numbering range and model settings regarding solver
- The model has to be numerically stable for the require simulation times (~2s)
- The simulation model should represent all setting parameters, as also realized in the real hardware
- The model has to approve a sufficient alignment with the validation tests, to be carried out

2 METHOD

This chapter contains a detailed description of the creation process of the Finite Element (FE) computer model as well as the experiments conducted to validate the latter.

The Workflow of the creation of the FE model of the sled testbed contains three main parts: model creation, model verification, and model validation (see figure 2-1). The model creation is the process of building the FE model on a basis of the CAD model (see subsection 2.1.1) in the finite element software (see subsection 2.1.2) and consists of sets of steps. Main steps are geometry simplification, meshing technique of test-rig, model start-up, definition of connection between single FE parts, assembling of the FE sub-models into the main FE model.

After creation the FE model, the verification is the second step in the workflow. This step controls and approves the quality of FE model and the assuring that the model works. In this research, the verification steps were mass check, element quality criteria and energy check.

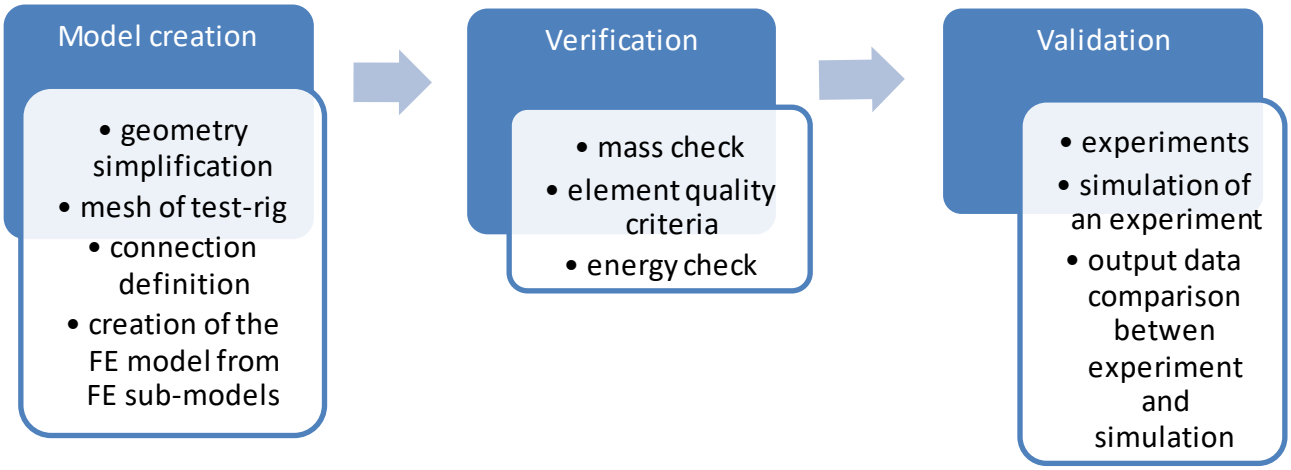

Figure 2-1: Workflow of creation of the FE model LowG

The last section of the workflow is the validation of the FE model, where the output data of the experiments were used for the validation. Therefore, for the comparison with the results from the experiments, different cases of simulation scenarios were created (see subsection 2.7).

2.1 Finite Element Model Creation

This sub-subsection covers a detailed description of the creation of the Finite Element (FE) Model of sled testbed with meshing strategy and model start-up as a well short description of the CAD model as starting point of FE model creation.

2.1.1 CAD model

The CAD model was made available at the start of this study to be the basis for the creation of the FE model, as a graphical representation is the reference for part dimension, location for a part, part interaction with each other, regrouping in subassemblies, etc. A CAD model contains detailed information about the parts that are built in real construction and it can be described as a detailed computational interpretation of hardware. The CAD model sled testbed was created in the CAD software *Creo,* and made in the neutral *step* file format.

In figure 2-2 is shown the CAD model of the sled testbed and in figure 2-3 the hardware.

Figure 2- 2: CAD model of sled testbed

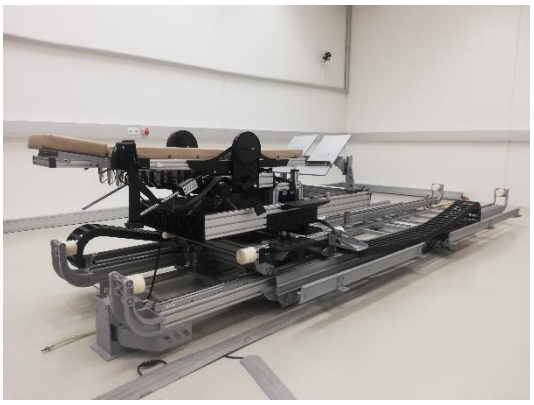

Figure 2- 3: Sled testbed in the lab

2.1.2 Finite Element Simulation Software

The simulation program used in this study is LSDyna, a FE-code for explicit and implicit methods for analysing the nonlinear response of structures [12], whereby the explicit solver is applied for this study. LSDyna has possibility to solve complex, real-world problems because of its automated contact analysis and wide range of material models [13]. Capabilities of the program are for example nonlinear dynamics, rigid body dynamics, quasi-static simulations, normal modes, linear statics, FE-rigid multi-body dynamics coupling, … [13]. Therefore, is a widely used FE solver to analyse e.g. the crash-behaviour of structures.

The reason for the application of this program is also because the THUMS model is also running in this code. The goal of this study was to build an FE model suitable for dynamic impact events and short simulation duration.

2.1.3 Meshing of test-rig

This sub-section describes the principle workflow that was followed in the course of the FE mesh of all necessary components. With FE-model creation is necessary to obtain a detailed response of structure that gives the most realistic outputs. The model consists of simple „finite“ elements that are defined in mesh, for which numerical solvable equations (element formulation) can be formulated. The procedure starts from with the generation updating of the CAD model up to final mass check with the following intermediate steps:

- Reduction of parts and type definition of remaining parts (1D, 2D, 3D)
- Clean-up geometry process and mesh
- Part simplification and part exchange process
- Connection determination between meshed parts in sum models
- Mesh-optimization using quality criteria
- Mesh clean up: free nodes, free edges, mesh overlap or duplicate elements etc.
- Sub-models reorganization
- Renumber IDs of elements, nodes
- Assembly and connection of all FE sub-models into one to create complete Finite element model
- Mass check and comparison with CAD model

The software used in FE model creation was the multi-disciplinary finite element pre-processor *Hyperworks*. It manages the generation of the large and most complex models, starting with the import of CAD geometry to exporting a ready-to-run solver file. The program *Hyperworks* is an integral part of

PLM (Product life cycle management). The focus is to prepare the model for the interpretation of behaviour in a real-life environment [14].

2.1.3.1 Part reduction and definition of remaining parts

The first modification step is to remove parts or exchange them with parts with simplified geometry. This is followed by the classification of remaining parts into 1D, 2D, and 3D (see sub-section 2.1.3), and definition of element type and size. To classify, remove and simplify CAD parts, a deeper understanding of the function and importance of parts is required.

The goal of this thesis is not to analyse forces impact on parts such as screws, screw nuts, screw plates, angle brackets, sliding blocks, rings, and bolts as this was already done at the design of the test-rig. Therefore, they are replaced with the time-efficient simplified representation described in the following sub-sections.

To reduce calculation time, the CAD assemblies "Dewetron" and motor are exchanged with a simple 3D FE model made of meshed cubes with an element size of 15 mm (see figure 2-4). As the mass of these components is relatively high, they have significant influence on the loads within the test-rig structure. Therefore, the simplified representation need to have same inertial properties.

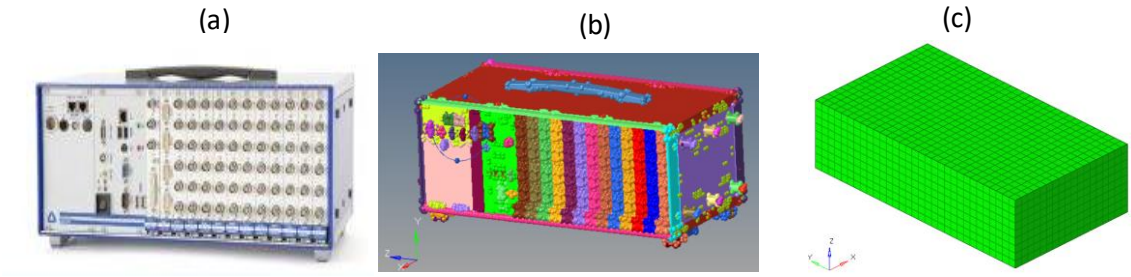

Figure 2-4: Data acquisition unit Dewetron: (a) hardware part; (b) CAD Model; (c) simplified representation in FE model

Another example is the motor (see figure 2-5) that moves the movable section of the hardware assembly. Therefore, in FE model is defined as the part that moves FE sub-models along the sled of FE sub-model "X-Sled".

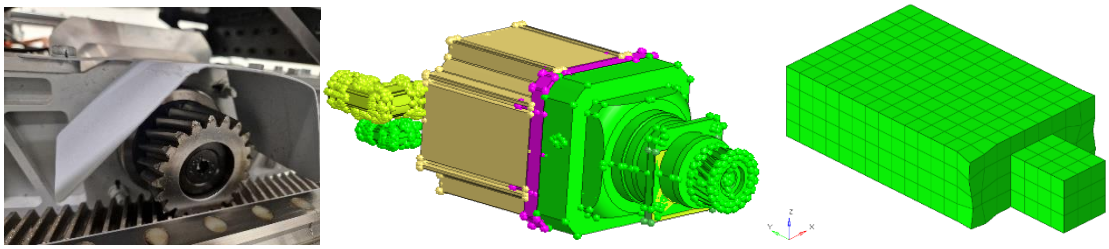

Figure 2-5: Data acquisition unit motor: (left) Gear connection motor – gear rack; (middle) CAD model; (right) Simplified representation in FE model

The main structural members of the LowG testbed are Item-profiles of different dimensions (e.g. 80x80, 80x40, 40x40 and 40x20). Because of their complex geometry, item profiles are also replaced with simplified FE-Model of the beam to reduce calculation time.

The simplified version of the beam consist of a shell beam, whereby the approximately shell properties are calculated in comparison with the item profile 80x80. This member was selected based on the assumption that the biggest stress and deformation appears on the largest item profiles. In the following, the detailed approach of the creation of the simplified version of the item beams is described:

The first step was the geometry simplification of the item profile to become 2D mesh with majority of quadratic elements (see figure 2-6). To become 3D mesh, the 2D mesh was extruded along the length of the item beam. The resulting element size was between 2 and 3mm.

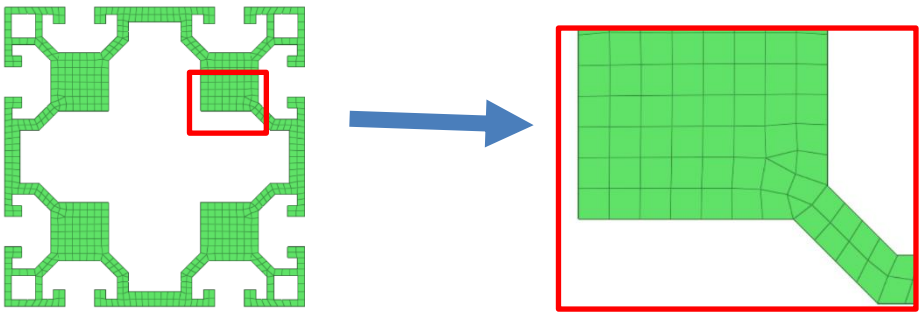

Figure 2-6: Detailed 2D FE Item profile simplified

Second step was the creation of the simplified FE-Model of the beam as quadratic cube with 2D shell elements with a size of 15mm (see figure 2-7). The simplified representation of the beam has the same outer dimensions as the detailed Item profile.

The figure 2-7 shows the FE model of the Item beam and the shell beam with the following dimensions: L (length) = 1500mm, A (profile) = 80x80mm. As can be seen in the figure, the FE model of the item beam has smaller elements and the amount of elements is noticeably bigger.

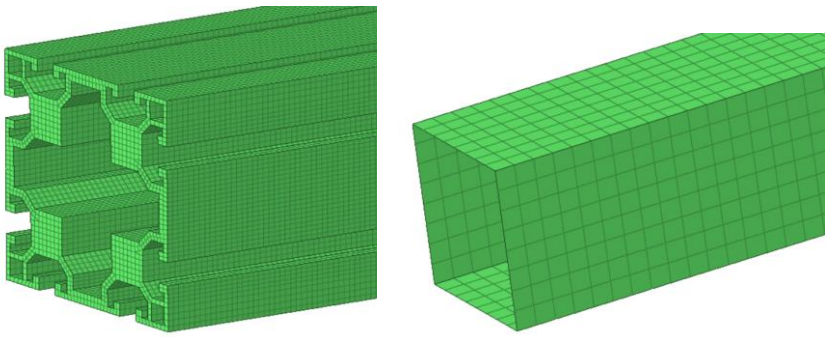

L=1500mm ; A=80x80mm
Item
Nodes: 442 820
Elements: 304 430
Calculation time: 10h
Shell
Nodes: 28 865
Elements: 28 800
Calculation time: 1min 45s

Figure 2-7: (left) FE Item model; (middle) FE shell model; (right) comparison Item/Shell FE Model

For an accurate definition of the shell properties, it was necessary to have data of the deformation of the beam in a representative loading condition (see figure 2-8). In this case, a bending of the profile under static force impact with certain profile length and dimension was selected, as this configuration is public available on the homepage *Item24* [15]. The compression calculation was the reference for further FE shell model definition.

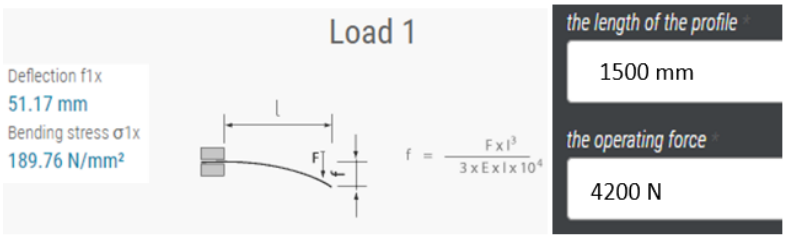

Figure 2-8: Deflection calculation example, [15]

The calculation of item profile 80x80 with a length of 1500mm was proceeded with a force of 4200 N, which is close to the plastic deformation area [15]. This was selected, as there is no plastic deformation expected in the testbed during the tests. The material properties of the item beam are unknown, and based on literature, as no material tests were made [12]. Compression calculation was the reference for further FE shell model definition. Compression calculation of item profile 80x80 with a length of 1500mm has proceeded with a force of 4200 N, close to the plastic deformation area [15].

The simulation setup consists of two boundary conditions: One constrained fixed side and the other with force in the direction perpendicular to profile length (see figure 2-9 and figure 2-10). Both boundary conditions are defined on one middle rigid node that is part of the set of nodes that includes all boundary nodes. The reason is to allocate the load on elements to have equal stress flow through the mesh.

Figure 2-9: FE-Model of an ITEM-beam

Figure 2-10: FE-Model of a shell beam

The simulation setup of the FE Item model and the FE shell part model have the same boundary conditions, obtaining one fixed constrained end and constant force load of 4200 N on the second end in a simulation duration of 500ms.

The goal was to reach a similar deflection with both FE-Models with the same length and outer dimensions subjected to a load of 4200N (see figure 2-11). However, the FE model of the item beam has deflection of the 57mm, slightly exceeding the reference from the source [15].

The simulation with the FE model shell beam was calculated to have similar deflection with the source result, with deflection of 50.26mm and the shell wall thickness of 6.1mm (see figure 2-11). In diagram below, the red curve shows the signal of the FE model of the shell beam, and the blue curve of the item beam.

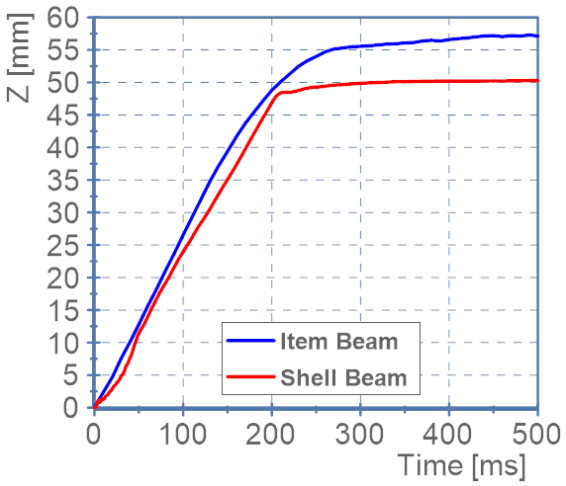

Figure 2-11: Simulation results displacement over time

The load force was defined as the ramp up function from zero to 200 ms in order to avoid the oscillations caused by the dynamic impact of the force. Moreover a damping coefficient was set 0.2 for this calculation.

2.1.3.2 1D elements

Components, that have one dimension very large compared to the other two dimensions, more specifically parts of which the length is greater than the width, height, or diameter are typically modelled as 1D elements. The shape of the 1D element is the line that is created by joining two nodes, which also represents the length. The other dimensions are defined by assigning respective cross sections to the line [16], although some 1D elements have possibility for example the diameter definition of a rod.

1D elements have a number of advantages such as faster solution computing because of only one element across the cross-section compared to 2D and 3D, meshing needs less effort, and design changes are easier for example, changing the cross-section of beam elements [16].

In the model of the test rig, drilling holes, screw connections are defined as 1D-constrained rigid bodies with the assumption that the screw connection is completely stiff and inflexible. The rigid body connects a group of nodes of each FE part. Figure 2-12 shows that screw connections are partly modelled as rigid body connection with bigger amounts of nodes. This makes the contact definition between surfaces of different parts obsolete, whose elements are adjacent.

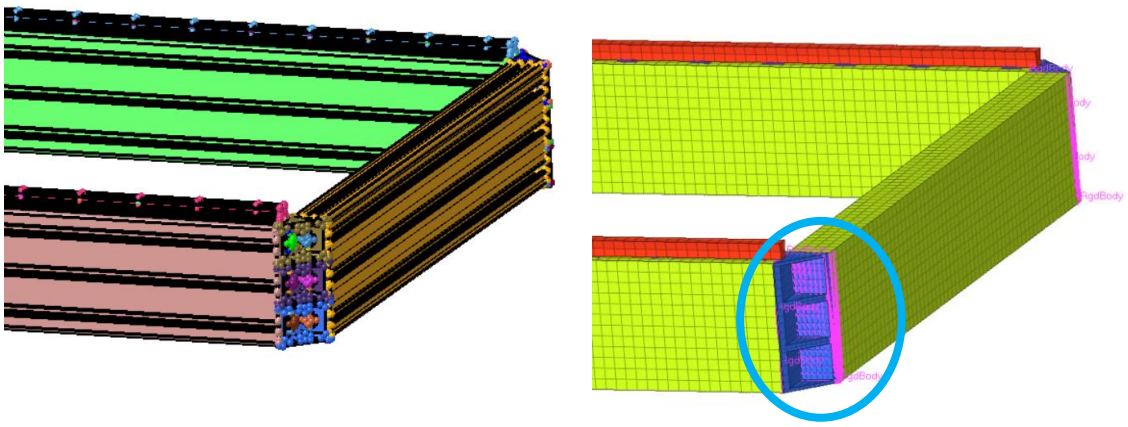

Figure 2-12: (left) Cut from CAD-model; (right) 1D rigid body connection example

The second example of 1D elements are 1D discrete and 1D beam elements. The support rods (see figure 2-13) that are connecting seat frame and seat backrest or as other example the potentiometers (see figure 2-14) in the foam of the seat cushion and seat back are defined in the FE model as 1D discrete elements.

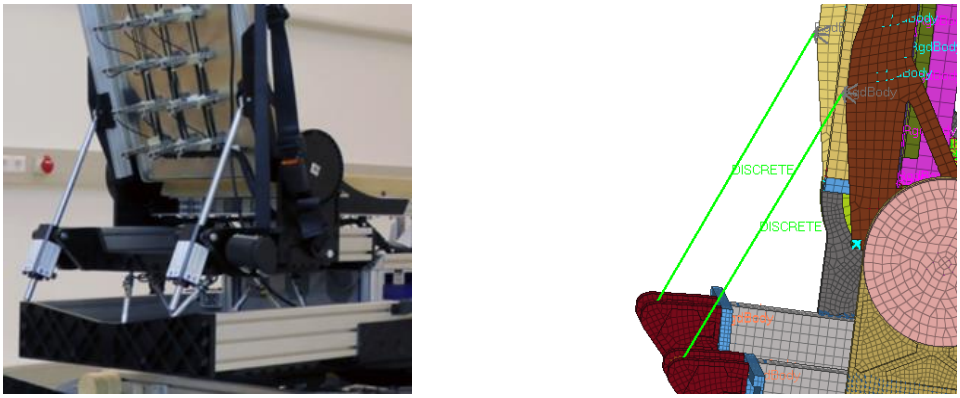

Figure 2- 13 : (left) rods, hardware; (right) FE model interpretation of rods as discrete element

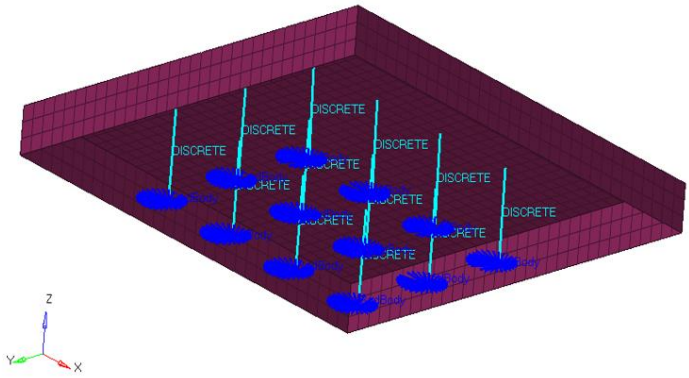

Figure 2- 14: FE model interpretation of potentiometers as discrete element

The rods between hexapod plates are defined as 1D beam elements as shown in figure 2-15. 1D beam elements are simplified elements that feature a constant cross-section along the beam. The advantage of beam element lies in its straightforward formulation and high accuracy in a short analysis time [17]. A further advantage is the possibility to analyse different cross-section by just changing the single parameters. A disadvantage is that not all effects can be captured, such as stress components and distribution through the thickness.

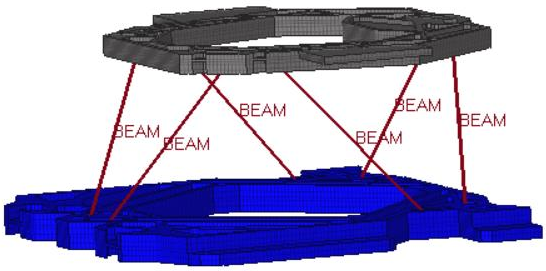

Figure 2- 15: 1D rigid body connection

2.1.3.3 2D elements

In general for 2D and 3D meshing, quadrilateral or rather hexahedron elements are preferred compared to tetrahedral elements. Quad/hex-elements are achieving great accuracy with a smaller amount of nodes in comparison with tri/tetra-elements [18]. On the other hand, it is more complex to achieve a quad/hex mesh complying with typical quality criteria, especially for 3D meshing. At mesh creation by complex geometries, tri/tetra elements have an advantage [18].

During the creation of the FE meshes of the single components, modelled using 2D or 3D elements, it was tried to minimize the number of tri/tetra elements.

Two Dimensional (2D) Elements, also commonly known as planar / shell elements are used for thin or sheet-based structures in which the 2D plane's dimensions are very large in comparison to the third dimension, the failure to be of bending deformation nature and consistent material properties are present over the entire model. They are simpler to model compared to 3D and solving time is faster than 3D models [18].

For the creation of the shell mesh, the following procedure was applied:

The first step, using the pre-processor Hypermesh, CAD parts under the same name and/or properties are isolated (see figure 2-16).

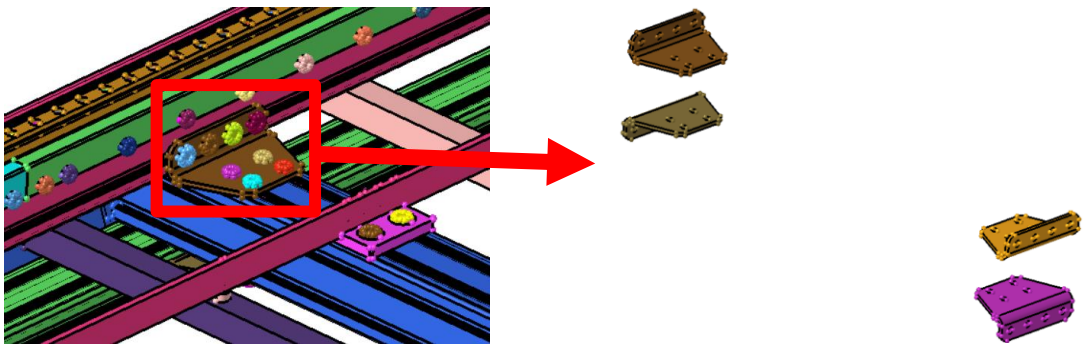

Figure 2- 16: (a) find the sheet metal part with the same properties (b) isolation of parts

The second step is to analyse the part and proceed with geometry simplification, more specifically to remove the radii and filets from the edges if applicable (see figure 2- 17). The geometry simplification is important to reduce the computing time, avoiding mesh with elements that have low-quality criteria, and stay in the defined range of the element size [18].

2D meshing was carried out on the mid-surface of the actual geometry (see Figure 2-17). This approach allows the omission of detailed volume mesh as the thickness of geometry is virtually assigned to the 2D Elements. The element thickness is assigned with half in the +Z direction (top) and the other half in the Z direction (bottom). The next step after the mid-surface procedure was geometry simplification to remove drilling holes.

The final step is the actual meshing, the discretisation of the geometry into finite elements. The range of element size is between 5 and 15 mm (see subsection 2.4 and 2.5). The size of an element was determined according to part size and its position and function.

Figure 2-17 shows an example of mesh optimization to avoid triangular elements if possible, where in this case the triangular element appears at the mesh transition point.

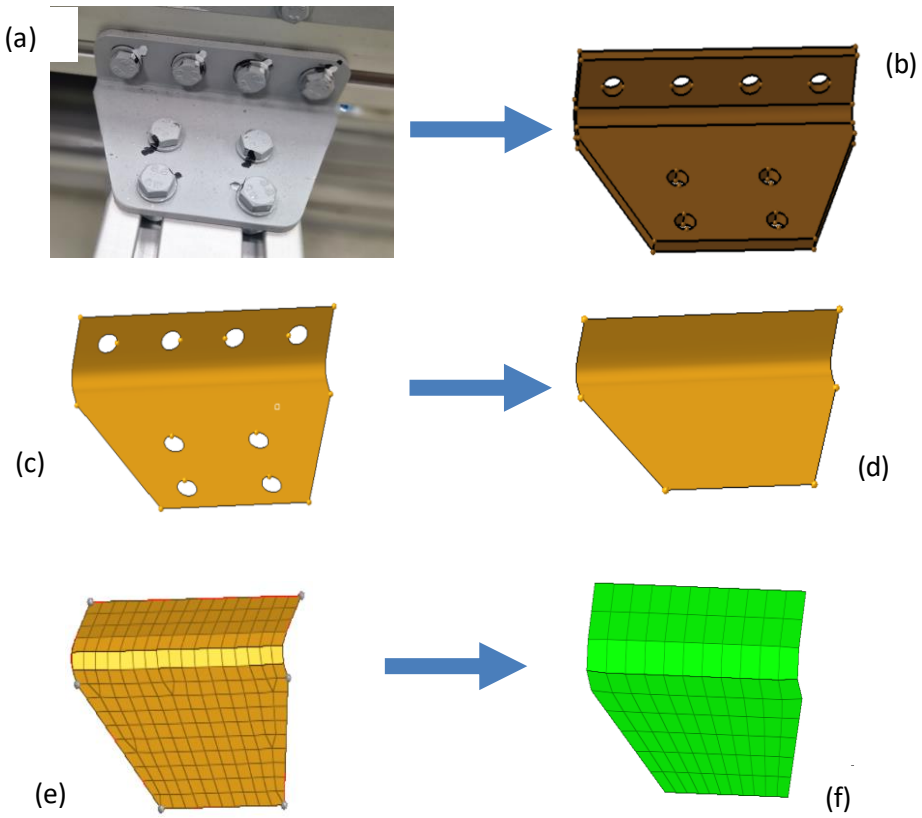

Figure 2- 17: Steps from hardware to optimized mesh -> (a) Hardware (b) CAD part: remove edge radius (c) Mid-surface (d) Remove drilling holes (e) Auto mesh FE part (f) Optimized mesh FE part

The LowG test-rig contains different sheet metal types, more specifically some are flat plates and some are bent. Bending sheet metals can have bigger and smaller bending radii. The bending radius of less than 2mm was removed and meshed with sharp edges (see figure 2-18).

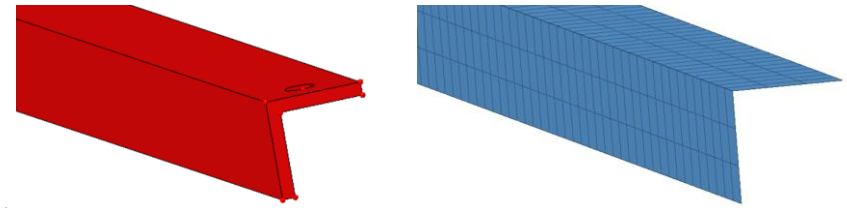

Figure 2- 18: Example of sheet metal with sharp edge

On the other hand bending radius bigger than 2mm was meshed with at least two elements and one node on the corner (see figure 2-19).

Figure 2- 19: Example of sheet metal with radius

2.1.3.4 3D elements

Components that cannot be represented properly with 1D or shell elements, 3D elements are used in meshing [19]. Such components are mainly thick-walled plates or parts with complex volumetric geometries such as support and connection plates, blocks, rails, rail carriage, absorber, rods, and seat foam.

The procedure of creating 3D meshes comprises the following steps:

In the first step, using the pre-processor *Hypermesh,* the CAD parts having the same name/properties are isolated (see Figure 2-20).

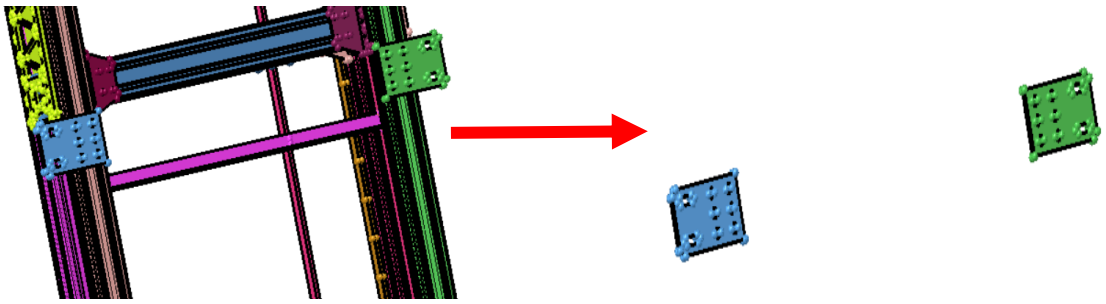

Figure 2- 20: (left) find the part with the same name/properties; (right) Isolation of parts

Selected surfaces of isolated parts are meshed with 2D mesh and then the 2D mesh is dragged out into 3D along the part thickness or length. The advantages of this procedure is reduction of mesh time, and the avoiding tetrahedron elements already by 2D in most cases.

To reduce computing time, geometry simplification is required. This was achieved by choosing the "simplest" surface for 2D mesh. For example (see Figure 2-21) by the creation of a 3D mesh of the base plate simplest surface is selected to create a 2D mesh and then dragged along the length of the plate. In such a way, filets, and drilling holes are automatically neglected and the 3D mesh contains only hexahedral elements of the same size.

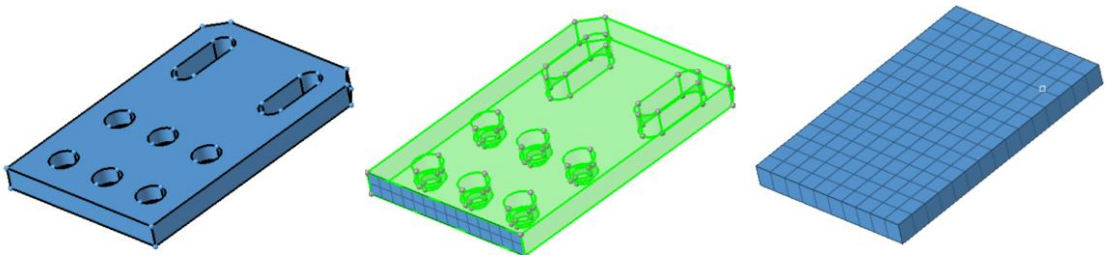

Figure 2- 21: Ground plate: (left) CAD part; (middle) 2D FE model; (right) 3D FE model

As shown in figure 2-22, support plates and long rods that do not contain the support ribs are FE part models with 3D mesh that contains almost only hexahedron elements.

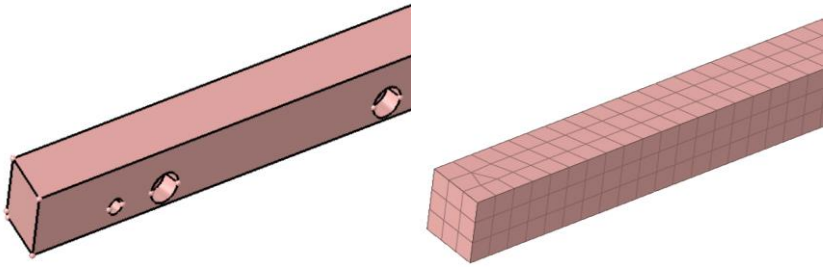

Figure 2- 22: Long rod with an angle edge: (left) CAD part; (right) FE model

In addition to the rather simple 3D parts, as shown above, the LowG testbed consists of plates with more complex geometry, whereby these plates are designed in the same way. They are set together from a base part and the part with support ribs (see figure 2-23), where the base part and support ribs have different thickness. It is not possible to extrude the 2D mesh along the thickness of the plate without the geometry adjustment, because the software *Hyperworks* cannot recognize contours from the ribs at the back-side of the plate.

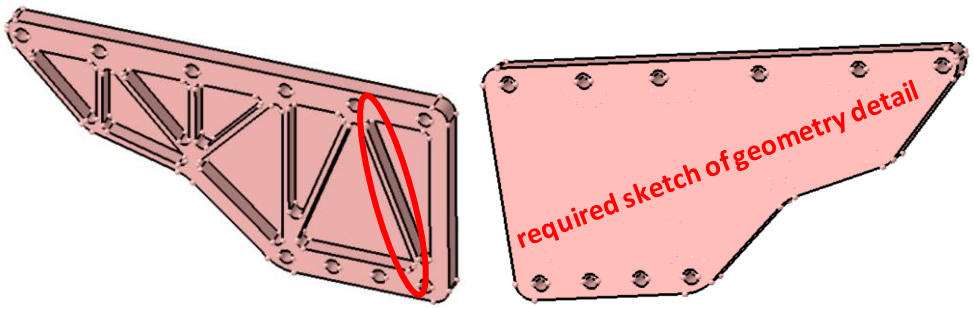

Figure 2- 23: (left) Front side of plate, ribs can be seen; (right) Back surface of plate suitable for 2D mesh

On the one hand, the goal of 3D meshing is to become the mesh that covers most of the geometric details of the part, except holes, smaller filets, and radius. On the other hand, the priority is to have the majority of hexahedral elements in the 3D mesh and that all neighbouring elements and nodes in the mesh are coincident. In other words in mesh should not be any nodes from elements that are not connecting the adjacent element.

The program *Hyperworks* has limitation when it comes to adjusting geometry and drawing sketches on the surfaces in comparison to the CAD software, for example *SolidWorks.* For that reason, the software *SolidWorks* was used for the geometric adjustment of parts, as described in the following:

Before meshing the selected plate was isolated (see figure 2-24) and saved as *step* file, and imported in *SolidWorks* for adjustment process. In *SolidWorks* the back surface of the part was redrawn with the required sketches.

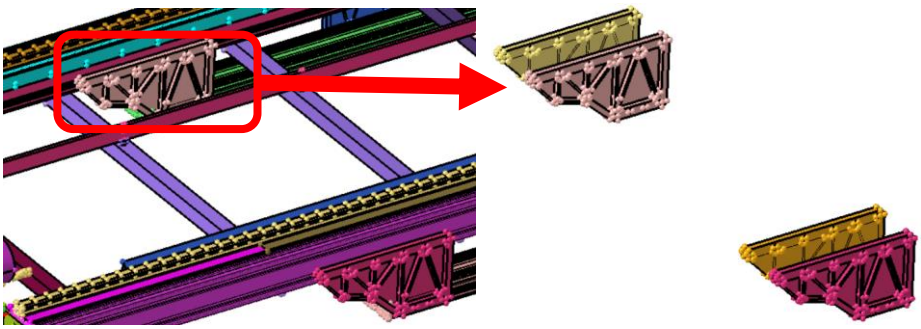

Figure 2- 24: (left) Selecting the part with the same name; (right) Isolation of parts

In the sketch the contour of the 3D shape of the plate from the front side is actually redrawn, to get the profiles from the support ribs on the sketch on the back-side of the plate.

The sketch contains a profile that is used in meshing to recognize which elements will represent the support ribs, which form the thickness of the plate, and finally which elements need to be deleted to define free volume between support ribs (see figure 2-25). Using that modified sketch *Hyperworks* recognizes the different surfaces (see figure 2-25). The next step was to select the surfaces and to make the 2D mesh. The advantage is that in the 2D mesh from each surface the nodes are approximately close to the nodes from neighbouring surfaces. Therefore, with the function *equivalence* those nodes will be set coincident.

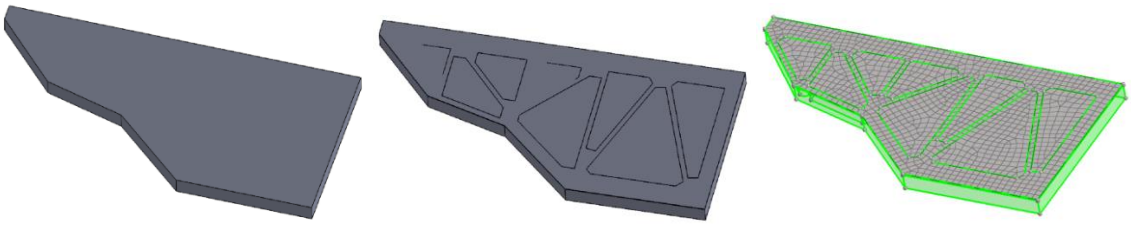

Figure 2- 25: Plate in *SolidWorks* back surface: (left) Without sketch (middle) With sketch; (left) 2D mesh generation in Hyperworks

Once the 2D mesh is created, the optimization of the latter is the next step. The 3D mesh is again dragged from the created 2D mesh, using different areas.

Figures 2-26 and 2-27 show that there are several varieties of support plates, but all of them have the similar structure, basis and support ribs.

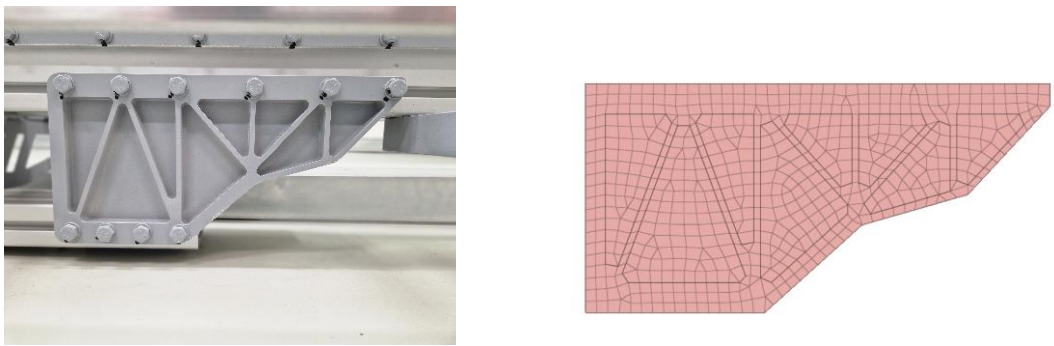

Figure 2- 26: Example of support plate: (left) Hardware; (right) FE model

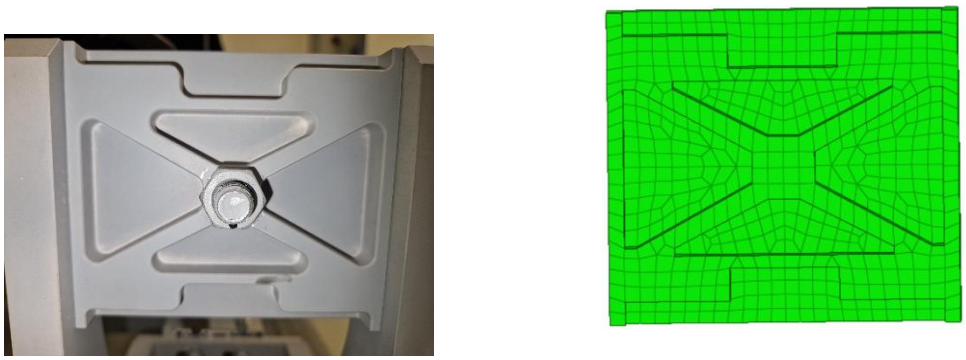

Figure 2-27: Example of support plate: (left) Hardware; (right) FE model

The most complex components in terms of mesh generation, were the hexapod plates (see figure 2-28). The preparation of the CAD part is similar to the support plates, only the hexapod plate does not have a flat back surface. The upper as well as the lower hexapod plate have two sides with different shapes. Consequently, the profile of the one side of the plate is chosen for further geometry adjustment in software *SolidWorks*. The advantage of hexapod plates is their symmetricity in width, which reduces part adjustment and meshing time.

Because of symmetricity, the part before adjustment was trimmed on one half of the part in *Hypermesh*, and after the 2D mesh was reflected again on the original dimension (see figure 2-28, 2-29, 2-30).

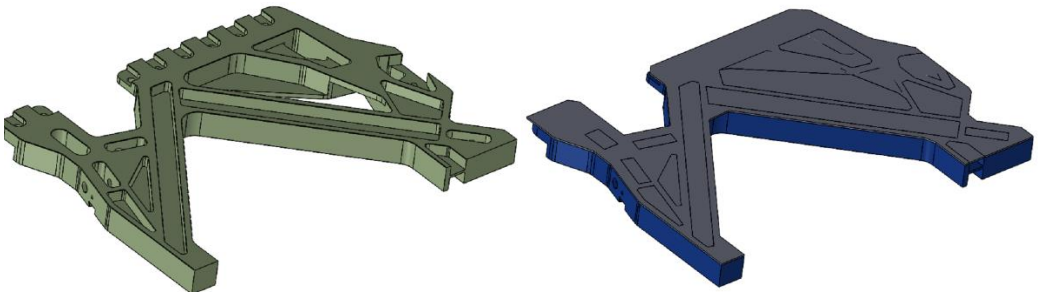

Figure 2-28: (left) Sketch on surface of one half of hexapod plate in *SolidWorks* software; (right) 2D mesh

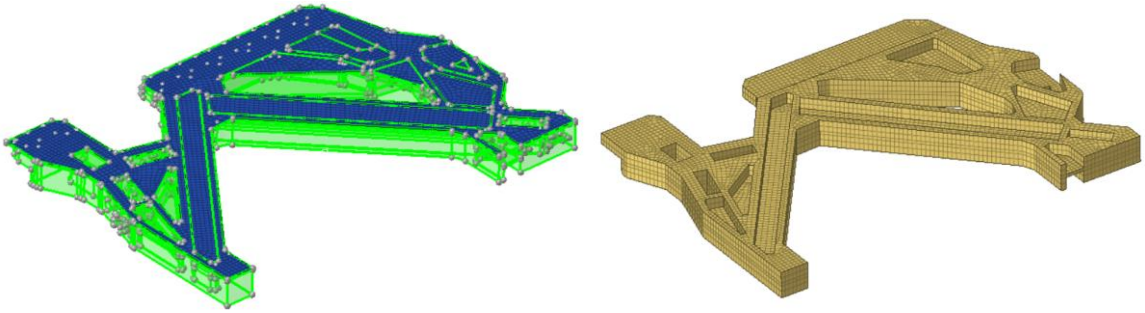

Figure 2-29: (left) 2D mesh; (right) 3D mesh

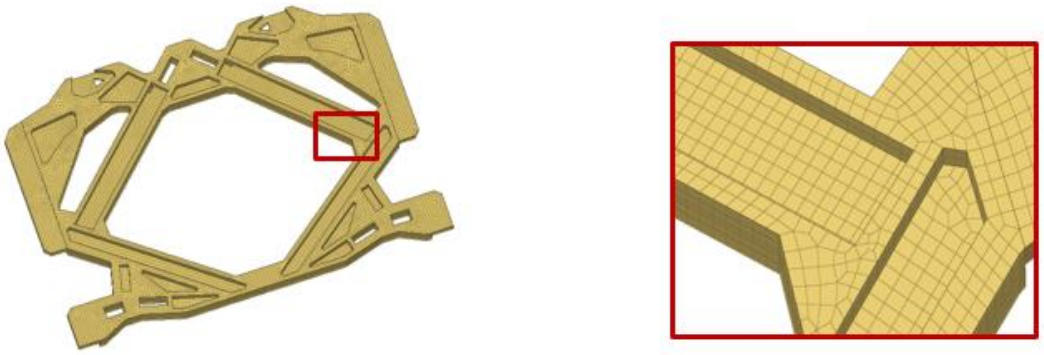

Figure 2- 30: (left) Hexapod plate; (right) Mesh in detail

2.1.4 Contact definition

To create a realistic FE model, the definition of contact surfaces between parts plays a major role. However, in order to reduce calculation time, the contacts between most of the adjacent surfaces in the model are not defined, as the rigid body connection is considered to be sufficient.

Still, several parts that will be explained in the following examples in this sub-section have surface contact definitions with the keyword *CONTACT_SURFACE_TO_SURFACE. The reason is to avoid overlapping or penetration of elements from one part into another, where there would be an influence on the simulation result.

Therefore, in the described examples the keyword *CONTACT_SRUFACE_TO_SURFACE is necessary, because without contact definition would come to penetration of elements. This keyword is a contact option between parts which surfaces are tight fitted together and pre-stressed in the initial configuration. At the beginning of a simulation this option turns off the nodal interpretation checks. In addition the contact forces are able to develop to remove the interpretations [12].

Figure 2-31 shows the CAD and FE model of the sled (X-Sled) and linear guide (Y-Sled) for better insight of contact relation between sled and linear guide. As can be seen, the contact profile from the adjacent parts was simplified in order to reduce calculation time and increase numerical stability.

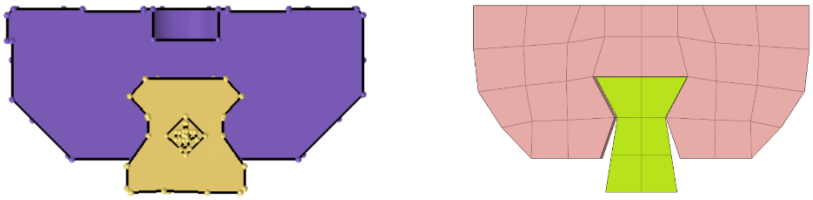

Figure 2- 31: Model sled (X-Sled) and linear guideway (Y-Sled) (left) CAD; (right) FE

The second example of a necessary contact definition with keyword *CONTACT_SURFACE_TO_SURFACE is the contact between the plates under the seat foam and also between plates under the foam on the seat back, so as between leather lining on the seat foams blocks and additional FE part models, either head impactor or steel plate depending on experiment type (see sub-section 2.7). Figure 2-32 shows the situation without and figure 2- 33 with defined contact. The case without defined contact gives inaccurate output data.

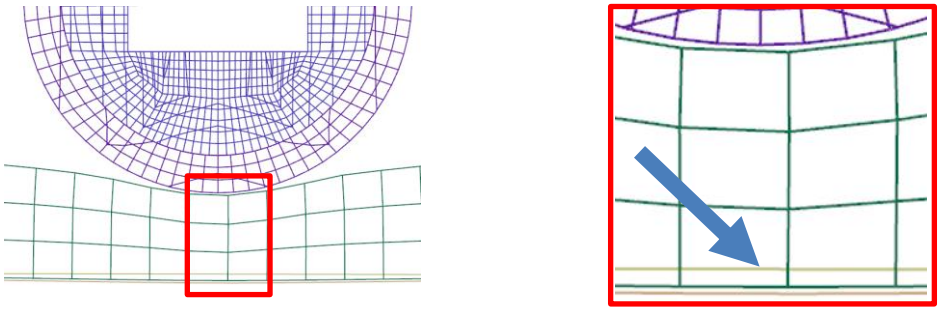

Figure 2- 32: Example without defined contact between parts in FE *Seat* model

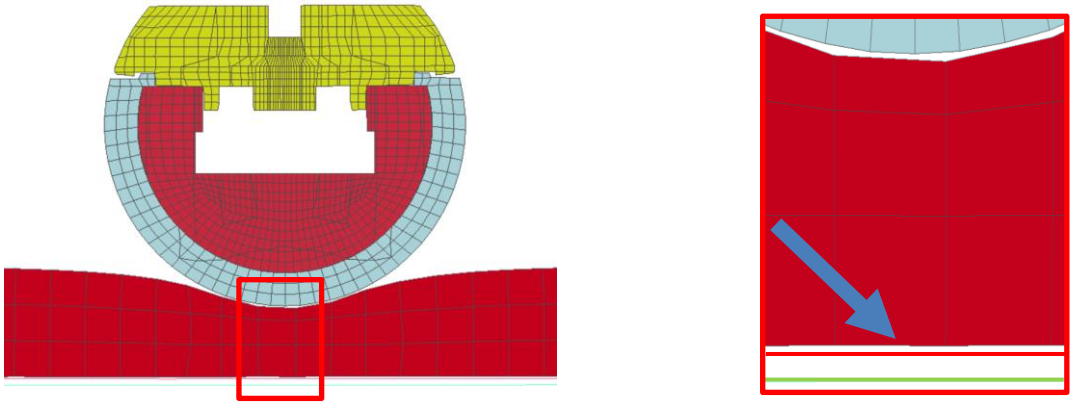

Figure 2- 33: Example with defined contact between parts in FE *Seat* model

2.2 Material and properties definition

The LowG sled testbed is made of parts with several material types such as aluminium, steel, rubber damper, seat foam, and leather in the FE model representative, material types are selected. Particularly at the definition of material properties in a FE model the consisted usage of the unit system is crucial, to prevent false results.

The unit system used for experiments and simulation of the FE model is as follow:

Table 2-1: unit system

Length : millimetre
Mass : kilogram
Time : millisecond
Force : kilo newton
Stress : mega pascal
Velocity: meter per second
Acceleration: meter per square second

For the material definition of aluminium and steel the Material Type 3 (see figure 2-35), and for rubber damper the Material Type 1 of LS Dyna is used. The reason is that from the rubber material are only the spring dampers that are installed on the edges of the "X-Sled", and they are not in focus of this study as the sled should never engage those in "normal" operation.

This material model Material Type 3 is suited to isotropic and kinematic hardening plasticity with the option of including rate effects. It is a very cost-effective model and is available for beams (Hughes-Liu and Truss), shells, and solid elements [12].

VARIABLE	DESCRIPTION
MID	Material identification. A unique number or label not exceeding 8 characters must be specified.
RO	Mass density.
E	Young's modulus.
PR	Poisson's ratio.
SIGY	Yield stress.
ETAN	Tangent modulus, see Figure M3-1
BETA	Hardening parameter, $0 < \beta' < 1$. See comments below.
SRC	Strain rate parameter, C, for Cowper Symonds strain rate model, see below. If zero, rate effects are not considered..

Figure 2-34: Description of variables of Mat_003 [12]

Table 2-2: Parameters for material definition of aluminium, steel, and rubber (source: Vehicle Safety Institute)

Material type	E	Nu	Density
unit	kN/mm	/	kg/mm^3
Steel	210	0.3	7.8x10^{-6}
Aluminium	70	0.3	2.78x10^{-6}
Rubber	2.3	0.49	1.18x10^{-6}

Material Type 57 was used for modelling of seat foams. This material type is used for material interpretation of highly compressible low density materials and activities such as seat compressions and padding [12]. Stress – strain relationship by those materials is highly nonlinear [12], shown in figure below.

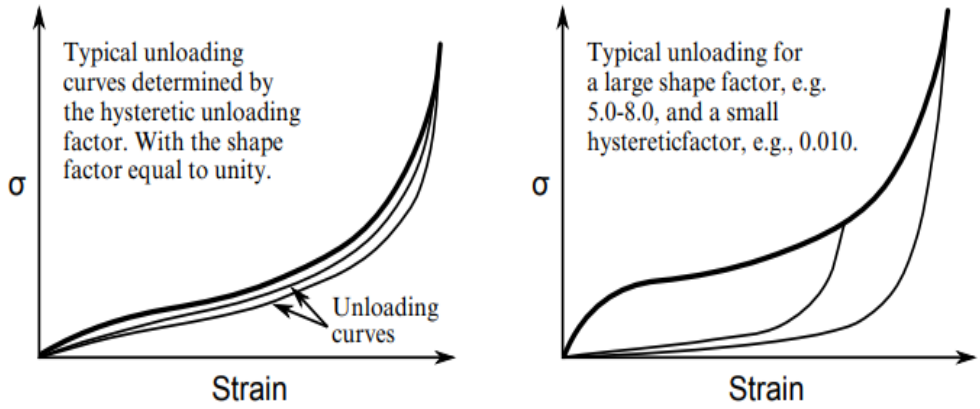

Figure 2-35: Behaviour of low density urethane foam model [12]

Required properties definition for seat foam in LS-DYNA as follow:

1. Density
2. Young's modulus
3. Poisson's ratio
4. Load Curve

The detailed interpretation of the seat foam material properties is described in subsection 2.7.2, together with the simulation setup used to validate seat foam material properties.

2.3 Sensor models

The LowG testbed comprises a number of sensors that capture reaction forces and the resulting deformation of the seat foam during an experiment. Those metrics are also derived in the numerical model of the testbench. The sensors as well as the modelling of the latter is described in the following:

Potentiometers (see figure 2-36 and 2-37) installed in seat foam and seat foam back are potentiometric position transducers with open system up to 100 mm [20].

They are suitable for mounting in closed devices with compact dimensions featuring a resolution less than 0.01 mm, and an outstanding linearity up to ±0.05 % [20].

Figure 2- 36: Potentiometer [20]

Figure 2- 37: Example of potentiometer in seat foam

At the top of the seat foam, below the leather lining, is a button attached to a cable that is connected with potentiometer. A spring is preloaded so that cable does not go slack at quick loadings. In the numerical model, the potentiometers are defined as discrete elements with material definition Material Type 1 (*MAT_ELASTIC). Therefore, the potentiometer is represented as a translational elastic spring located between two nodes with only one degree of freedom.

The output data is the length change of the discrete elements that are interpreting potentiometers and the file *deforce* is the file that contains the output. Discrete elements are stretching through the FE model of the seat and the FE model of the back seat.

On the bottom of the seat and the back seat are discrete elements connected with the frame plate with rigid body connections and on the top with the nodes from the FE interpretation of the leather cover (see figure 2-38).

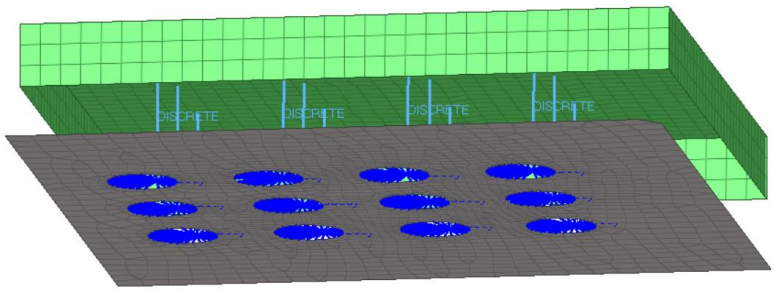

Figure 2- 38: Potentiometers connected with frame plate and the leather, seat

Sensors installed on hexapod rods are strain gauges for experimental stress analysis with high performance (see figure 2-39). Type used on hexapod rods is LY13-6/120. Y series foil strain gauges (SG) can be used in many areas, for static or dynamic stress analysis. Sensors are robust, flexible and with high accuracy [21].

Figure 2- 39: (left) Example of sensor installed on hexapod rod; (rigth) Example of hexapod rods indication on hardware, clockwise

On each hexapod rod is attached one sensor in clockwise direction, were first sensor named HEX_force1 is right front. In FE model the element beams that are representing hexapod rods are named and positioned according to definition of sensors attached on hexapod rods (see Figure 2-40).

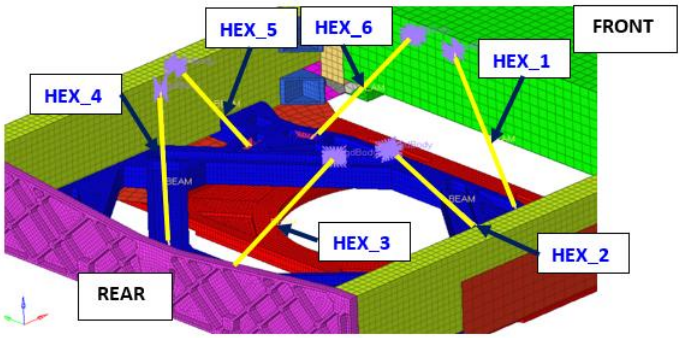

Figure 2-40: Hexapod rods indication

In the numerical model, the hexapod rods are defined as beam elements (see subsection 2.1.3.2). The output data are axial resultant forces, shear resultant forces, torsion moments, and the outputs are saved in the file *elout*. In order to create axial loading in the rods only, the rods are connection to the plates with spherical joints. This setup is also represented in the simulation model.

2.4 Structure and parameterisation of FE model

The first step in the creation of the FE model was to define a range of numbers of FE models. Thereby following FE Models are considered at the creation of the LowG FE Model: Total Human Model for Safety (THUMS), Global Human Body Models Consortium (GHBMC), and VIVA OpenHBM finite element 50th percentile male occupant mode.

Table 2-3: number of ranges of FE models

FE Model	Number Ranges
Thums	80.000.000 – 91.000.000
GHMBC	1.000.000 – 10.000.000
VIVA	0 – 1.000.000
LowG	20.000.000 – 30.000.000

The FE model has a total of 23 *.k* files and is set together from different of FE sub-models, whereby each FE sub-model is saved in own .k file. That concept of the FE model creation enables the parametrization of the adjustment of FE model, for example different angle of the seat or different start position of the movable FE sub-models.

The advantage of the parametrization is the better usability and time saving during the creation of the testbed setup for the discrete simulation scenarios. Without parametrization, the adjustment of the FE model would be much more complex, as for any new simulation scenario different parameters as for example angle, start translational position, height position would require manual

adjustment or even re-meshing. With parametrization, the sub-models are according to their defined degrees of fredom only constrained FE sub-model is “X-Sled” fully constrained.

In the model of the Lowg testbed, the parametrization is defined in *LSDyna* using the keyword for defining one parameter *PARAMETER. The keyword contains the variable and its value that defines the angle for rotation or distance in translation. In the model, there is a separate .k file, containing the parameter values.

In the main file are all other .k files included using the keyword *INCLUDE and *INCLUDE_TRANSFORM, whereby the .k files from FE sub-models are called with the *INCLUDE_TRANSFORM. To define the position of the FE sub-models, in the main .k file for each FE-sub-model the keyword *DEFINE_TRANSFORMATION is defined for the setting the initial position of each FE sub-model. The last step for the creation of the parametrization is the definition of the connection between parameters and the FE sub-models. Therefore, in the keyword *DEFINE_TRANSFORMATION the name of the variables defined in the parametrisation .k file is added.

The table 2-4 shows the list of the .k files and their function and the structure of the FE model. Each .k file that defines the FE sub-model contains the mesh as well the material and the properties of each meshed part in the sub-model.

Table 2- 4: Model structure

File name	Description
00_Master	Main file that includes all other files together to create the FE model of testbed
00_Control_Database	Contains definition of the time simulation, all output codes
0_Contact	Contains contact definition between FE sub-models
0_Element_Discrete	Defines the discrete elements between FE sub-models (back-seat and seat frame)
0_Load	Contains the load definition on the FE model, for example the gravity
0_Parameter	Contains the parameter definition
01_X_Sled_Rigid	Definition of the rigid body connection between FE sub-models “X-Sled” and “Y-Sled”
02_Rotating_Plate_Rigid	Definition of rigid body connection between FE sub-models “Y-Sled” and “Base-Frame”
03_Rigid_Body_PedalPlate-Base_Frame	Definition of rigid body connection between FE sub-models “Pedal-Platte” and “Base Frame”
03_Rigid_Body_Seat-Base_Frame	Definition of rigid body connection between FE sub-models “Seat Assembly” and “Base Frame”
04_Rigid_Body_Seat	Definition of the rigid body connection between FE sub-models “Seat Assembly”
05_Rigid_Body_Pedal_Plate	Definition of rigid body connection between FE sub-models “Pedal Plate Assembly”
01_X-Sled	FE sub-model of the “X-Sled” (see figure 2-42)
02_Y-Sled	FE sub-model of the “Y-Sled” (see figure 2-43)
03_Base_Frame	FE sub-model of the “Base Frame” (see figure 2-43)
04_Seat	FE sub-model of the “Seat” (see figure 2-44)
04_Back_Seat	FE sub-model of the “Back-Seat” (see figure 2-44)
04_Seat_Frame	FE sub-model of the “Seat Frame” (see figure 2-44)
05_Pedal_Plate_01	FE sub-model of the “Pedal Plate” (see figure 2-45)
05_Pedal_Plate_02	FE sub-model of the “Pedal Carriage” (see figure 2-45)
05_Pedal_Plate_03	FE sub-model of the “Pedal Frame” (see figure 2-45)

The following images illustrate the FE-Models of the different sub-assemblies:

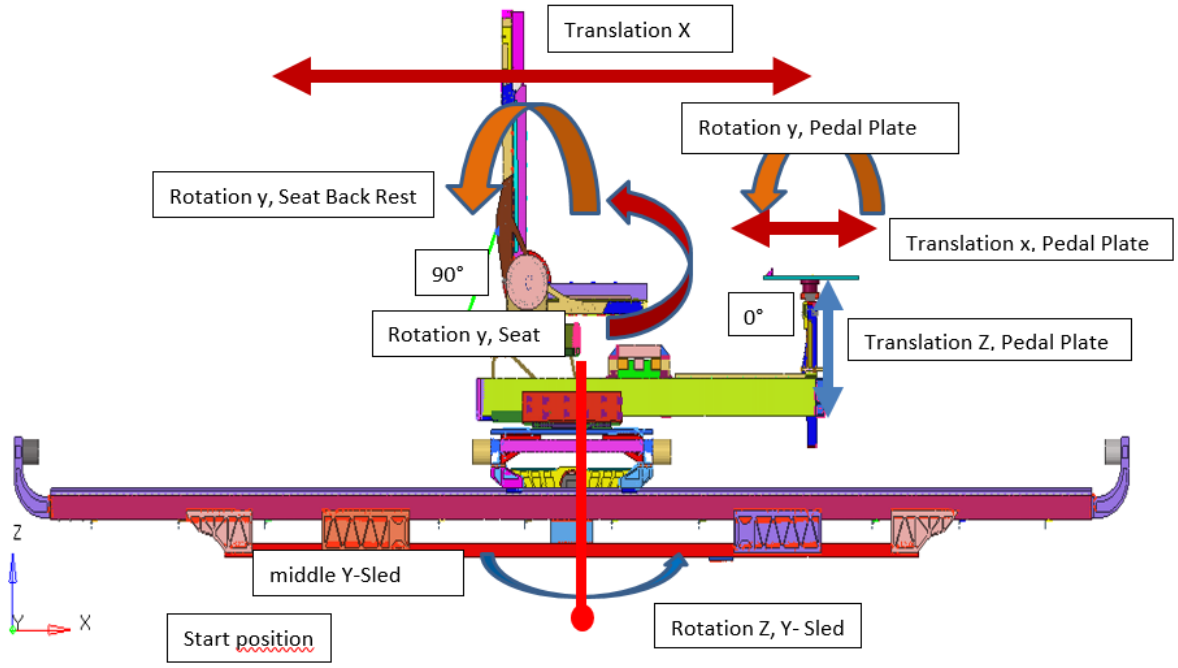

Figure 2-41: FE model in nominal position

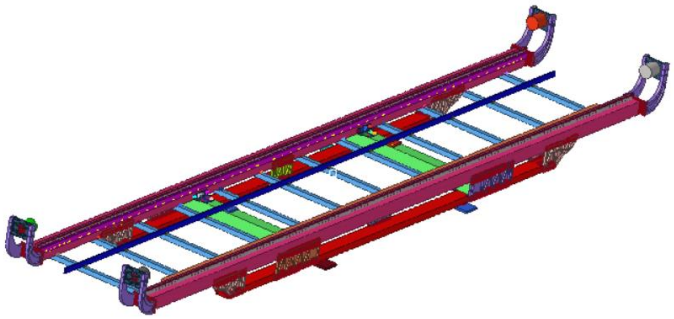

Figure 2-42: "X-sled"

.

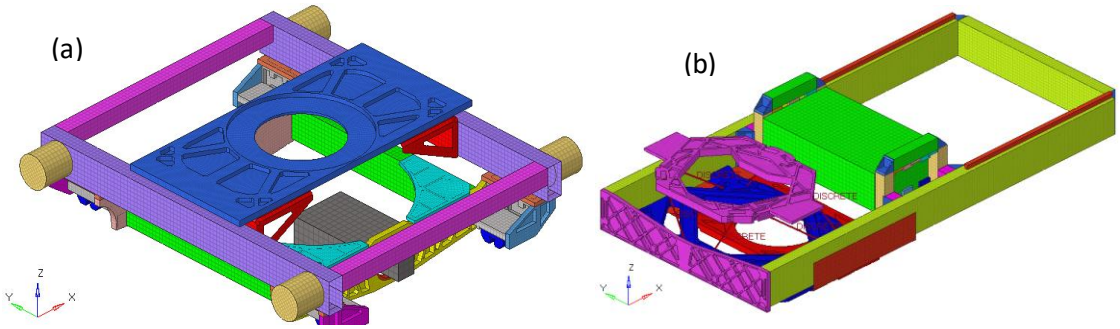

Figure 2-43: (a) Y-sled; (b) Base frame

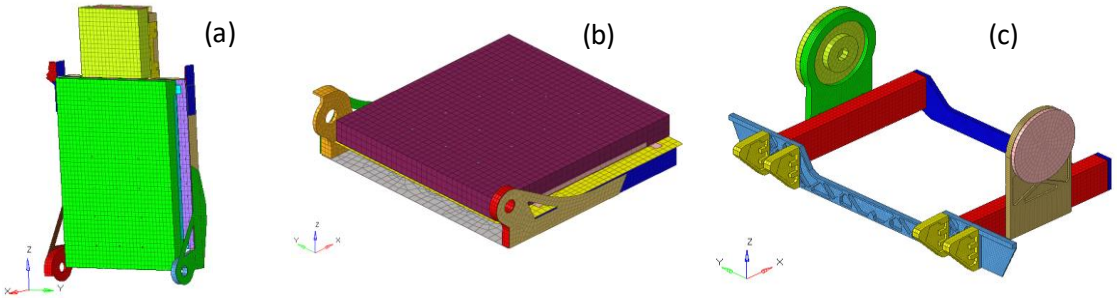

Figure 2-44: (a) "Seat Backrest"; (b) "Seat"; (c) "Seat Frame"

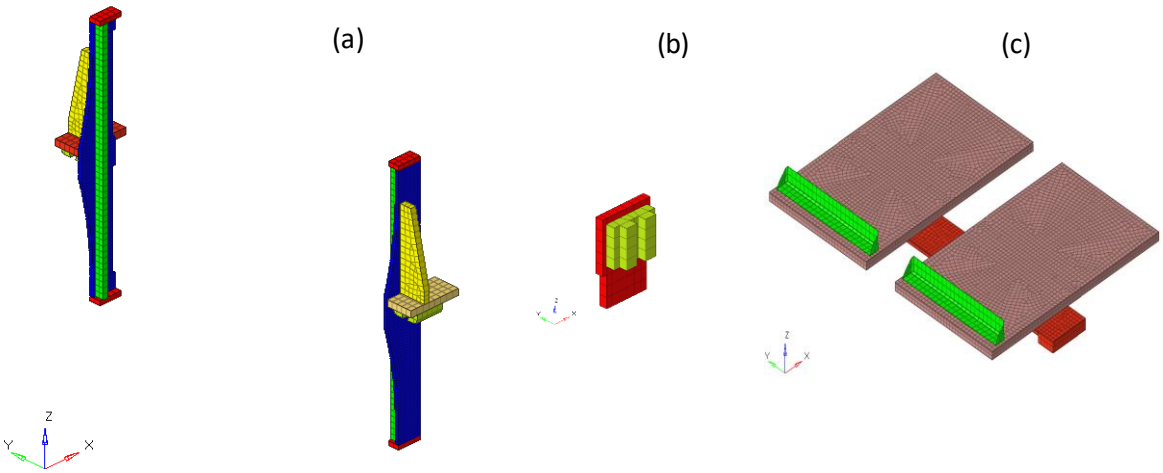

Figure 2-45: (a) "Pedal Frame"; (b) "Pedal Carriage"; (c) "Pedal Plate";

2.5 Model verification

Subsequent to the model creation and principal functional checks, the model has to be verified regarding quality criteria and plausibility. In the following, the evaluations with respect to different criteria are described.

2.5.1 Mesh Quality Criteria

Quality Criteria plays an important role in the accuracy and stability of Finite Element Analysis, to identify mesh elements with poor quality and improve them. The mesh quality influences convergence, the accuracy of the solution, and the required computing time [22].

The following quality criteria were used in this study the software *HyperMesh* enables the straightforward check of the latter*:*

- Warpage angle
- Aspect Ratio
- Skewness
- Minimum and maximum length of the elements

The smoothness is not available to check with the software *HyperMesh,* however this quality criterion was also considered during the meshing process. The assessment of the model with respect to these criteria is summarized in chapter at the end of this chapter. In the following, the single criteria are briefly described:

The warpage angel is the angle by which an element deviates from being planar. This check applies on the quad elements. Quad element surface is divided in two surfaces with the diagonal and each surface has its normal vector (see figure 2-46). The angle between those two normal vectors is the warpage angle [23].

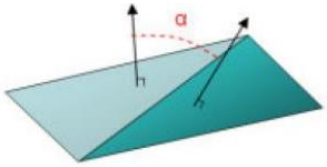

Figure 2-46: Example of the warpage, angle between two normal [23]

The aspect ratio the ratio between the longest edge of an element and its shortest edge or shortest distance from a corner node to the opposing edge (see figure 2-47). In *Hyperworks*, the ratio of 5:1 is the highest ratio rated acceptable and value of ratio should be under 5:1 [23].

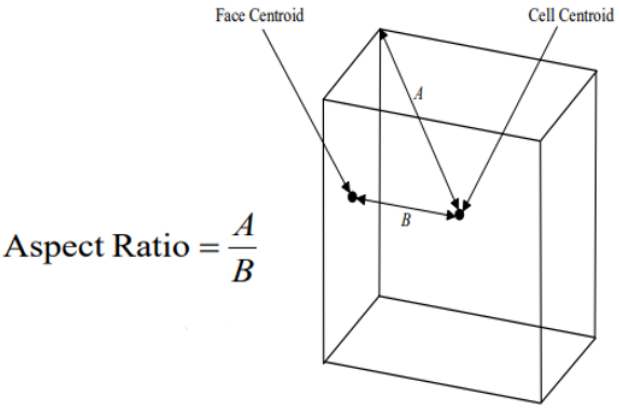

Figure 2-47: Aspect Ratio [22]

In figure 2-48 3D elements with a bad aspect ratio are shown.

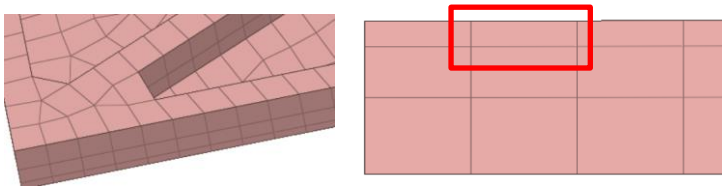

Figure 2- 48: example of bad aspect ratio quality

The skewness is an angle criterion, and is differently defined for tri/tetra and hexa/quad elements. For hexa/quad elements the skewness is calculated by finding the minimum angle between two lines joining the opposide mid-sides of the element [23]. For the check quality check in *Hyperworks*, values of the skewness angle higher than 60 degrees result in a warning that elements are not satisfying the skewness quality check.

The figure 2-49 shows the sketch with the skewness definition by hex/quad elements and for tetra/tri elements.

Figure 2- 49: Skewness angle (left) hexa/quad elements [22] ; (right) tetra/tri elements [23]

The figure below shows the example of bad skewness of hexahedral elements in mesh.

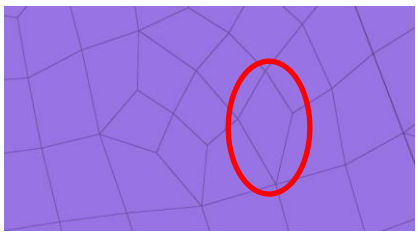

Figure 2- 50: example of low quality of skewness

During the creation of the FE model, to satisfy the quality criteria was most difficult for the created 3D mesh. Sometimes was not possible to obtain optimal quality criteria and the same time be within the defined range of element size that is between 5 and 15mm and create predominantly of hexahedron elements in the mesh.

The reason is the complex geometry of CAD parts, more specifically of support plates and hexapod plates. The support plates are shaped to obtain stiffness but to reduce weight.

Because of that they have a full volume thickness of 2mm but stiffening ribs are 10mm tall and between 2-5 mm wide, depending on the support plate. Those dimensions are not allowing meshing to respect defined element sizes. Therefore, the threshold for the quality criteria of those parts are not met for many elements. In figure 2-51 the example with an FE model of a support plate is shown, where elements of support ribs and plate thickness are examples of low skewness and aspect ratio.

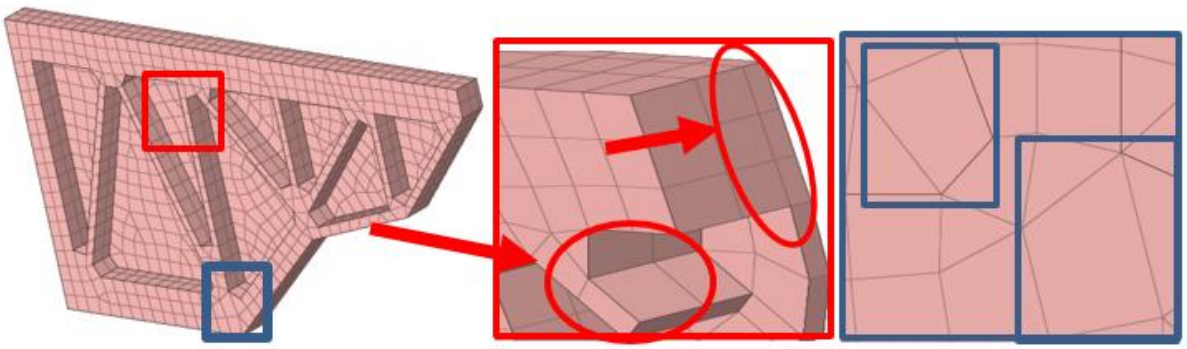

Figure 2-51: example FE part, support plate; (left) support plate; (middle) "AR" and Smoothness; (right) Skewness

The aim of the smoothness criterion is to achieve, that the element size should be changing continuously (see figure 2-52). The smoothness lies between zero and one, and the larger smoothness implies a bigger alteration between adjacent elements. In an ideal case, the alteration rate should not cross 20% [22].

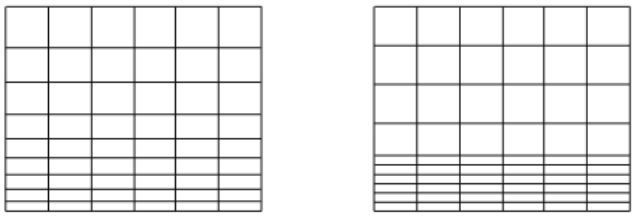

Figure 2-52: (left) continuously -> good; (right) rapidly -> bad [22]

The smoothness was hard to satisfy when comes to the 3D meshing of the support plates (see figure 2-53) because the thickness of the plates was 2mm and the height of the support ribs up to 15mm.

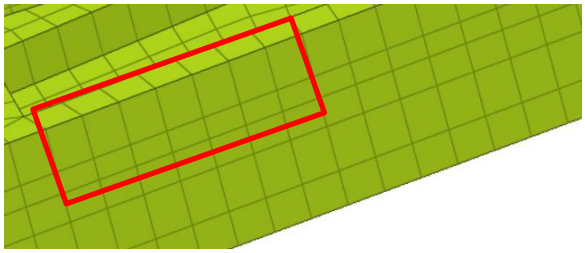

Figure 2-53: example of low smoothness quality

The following table represents the results from the quality check criteria as described in the chapter for the 2D and 3D elements.

Table 2-5: Quality criteria values

Element Type	2D	3D
Number of elements	99110	244922
Aspect Ratio, Nr elements	12	640
Aspect Ratio, max	15,78	1784
Skewness, Nr elements	0	13
Skewness, max. angle	58,44	90
Warpage, Nr elements	94	313
Warpage, max.	180	313
Length max (15mm), Nr. el.	319	13670
Length min (5mm), Nr. el.	346	188695

2.5.2 Mass check

The mass check is relevant because of the impact of the moment of inertia. Therefore, with greater difference of mass between the hardware and the FE model of the sled testbed the moment of inertia will be different and so the output data of simulation. However, by nonstationary parts the difference between the masses plays bigger role in output data of simulation then by stationary parts, for example the FE-model of the "X-Sled". The following figures are representing the masses of the FE sub-models and of the CAD sub-models.

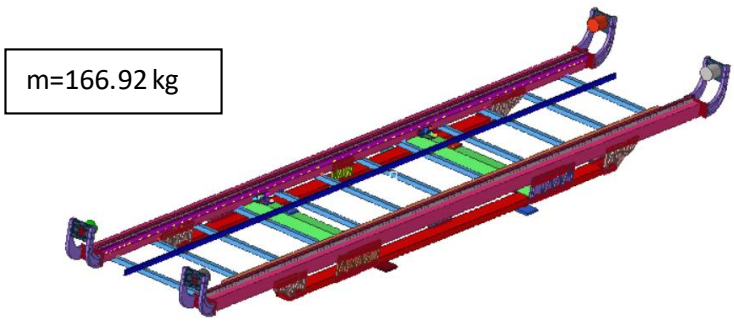

Figure 2- 54: FE model of „X-Sled“

Figure 2- 55: CAD model of „X-Sled“

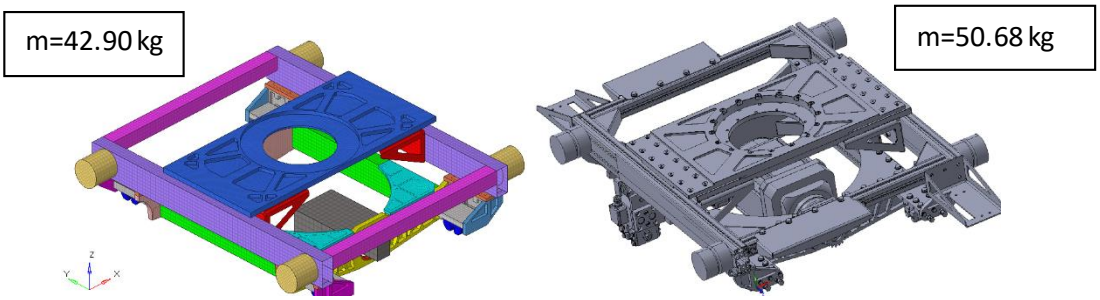

Figure 2- 56: „Y-Sled“ (a) CAD Model; (b) FE model

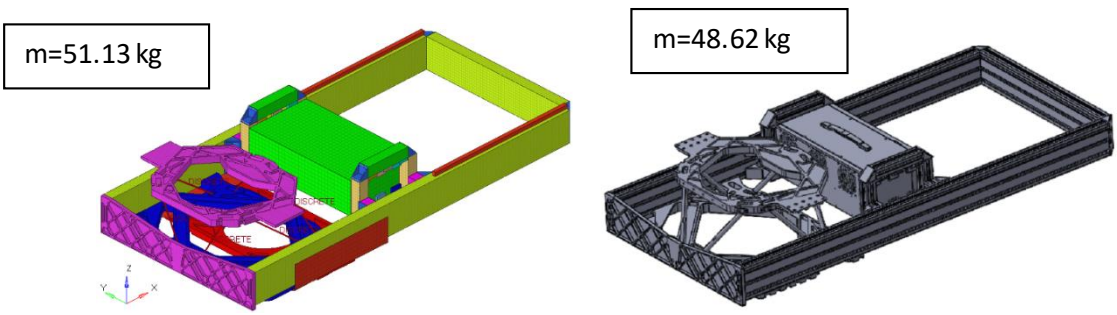

Figure 2- 57: „Base frame“ (a) CAD Model; (b) FE model

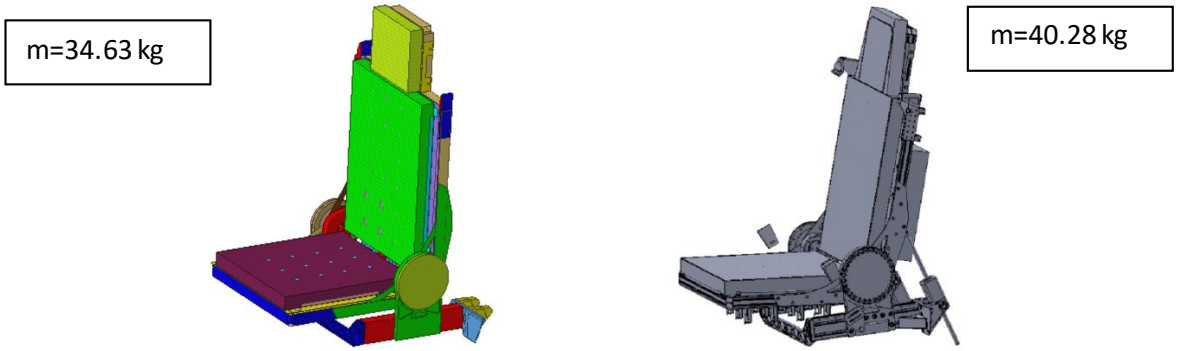

Figure 2- 58: „Seat assembly“ (a) CAD Model; (b) FE model

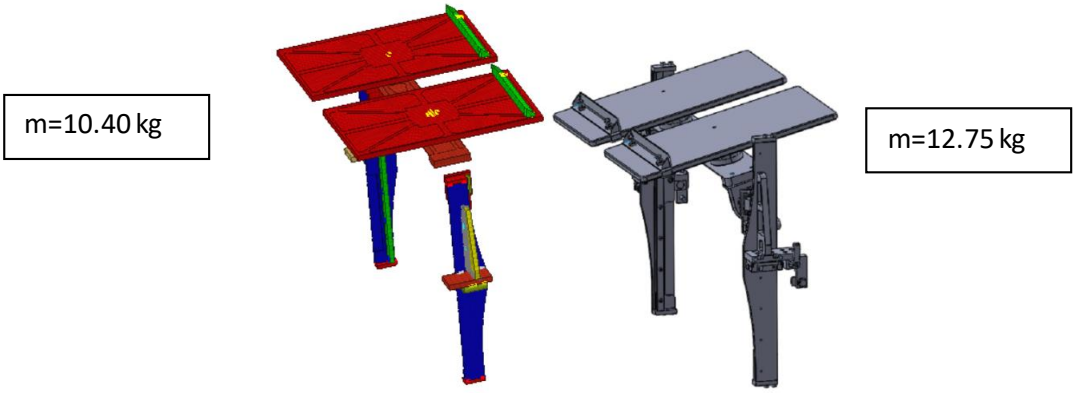

Figure 2- 59: „Pedal plate assembly“ (a) CAD Model; (b) FE model

Table 2- 6: Deviation of the weight

Assembly	Subtracted weight (FE model – CAD model) [kg]
X-sled	-22.54
Y-sled	-8.08
Base frame	-2.51
Seat assembly	-5.65
Pedal plate assembly	-2.35

As shown in the table 2-6, the FE model is lighter than CAD model. The reason could be that the all connection parts as screws, nuts and others are exchanged with the massless 1D rigid bodies. Another assumption is that, the potentiometers are represented as 1D discrete element, but in reality they system consist of several parts, and when the test-rig contains bigger amount of potentiometers, that could make and influence on the weight. However, the biggest weight deviation lies in the assembly of the “X-sled”, the completely fix constrained part. In further studies, the weight of the

assemblies should be more in detail analyzed and adjusted (material definition, adding weight to compensate the "lost" weight with the 1D rigid bodies, …).

2.5.3 Energy balance

When checking the plausibility of the model output, one crucial indicator is the reaching of the balance of the energy at the end of the simulation, whereby "total energy" should be equal the sum of "initial total energy" plus the "external work".

The energy data is printed in the *d3hsp* and *glstat* files forming a useful check on an analysis [19]. The energy balance equation defined in the LSDyna manual is in this research adjusted as follows:

$$E_{kin} + E_{int} + E_{damp} + E_{hg} = W_{ext}$$

E_{kin} is the current kinetic energy,

E_{int} is the current internal energy, and its base is the six components of stress and strain

E_{damp} is the current damping energy,

E_{hg} is the current hourglass energy,

W_{ext} is the energy external work, and includes the work that is done by forces pressures. Also includes the work done by displacement, velocity or acceleration of boundary conditions [12].

There are also other important measures to check the plausibility of simulation results which are based on control energy, mass, and force. At the simulation start, the contact force is zero, contact energy is smaller or equal to 1% of the total energy. FE surfaces that are getting in contact do not cross each other and surfaces getting in contact do not get trapped one in the other.

During simulation, the total energy should remain constant with a tolerance of 15% and the artificial mass increase is less or equals to 3%. Artificial energy (contact energy and hourglass energy) ≤15% of the total energy and hourglass energy ≤ 10% of the total energy [24].

Figures 2- 60 and 2-61 are showing the energy diagrams. They are containing the energies that are involved in the system of the FE model simulation. The total energy is equal to the external work. In dynamic load condition, the hourglass energy is negligible small, and the damping energy increases during the impact of the impactor on the seat. The increase and decrease of the kinetic energy is the fall of the impactor, where the kinetic energy is zero when the seat compression reaches its maximum. In that moment the internal energy has the highest value.

In the quasi-static load condition, the damping and internal energy are bigger, and the curves are after reaching the stationary state (full gravity load) remain almost constant.

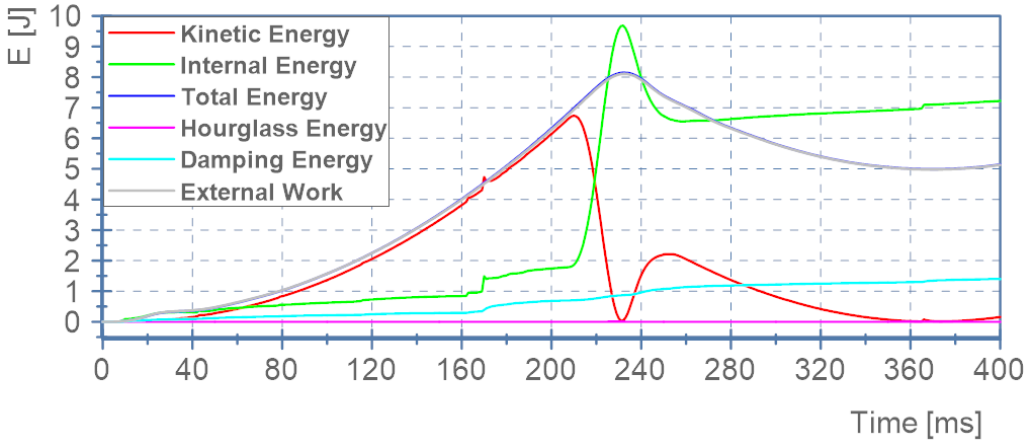

Figure 2- 60: Diagram with energy system, Test 1, head impactor child impacts the seat

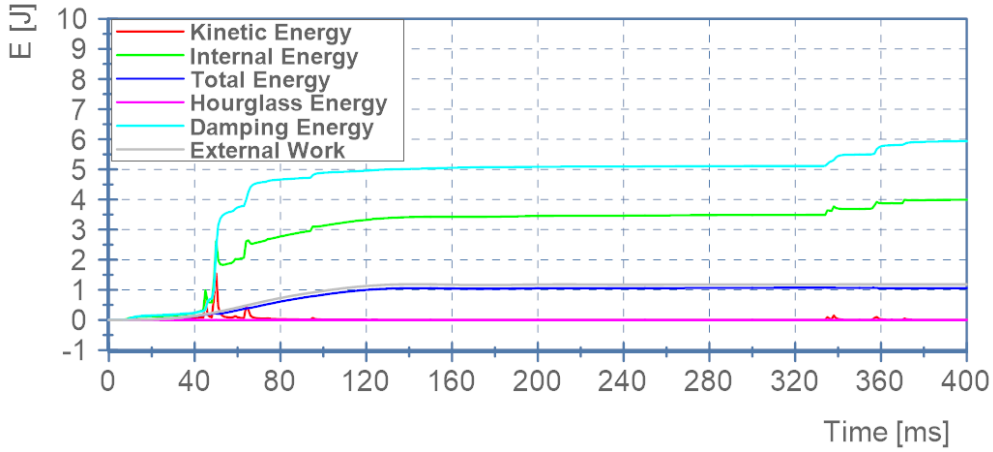

Figure 2- 61: Diagram with energy system, Test 1 (head impactor child impacts the seat)

2.6 Validation of simulation model

This sub-section describes two experimental methods that were used to validate the model. Thereby the test data were compared with the output of corresponding numerical simulations. By adjusting the simulation model (e.g. material characteristic of the seat foam) found differences were minimized. In the following, the experiments carried out are described in detail.

2.6.1 Seat Load Test

This sub-section describes an experiment that was carried out to obtain quasi-static load on the seat. There are six support rods with applied strain gauges between two hexapod plates (top: seat, low: frame) that prove the reaction forces and moments of the seat with the sled frame (see Figure 2-62).

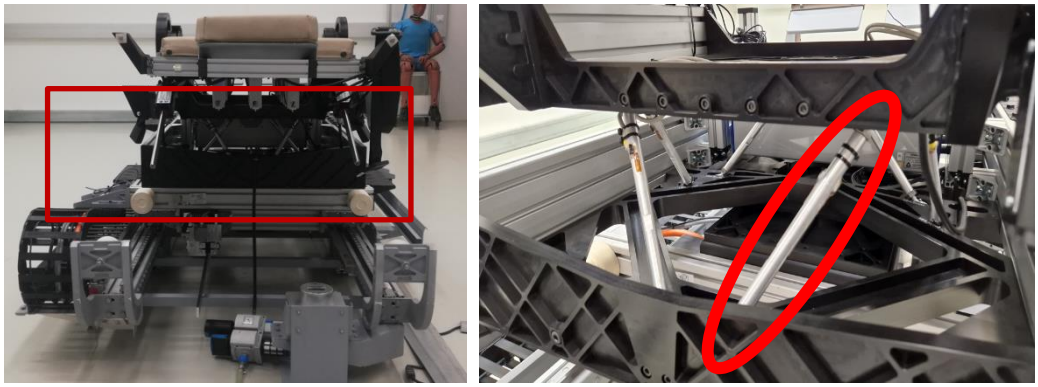

Figure 2- 62: (left) Connection of seat with base frame; (right) Hexapod rods

A steel plate (see figure 2-63) with dimensions 300x300x66 mm and with a mass of 46.6 kilogram is used as ballast in the experiment. Its purpose was to achieve a quasi-static load on the seat and thereof resulting forces in the hexapod rods.

Figure 2- 63: Steel plate used as ballast (left) Weight measure; (right) Thickness measurement

The seat cushion and seat back were set as close as possible to a horizontal position, although zero degrees angle was not possible to achieve for both sub-assemblies (see Figure 2-64, see section 2.6.2).

Figure 2-64: Seat cushion and seat back position

Figure 2-65 shows the angle adjustment of the back seat and the seat relative to horizontal. The seat cushion could be set horizontally, whereas the seatback angle relative to horizontal is 1.4 degrees. All movable parts of hardware were constrained with the brake system, so there is no movements during the test.

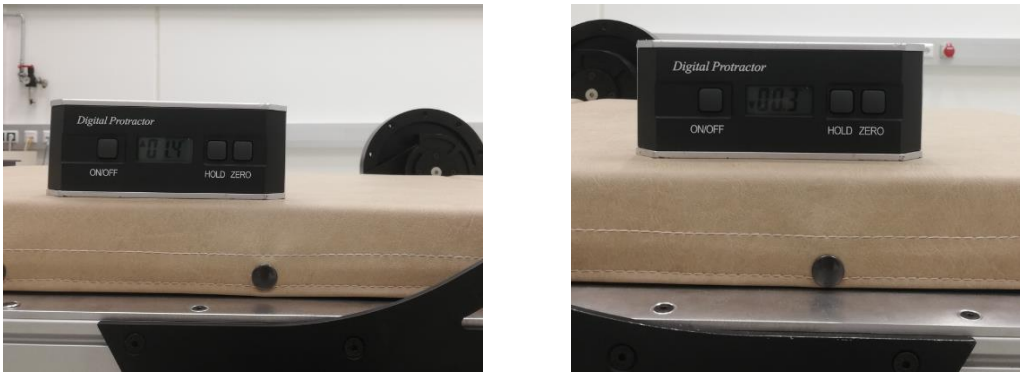

Figure 2-65: Seat angles, (left) Seatback, (right) Seat cushion

During each attempt of the experiment, the steel plate was manually put on the seat or on the seatbacks, at different locations. To disregard oscillations in the first hundreds of milliseconds of the experiment resulting from the repositioning of the ballast plate, the duration time of measurement was set to 45 seconds to reach an idle state and to get more accurate data.

The purpose of the experiment is the comparison of measured data with the simulation. Hexapod rods' positions are not vertical but at a certain angle and do not orient at the same angle relative to Z-axis which gives different resultant force for each rod as load output. The rod length can be adjusted in the test rig with for example compensating manufacturing tolerances what can have significant influence on the force distribution. Therefore in the FE model, beam elements that are representing the rods should be positioned as hexapod rods so that simulation gives the same outputs as the experiment.

The experiment consists of six attempts, where each attempt defines one position of the steel plate on the seat foam or seat back as follows:

Table 2-7: Test number with position plate on seat type

Test number	Position of plate
Test 1	seat middle
Test 2	seat front left
Test 3	seat front right
Test 4	seat backrest middle
Test 5	seat backrest up right

Test 1 (see Figure 2-66 (left)) and Test 4 (see Figure 2-67 (right)) are symmetric loading tests and are used for plausibilisation of the data. Theoretically, symmetric rods should give the same outputs.

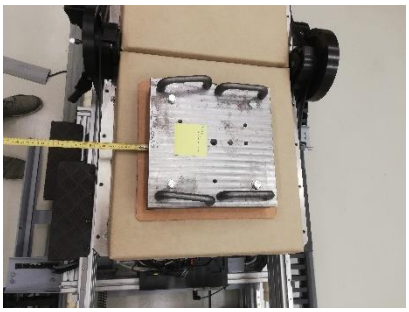

Figure 2-66: (left) Test 1, seat middle; (right) Test 2, seat front left

Figure 2-67: (left) Test 3, seat front right; (right) Test 4, seat backrest middle

Figure 2-68: Test 5, seat backrest up right

The output data of the experiment are the forces of the six hexapod rods, that results from the weight of the seat and the ballast. Before the loading with the ballast, the forces were set to zero. This is typically done prior to an experiment in order to achieve a comparable starting point for the resulting data.

In the remaining four measurements, the ballast was moved to a new position and lifted shortly, to also have a phase in the results, in which only the seat weight is acting on the hexapod rods.

This enables the comparison of the forces for the different loading configurations, and also for the comparison with simulation results. In the further analysis, the phase with seat weight was set to zero, to measure the delta forces resulting from the ballast in different locations.

2.6.2 Head Fall Test

This sub-section describes the head impactor free fall experiments that were carried out to validate the simulation model. In the experiments two different head impactors are used, as typically applied for the assessment of the injury risk of vulnerable road users when impacting the hood of a car (see table 2-8) [25].

The experiment goal is a determination of seat foam properties as well the dynamic impact loading on hexapod rods. Relevant measurement devices are potentiometers (see figure 2-69), installed in the seat cushion and the backseat, the acceleration sensor in the head COG and again the hexapod rods.

Table 2-8: Impactor data [25]

Head impactor Type:	Diameter [mm]:	Weight [kg]:
Adult, Euro NCAP / J-NCAP	165	4.58
Child, Euro NCAP / J-NCAP	165	3.45

Figure 2-69: Head impactor Adult

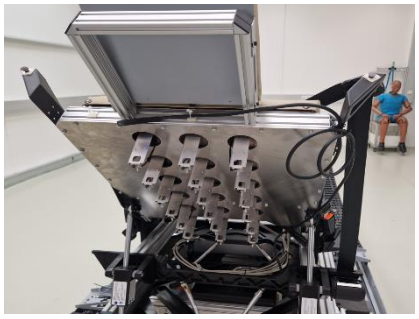

Figure 2-70: (left) Seat backrest potentiometer; (right) Seat potentiometer

All movable hardware is constrained with a brake system, so there is no movement during the test procedure (see figure 2-64). The seat cushion and seat back were set as close as possible to horizontal position, although zero degrees angle was not possible to achieve as already described in 2.6.1.

Each head impactor, adult and child, contain a three-axis sensor for acceleration Model 1203 Accelerometer (see figure 2-71). The signal is further is used to calculate the velocity and displacement of the impactor. The sensor is a small triaxial device created for vehicle impact and road testing. Its ranges are 50 g to 1000 g and frequency response to 3000 Hz [26].

Figure 2- 71: Model 1203 Accelerometer [26]

The target impact positions of the head impactors are marked on the seat cover above potentiometers, as well as the target-position between the potentiometers SP-R2_mi and SP-R3_mi.

The positions on the seatback cover are marked in the same way, above the potentiometers LP_R4_mi and LP_R3_mi, as well the target position between them (see figure 2-72, 2-73 and figure 2-74).

Figure 2-72: (left) Potentiometer Position Marking; (right) Height Setup

The tests, at which the impactor falls on the position above potentiometers are used for validation of the simulation to determine the scale factor of the foam. The additional tests at which the impactor falls on the target position between potentiometers is used for the further validation of the simulation with another configuration, in particular to control the simulations for the scale factor determination.

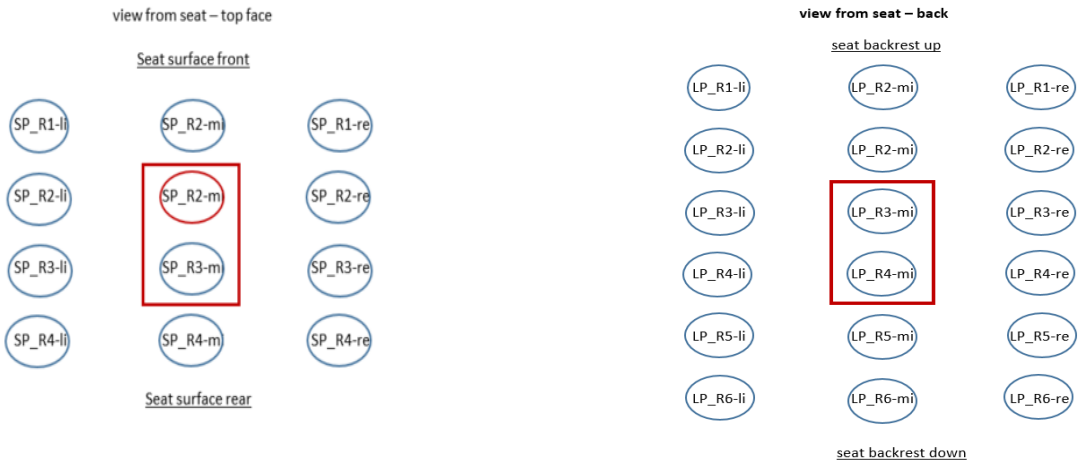

Figure 2- 73: (left) Seat potentiometer pattern; (right) Seatback potentiometer pattern

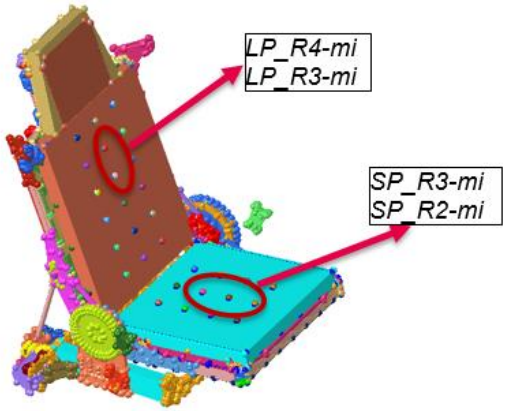

Figure 2- 74: CAD seat model, *with potentiometer locations*

The parameters to be varied in the course of the experiments are the height of the free fall, the impact location and the used impactor.

In total, five experiment configurations were defined set foam properties (S01 – S05), whereby in each configuration three test repetitions were carried out (T1, T2 and T3).

Height and position of head impactor adult/child was defined with combined vertical and horizontal laser light as follows. The height was set with horizontal line: to 150mm for the adult head impactor, and to 300mm for the child head impactor. For precise height definition, a clear edge of the impactor (end of the rubber skin) was aligned with the laser.

The actual height of the top of the head impactor child: 300 - 106=194mm

The actual height of the top of the head impactor adult: 150 – 106=44mm

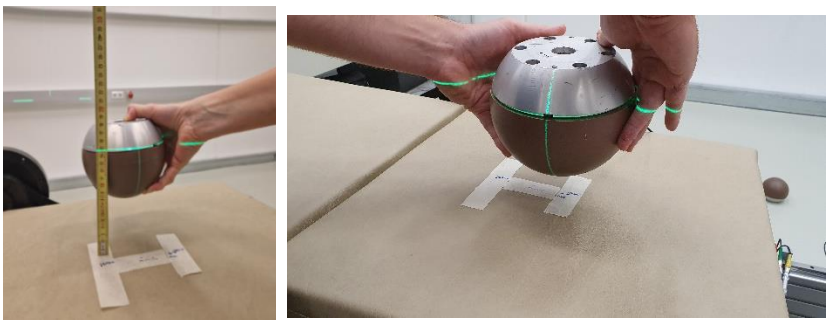

Figure 2- 75: (left) Head impactor adult fall between two potis; (right) horizontal and vertical laser light for adjustment

The impact location of head impactor adult/child was set with vertical laser line on the defined position, either potentiometer position or position between two potentiometers.

Free fall start position by each attempt was set with the hand (see figures 2-76, 2-77).

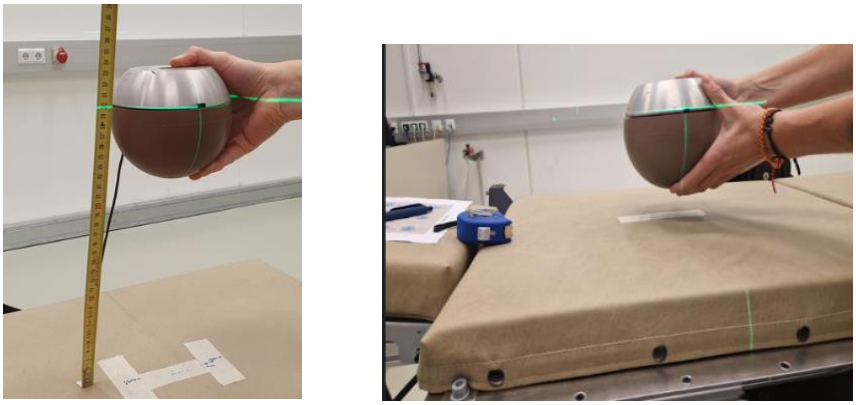

Figure 2- 76: (left) Head child impactor between two potis seatback; (right) Head adult fall on between two potis

In these experiments only outputs in Z-axis are evaluated, because the outputs in Y- and X-direction are negligibly small in comparison to the outputs in Z-axis when the impactor is falling straight.

Relevant outputs in Y- and X-axis are indicating, that the head impactor is not falling straight but it comes to rotation. That occurrence is possible due to the manual release of the head impactor. The experiment results are described and analysed in the chapter 3.1.2.

2.7 Simulation setup of FE model

Before using the FE model of the sled testbed for simulation together with HBM under dynamic conditions, a validation of the FE model is required. The validation is thereby realized as a stepwise approach, starting with simple component tests under quasi-static conditions up to the plausibilisation of the model response in combination with a numerical HBM under dynamic load.

Therefore, three sets of adjusted FE models for the simulation of two experiments were prepared, one quasi-static loading of the seat and additionally a dynamic impact of the head impactor on the seat. Using these models, the initial correlation with the respective tests results was assessed, followed by an adjustment of selected model parameters (e.g. foam stiffness of seat foam)

This model optimization process was used to improve the FE model parameters to get more accurate and realistic outputs before a more complex simulation. Both sets of FE models were simulated only with the impact of gravity.

2.7.1 FE model setup for quasi-static load condition– Seat load test

As in the experiments, the complete FE sled testbed model is simulated with loading the seat or seatback.

An additional FE sub-model represents the steel plate with the same dimensions and weight as used in the experiment (see figure 2-77).

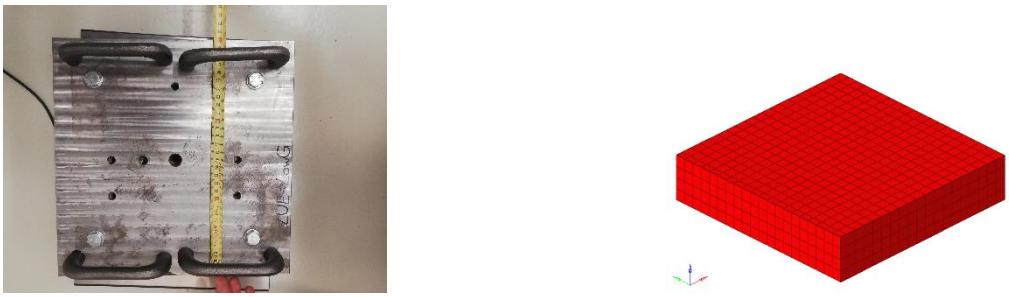

Figure 2- 77: (left) Steel plate (right) FE sub-model of steel plate

The FE sub-models "Seat backrest" and "Seat" are set horizontally and all FE sub-models are fixed so there is no movement during the simulation (see figure 2-78).

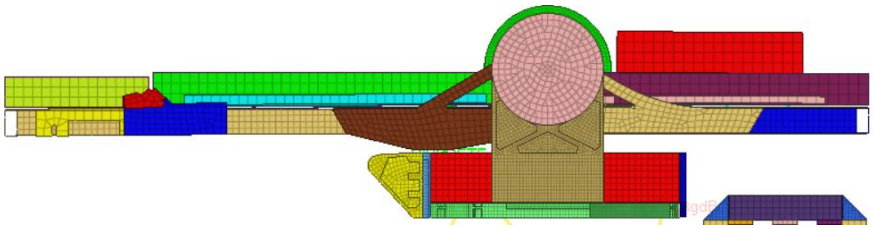

Figure 2- 78: Horizontal position of seat and seatback

As described in section 2.6.2, in the experiment the oscillations occurred in the beginning, resulting from the repositioning of the ballast. This phase disregarded the analysis of the data and also in the comparison with corresponding simulation results. Also in the simulation, significant oscillation is present but for a different occasion. Figure 2-79 shows that at the start condition of the simulation the steel plate is set on the seat, which means there is no oscillation influence by putting the steel plate on the seat, which on the other hand was the case during the experiment.

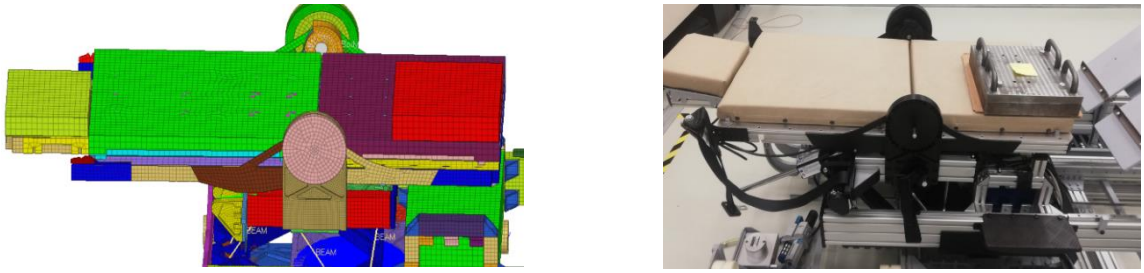

Figure 2- 79: FE model setup example (left) compared with experiment (right)

On the other hand, the oscillation in the simulation results from the impact of the gravity, as the testbed is unstressed at the initialisation of the simulation. The deformation of the testbed starts at the beginning of the simulation, amplified the plate positioned on the seat or seatback. The instantaneous deformation to the static equilibrium induces the described oscillations.

To reduce latter, modifications in the model were made: increase of simulation time, load definition, damping coefficient, type of FE element that describes hexapod rod, spring value of FE element, a joint connection between hexapod rods and hexapod plates. The different steps are explained in more detail in the following.

Using the first model status, the influence of simulation time, damping coefficient, type of FE element of hexapod rod, and its spring values was analysed. The damping coefficient was set at 0.1, the element spring value at 100 kN/mm, and FE discrete elements for hexapod rods. The simulation output enabled several conclusions (see Figure 2-80).

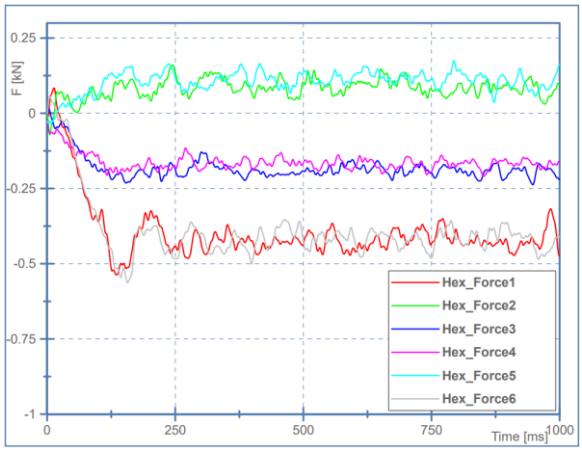

Figure 2-80: Simulation output data resultant forces, gravity only

The first conclusion was, that the simulation time has to be longer than 200 ms to get accurate output data, followed secondly by the decrease stiffness of the hexapod rods to a value 1 kN/mm (see figure 2-81). This was followed by an exchange of the discrete elements with a beam element, the definition of the spherical joints as a connection between FE hexapod plate models and FE beam elements and finally the increase of the damping coefficient on the value of 0.5 (see figure 2-81).

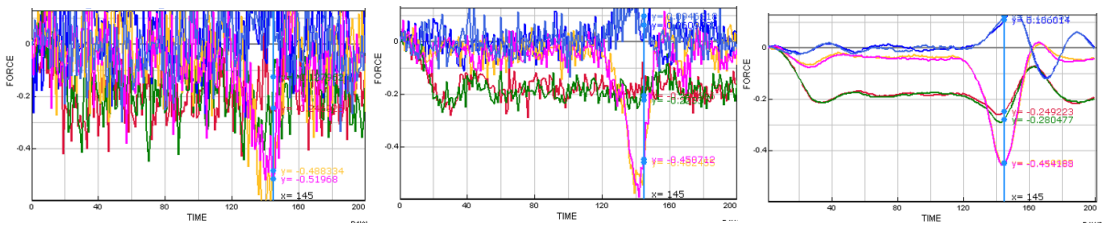

Figure 2-81 simulation output data resultant forces: (left) K=1000 kN/mm; (middle) K=100kN/mm; (right) K=1kN/mm

The last modification in the model was to investigate the impact of the gravity curve definition. The first definition was a constant value of gravity, more specifically from zero to the end of the simulation the gravity has a value of 9.81 m/s².

This was replaced with a gravity curve as function of time, that consist of two parts, the first part is ramped up to its full amount of 9.81 m/s² and the second is a constant value. A linear increase of gravity with a duration from zero to 100ms was a goal to reduce the unrealistic impact of gravity function on the simulation.

By comparing output data from those simulations it can be concluded firstly, that the linear increase of gravity or a constant value of gravity from begin does not influence output data and further, that the oscillations could be completely removed (see figure 2-82).

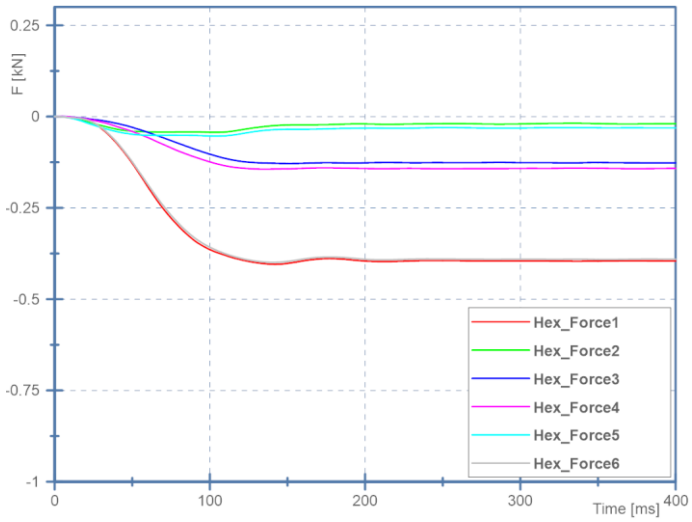

Figure 2-82: Simulation output data resultant forces, gravity only

The removal of the oscillations was one big step forward in the improvement process of the model. Further, minor misalignments in the hexapod rods could be identified and subsequently removed by checking the resulting forces for symmetry in load cases Test 1 and Test 4. Finally the modelling of the connection of the beams representing the hexapod rods with the hexapod plates needed to be updated in order to achieve only axial loads in the rods, as in the experiment.

Having improved the model with the updates described above, the next step is a validation of the FE model, more specifically comparing the simulation output with corresponding experimental data.

2.7.2 FE model setup for dynamic load condition – head impactor

This sub-section describes the creation of the FE model for head impactor freefall simulations. According to the experiment, there are five different simulation variations, with head impactor (see figure 2-83) adult and child.

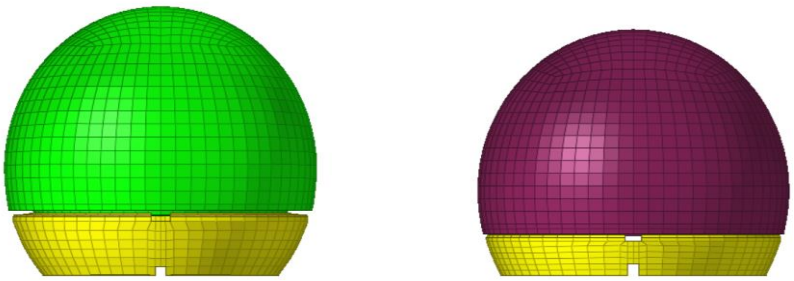

Figure 2-83: (left) FE Head impactor adult; (right) FE Head impactor child

The FE model setup is consistent with the experiment setup. The FE sub-model head impactors are commercial, validated models of the impactors used in the experiment. In the FE model of head impactor, the accelerometer output data is defined with keyword *DATABASE_HISTORY_NODE_ID what gives nodal point data. The output available comprises X, Y, Z-axis and resultant motions as follow: displacement, velocity, acceleration, rot-displacement, rot-velocity, rot-acceleration. No additional FE model was defined for the accelerometer [12].

The start position is set at the same height as for the impactors in the experiments (see section 2.6.2).

The FE sub-models "Seat backrest" and "Seat" are set horizontally and all FE sub-models are fix constrained so there is no movement during simulation except the free fall of the FE head impactor adult/child model.

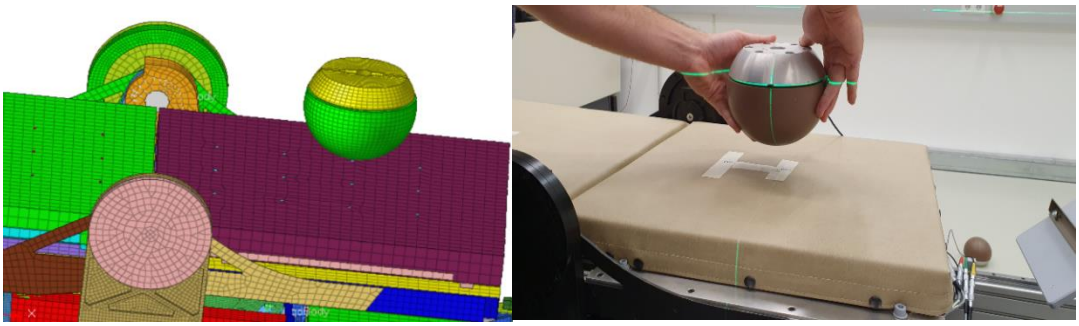

Figure 2-84: (left) Simulation setup FE Head impactor model; (right) Experiment setup Head impactor

The goal was to compare simulation results with test data to check if the simulation gives realistic output data, in particular the compression of the seat and the acceleration of the head impactor during the first impact.

Parameters such as the type of FE element that describes potentiometers, the spring stiffness value of latter, and the curve that describes seat foam properties were identified to be parameters that unexpectedly influence the correlation of simulation and test as follows.

The spring stiffness of the discrete elements that are representing potentiometers in the seat and seat back influence the compression of the seat foam as well the acceleration of the impactor. Its value was reduced on $1x10^{-7}$N/mm, because initial setting with 1N/mm turned out to be still too stiff. The described comparison between simulations with different values of spring stiffness of the discrete elements is shown in figure 2-85.

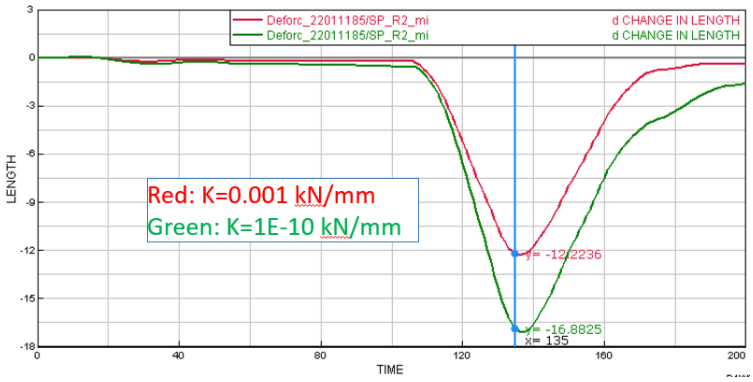

Figure 2-85: Comparison of two different spring-stiffness values, seat compression output

The second parameter that has an unexpected influence on seat compression as well as on the acceleration of the impactor is ramping up of the seat-foam stiffness at high compression, as defined in the model. The last value in table (representing stress over volumetric strain) is typically set to high values in order to prevent numerical instability of the material. It was not found, that the last value was chosen too high in initial model (carried over from other seat) (see figure 2-86).

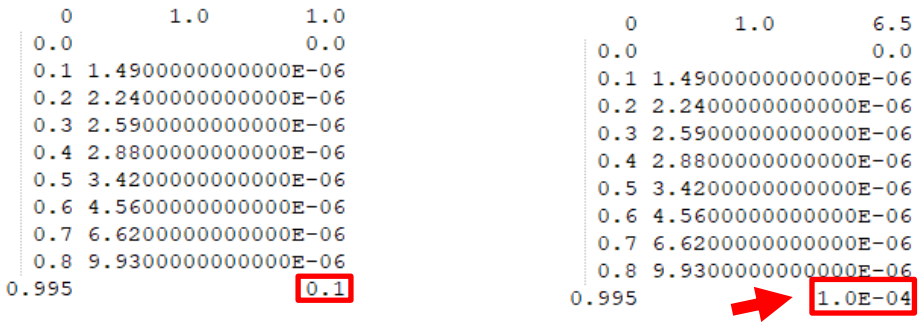

Figure 2- 86: stress-strain curve, *.k file* (left) typical set; (right) adjusted

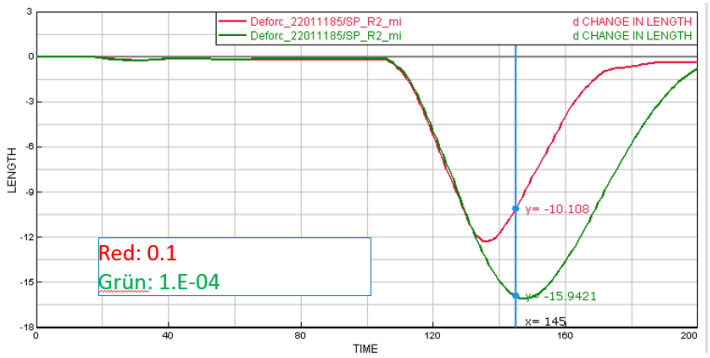

Figure 2- 87: Influence on deformation of seat foam

To reduce the calculation time, the simulation duration of the FE model for the tests with the adult head impactor is 200ms and of the FE model for the test with the child head impactor is 300ms, because of the different start height positions between those test types and it is the same as the start height by experiment (see section 2.6.2).

The gravity is the only load defined in the simulation as well as in the experiment, and the seat must be in the static equilibrium when the head impactor is in collision with the seat.

As described for the seat load test, in the model, the gravity is defined as a ramping up function, to reduce the oscillation that occurs resulting from the impact of the gravity load on the model.

In order to clarify the influence of the defined gravity curve, the output data two types of simulation with two different types of gravity curves were compared.

One simulation is run with a constant gravity load value of 9.81 m/s², the respective signal is named Signal_Compression_01. In the second simulation, Signal_Compression_02, is the gravity load defined as the "two-part" curve, or rather first part is a linear ramp-up function from zero to 20ms and the second part a constant value (see figure 2-88).

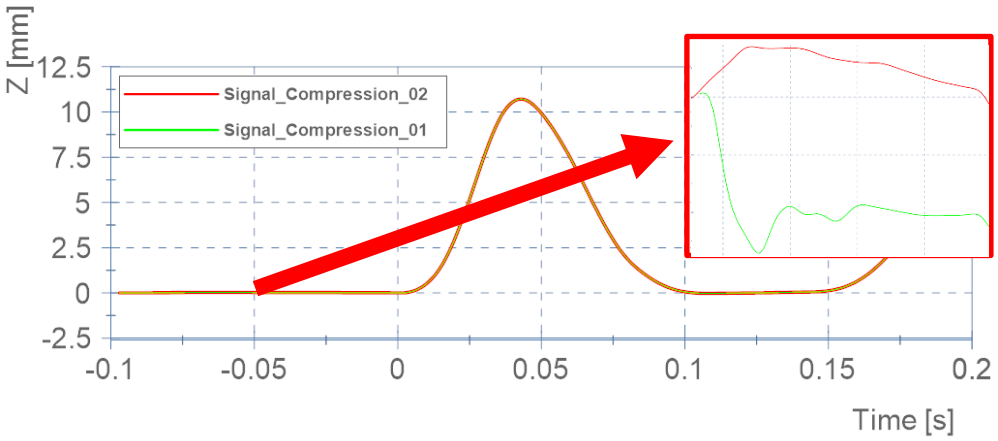

Figure 2- 88: Influence of gravity definition on seat compression

The diagram in figure 2-88 shows, when gravity starts with a constant value then has a bigger impact on the oscillation of the model. On the other hand, when gravity is defined from start as a linear function, then the impact on oscillation is smaller.

2.8 Model implementation: Sled LowG + THUMS v6

This section describes the implementation of the Human Body Model together with the created FE model of the sled testbed to approve the stable running simulation for the required duration.

The selcted HBM for the is simulations is the THUMS v6. Hovewer, in the simulation setup also the THUMS v4 was implemented for the comparison with the simulation that includes THUMS v6. As described in chapter 1, the THUMS v6 is the HBM that features a representation of muscle and can represent the scenario with the muscle condition of passive, relaxed, and braced drivers (see subsection 1.1). The THUMS v4 represents the case when the muscles are not activated, and by THUMS v6 the muscles are activated during the braking manoeuvre.

The implementation of the HBM in the simulation with the FE model of sled is realised as follows:

The first 0.2 s of the simulation are used for settling the HBM on the seat. The HBM was placed 1mm above he seat and in the first 0.2 s the only load was the gravity. The reason is that in first 0.2 s, the gravity reaches increases to 1 g (see figure 2-89).

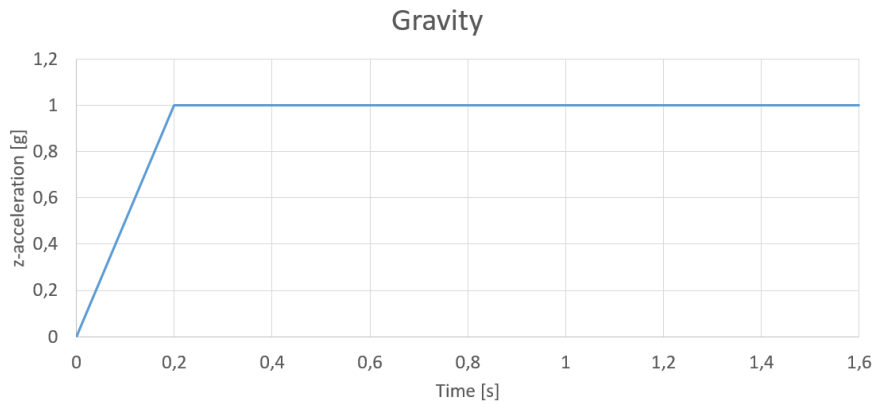

Figure 2-89: Gravity load [g] during the simulation

After the first 0.2s, the velocity of all the nodes was reset to zero, to stop any further seating procedure-related movements. This procedure is a very rough representation of achieving a static equilibrium of the passenger in the seat while seating.

The simulation duration was set to 1.6 s because of the lenght limitation of the sled. Therefore, only scenarios of the braking manoeuvre within this lenght will be possible to investigate. Figure 2-90 shows the diagram withe the acceleration, velocity and displacement curves of the sled. The acceleration was the measured value, where the velocity and the displacement are calculated values.

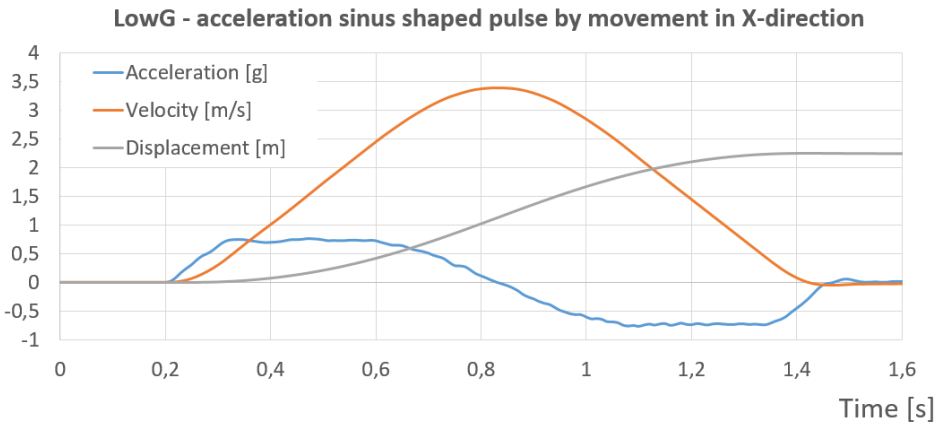

Figure 2-90: Acceleration, velocity, displacement of the sled

Figure 2-91 shows the start of the simulation, where the HBM is 1mm above the seat.

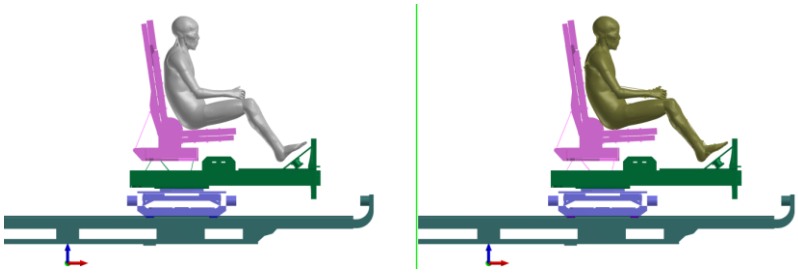

Figure 2- 91: Initialisation of Simulation with HBM (t=0.0 s); (left) THUMS V4; (right) THUMS V6

3 RESULTS

In this chapter the results from experiments and simulations are represented followed by their comparison to prove the accuracy of validation. To be able to compare the output data, a number of calculation steps were (e.g. offset correction, filtering, unit conversion, ...). These steps, as well as the visualization of the data in charts and diagrams was done using the program *Diadem*.

3.1 Presentation of experimental results

In this sub-section the results of the experiments with the ballast plate and the experiments with the head impactor are shown. For presenting the output data in diagrams, the parameters of abscissa and ordinate values were adjusted with several steps of Filter Function, Offset Correction and Scaling.

3.1.1 Experiment results with quasi-static loading condition – seat load test

The goal of the experiment was to get accurate output data for validation simulation by achieving a quasi-static load on the seat and thereof resulting forces in the hexapod rods (see subsection 2.6.1). The input is the impact of the weight of parts that are installed on hexapod rods. The output is the sum of the weight of testbed and additional weight in the case when the steel plate is placed on the seat.

In figure 3-1 the necessary steps of signal adjustment are shown, the single steps are described in the following:

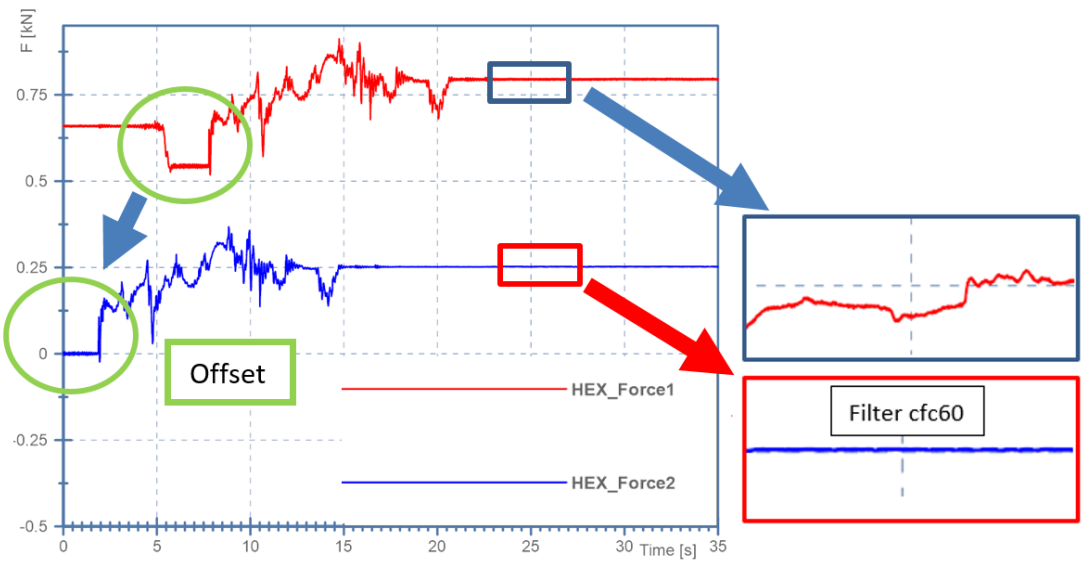

Figure 3-1: Example of diagram adjustment with filter and offset parameter

The original-measurement signal is represented as red curve and named with HEX_Force1, and the adjusted signal is represented as blue curve named with HEX_Force2. Therefore two steps were necessary, to be done:

As a second step the signal was offset in time, as well as on the amplitude:

The original-measurement signal has the start approximately five seconds before the experiment start. In the red curve in the figure 3-1 a drop to a constant force of approx. 0.5kN is seen the fifth seconds acquisition time for a duration of about two seconds. During that period, the ballast is shortly lifted to enable the correction of the force signal by the net weight of the seat.

The time channel was corrected approximately five seconds with the offset, so that the start of the experiment and measurement are synchronised. Next step, the force channel was corrected with the offset, so that the experiment starts with the force of zero. The reason for adjustment better comparability of the data in the different test configurations.

For the very first test this procedure was not necessary, because ballast plate was not initially placed on the seat.

Test 1 – Ballast on seat cushion, centred

With Test 1 plausibility of the output data from hexapod rods can be approved, as they should be theoretically symmetric. More specifically, X-axis is a symmetry line, which means that (see figure 3-2) hexapod rods are symmetric to each other as follows: rods 1 and 6, rods 2 and 5, and rods 3 and 4. In figure 3-2 the hexapod rods indication is shown.

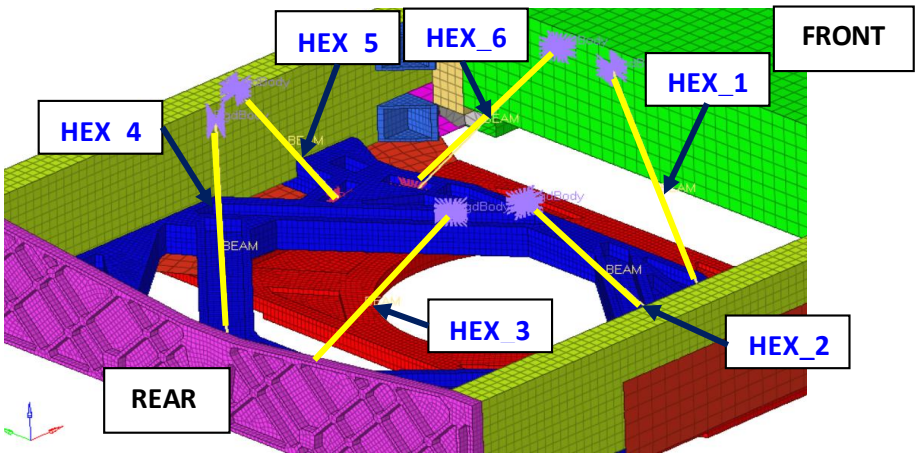

Figure 3- 2: Hexapod rods indication

Test 1 gives output data for the case when the ballast is on the middle of the seat foam, as can be seen in figure 3-3.

Figure 3-3: Test 1, seat middle

In figure 3-4 the resulting hexapod forces of Test 1, with the ballast positioned in the middle of the seat are shown. Each curve in following diagram represents one signal of resultant force of one hexapod rod. Each curve is named after the hexapod rod and visualized in different colour, as shown below.

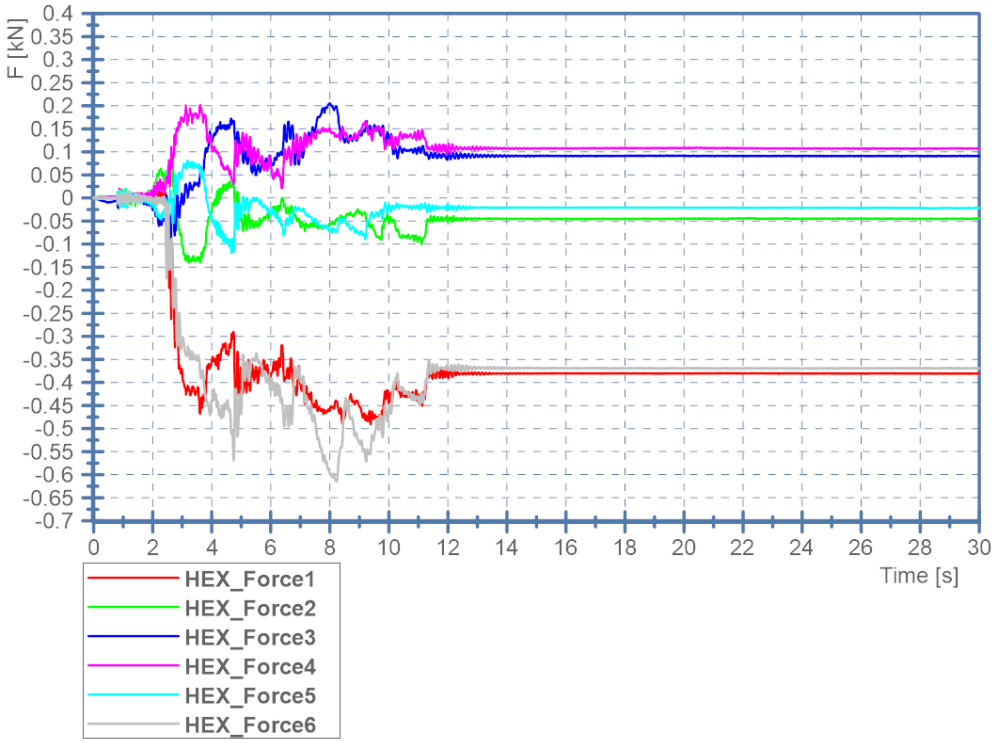

Figure 3-4: Test 1, steel plate located on the seat middle

In the diagram it can be seen, that there is a minor deviation of the output data between symmetrical hexapod rods. The reason for deviations could be the positioning of the steel plate possibly not exactly on the middle of the seat. Alternatively it could also result from slightly differing lengths of the pairs of rods – the effective length is manually set by threads and lock-nuts.

Test 2 – Ballast on seat cushion, front left

Figure 3-5 shows a testbed setup of Test 2, where the ballast plate is located at the front left corner on the seat foam.

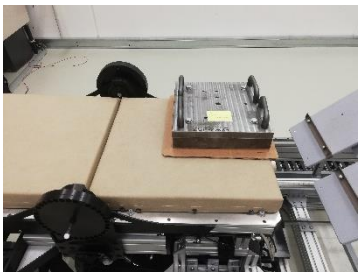

Figure 3-5: Test 2, steel plate on the front left side of the seat

In this test, there is no symmetry and the output data from symmetric hexapod rods are deviating more amongst each other, as can be seen in figure 3-6.

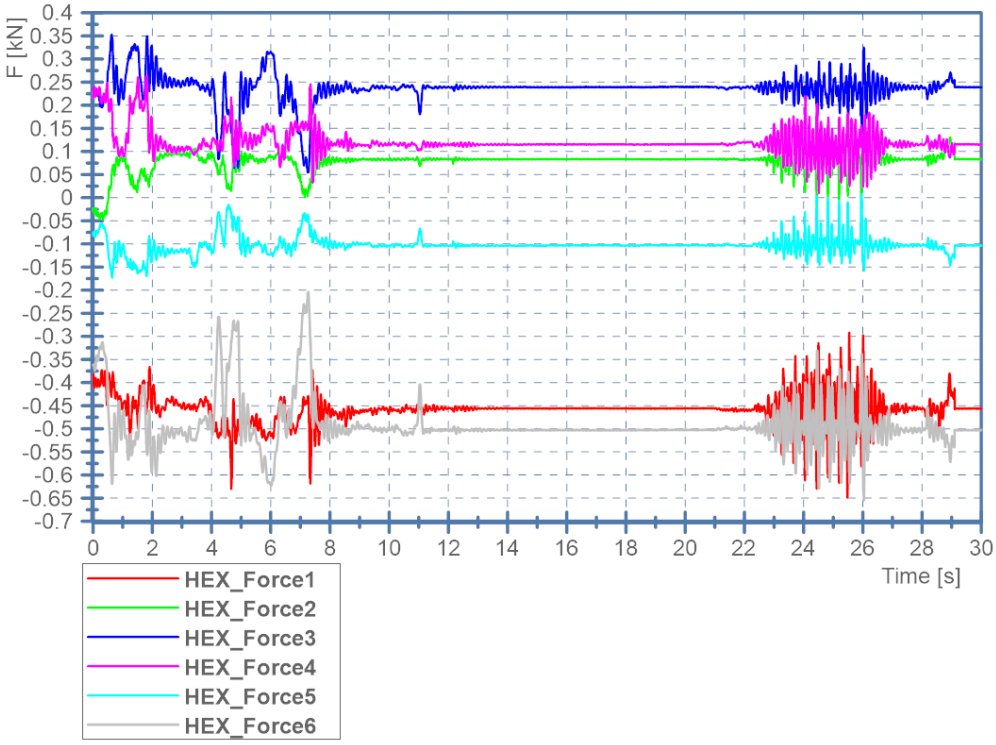

Figure 3-6: Test 2, steel plate located on the seat front left

The rear and middle hexapod rods show greater deviation than front ones.

Test 3 – Ballast on seat cushion, rear right

In figure 3-7 the testbed setup of Test 3 can be seen, where the ballast plate is located at the front right on the seat foam.

Figure 3- 7: Test 3, the steel plate on the front left side of the seat

Also in this test, there is no symmetry in the loading and the output data from the hexapod rods are deviating, whereby rear and middle hexapod rods have greater deviation than front ones. In figure 3-8 the force-time curves of Test 3 are displayed.

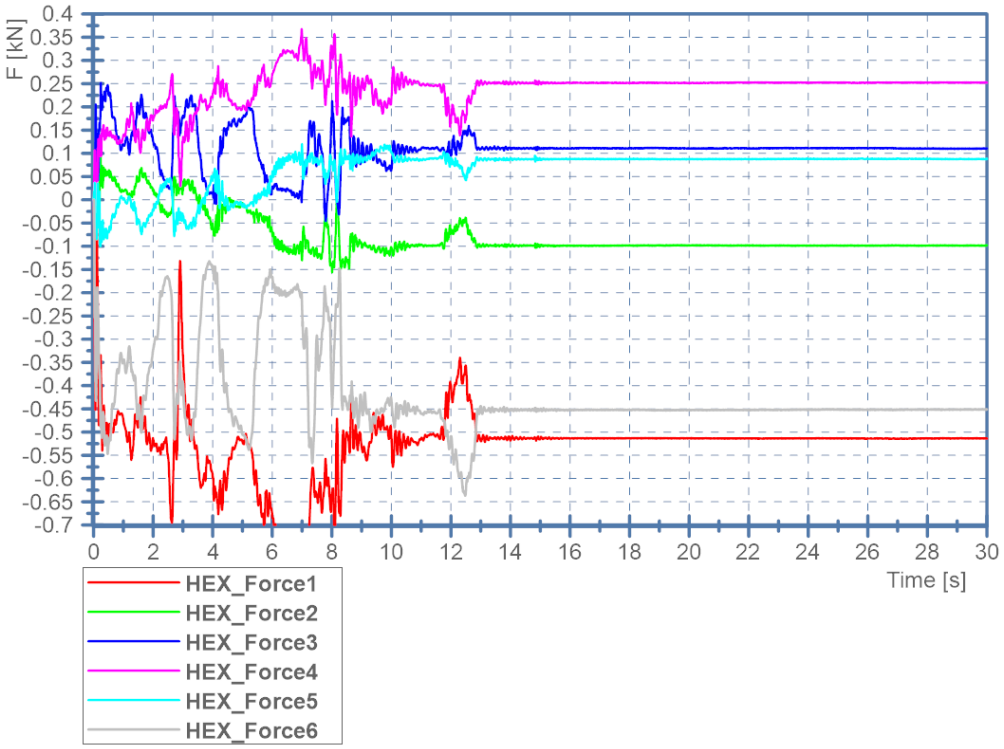

Figure 3- 8: Test 3, the steel plate located on the seat front right

The difference between Test 2, seat front left, and Test 3, seat front right, lies in the opposite deviation of output data. The conclusion is, where the ballast directly impacts the seat above the

sensors attached to the rods, occurs the greater deviation in the output data between the symmetric rods.

Test 4 – Ballast on seat back, centred

Test 4 is again a symmetric load-case, which enables outputs for plausibility as already described in Test 1. Figure 3-9 shows the testbed setup with the ballast plate placed centred on the seatback.

Figure 3-9: Test 4, steel plate on the middle of the back seat

As shown in the diagram 3-10, results are plausible, as three pairs of curves are seen. However, the results differ significantly from Test 1 (ballast on the middle of the seat foam), considering the direction of the forces in the different hexapod rods.

Figure 3-10: Test 4, steel plate located on the backrest seat middle

The hexapod rods 1 and 6 are loaded in tension (positive sign at signals HEX_FORCE_1 and HEX_FORCE_6) and the rods 3 and 4 are loaded in compression (negative signs and for the signals HEX_FORCE_3 and HEX_FORCE_4). This loading indicating a tilting moment to the back of the seat, which was opposite in Test 1. Moreover, the amplitudes of the signals are greater than in Test 1, because there is also a bigger distance between the ballast and hexapod rods. That leads to a bigger bending moments what results in higher force amplitudes for the hexapod leads to greater signals.

Test 5 – Ballast on seat back, rear right

In figure 3-11 the testbed setup of Test 5, with the ballast positioned on the rear right side of the seat back foam, is shown.

Figure 3-11: Test 5, steel plate on the rear right of the backseat

As can be seen in figure 3-12, the output data from symmetric hexapod rods are deviating, where rear and middle hexapod rods have greater deviation than front ones.

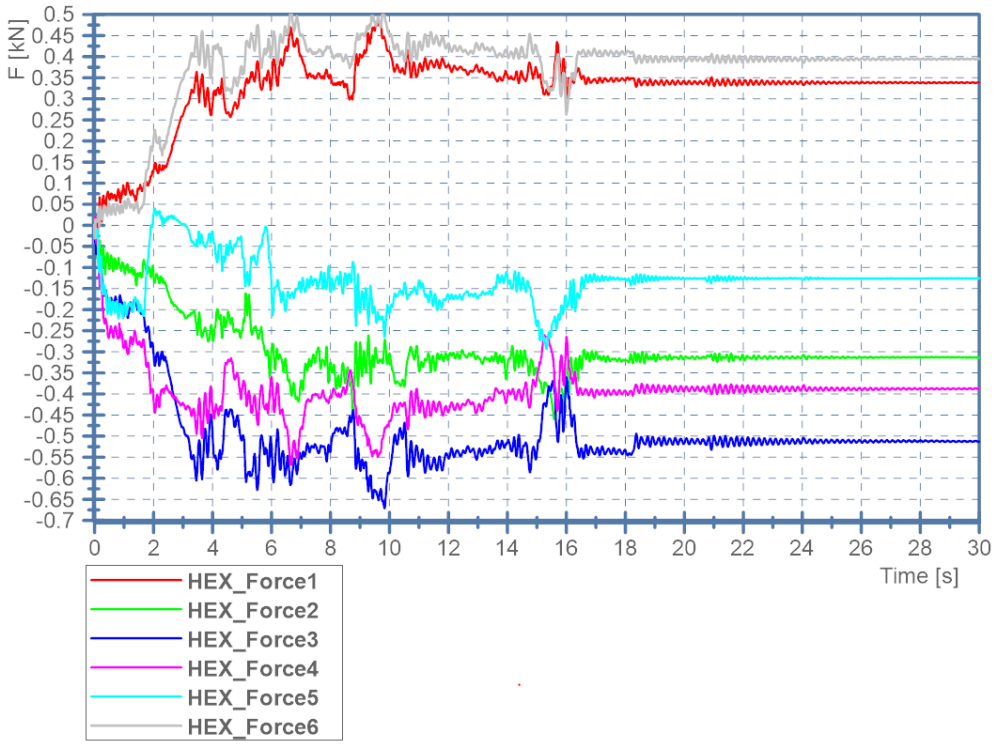

Figure 3- 12: Test 5, steel plate located on the backrest seat rear right

Due to the biggest distance of the ballast plate to the hexapod, in this configurations also the highest forces are seen. In the following chart the hexapod forces of the different rods are displayed for all tests. The output data are the resultant forces of the hexapod rods in kN.

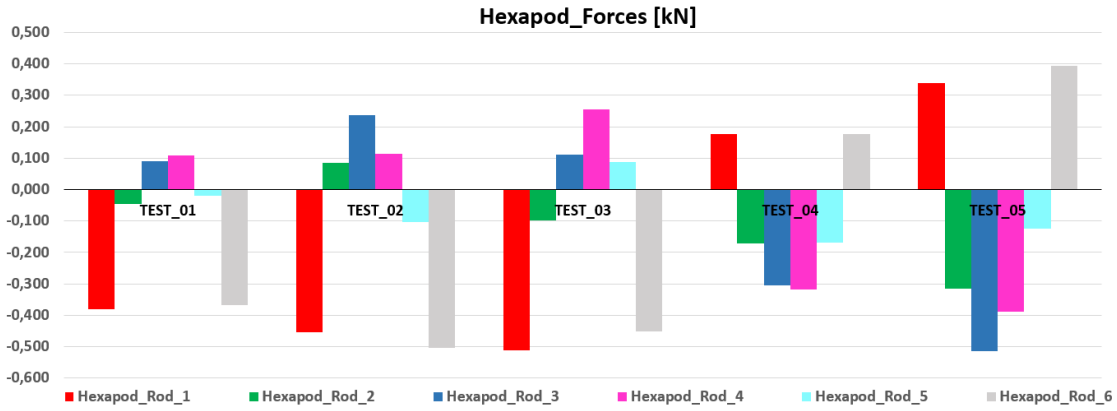

Figure 3- 13: interpretation of the tests in chart flow

As mentioned above, for Test 1 and Test 5, the 3 pairs of rods (1 and 6, 2 and 5 as well as 3 and 4) theoretically give the identical forces in symmetric loading conditions. As can be seen in the chart, the symmetric load cases Test 1 and Test 5 show a clear correlation for the pairs of rods.

3.1.2 Experiment results with dynamic loading condition – head impactor fall test

In this sub-section the results of the experiments with the adult head impactor and the child head impactor are shown. The goals of these experiments are the analysis of the load in the head impactor, as basis for the determination of seat foam properties, and also the analysis of the dynamic impact loading on the hexapod rods.

Calculated signals and captured metrics are seat foam compression in the discrete locations of the potentiometers, the head impactor acceleration, head impactor velocity, and the resultant forces in the hexapod rods. Each test was repeated three times. In the following, only selected data is analysed, the complete set of data is shown in the appendix.

To enable the analysis of the test reading of the results in diagrams and the signals needed to be adjusted as follows (see figure 3-14). The procedure is described using an impact test with the child head impactor as example.

For effective reading of the results in diagrams the signals were adjusted as follows (see figure 3-14). The diagrams in the following figures 3-14, 3-15, 3-16, 3-17 are examples of the acceleration signal of the child head impactor.

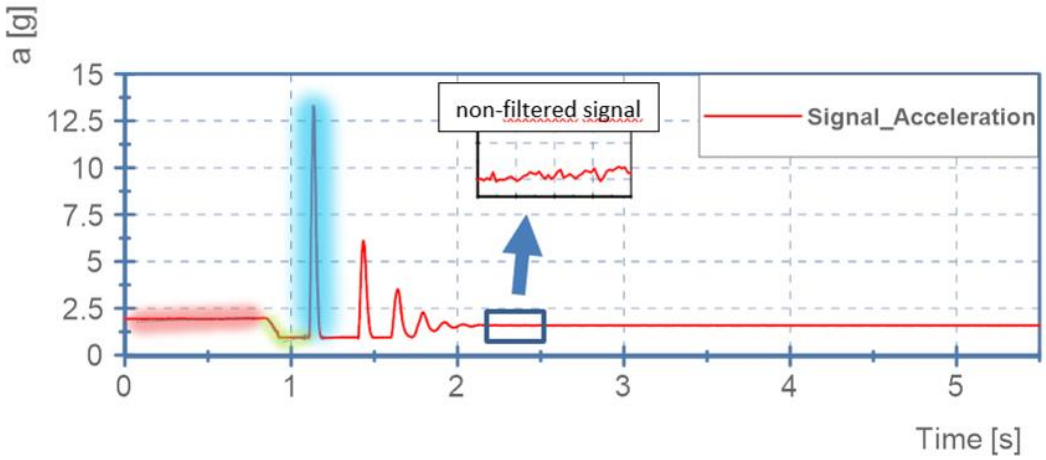

Figure 3- 14: Example of unadjusted experiment result, head impactor acceleration

As shown in the figure 3-14, the acceleration signal that was used for the validation can be divided into three phases:

- the first phase, marked red, is the time before the fall starts
- the second phase, marked green, represents the time of the free fall of the head impactor
- the third phase, marked blue shows the deceleration of the head impactor, resulting from the compression of the seat foam

The first step was to filter the original-measurement signal with filter CFC 60 (see figure 3-15). Once the signal is filtered, the goals is to correct the channel time with an offset to set the zero time at the start of the third phase, start of the seat compression. That contact point is interpreted in the diagram as the lowest point of the curve before the signal increases in the positive direction (see figure 3-15). That spot can be found once the signal is zoomed in and the bottom peak value appears.

The corrected time channel is used also for the visualisation of the output signal of the seat compression and velocity of the head impactor.

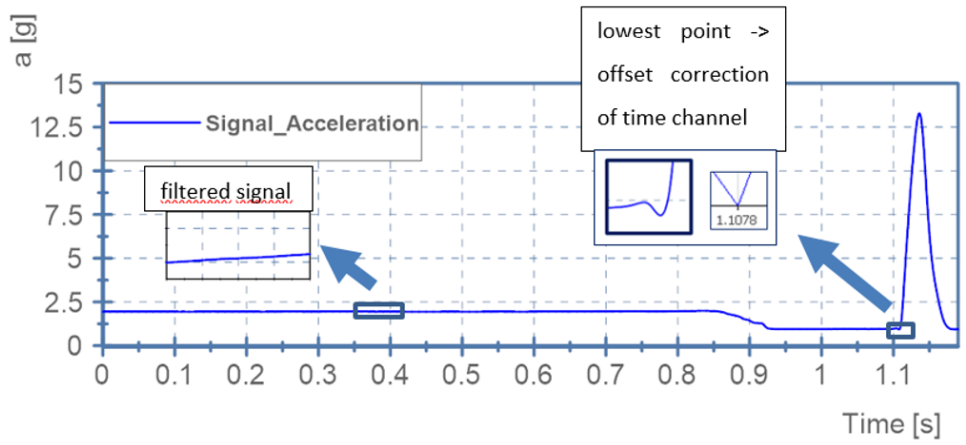

Figure 3-15: Example of filtered signal, head impactor acceleration

For a proper comparison with the simulation data, the acceleration unit is converted from g to m/s². The last step was to make an offset of the acceleration channel to subtract the first channel value, because the experiment started in stationary state (see figure 3-16). In the figure 3-16 it can be seen that the freefall duration is approximately 0.3 s. This duration of the free fall of the impactor is less for the adult head impactor (approx. 0.1s), because of the different fall height.

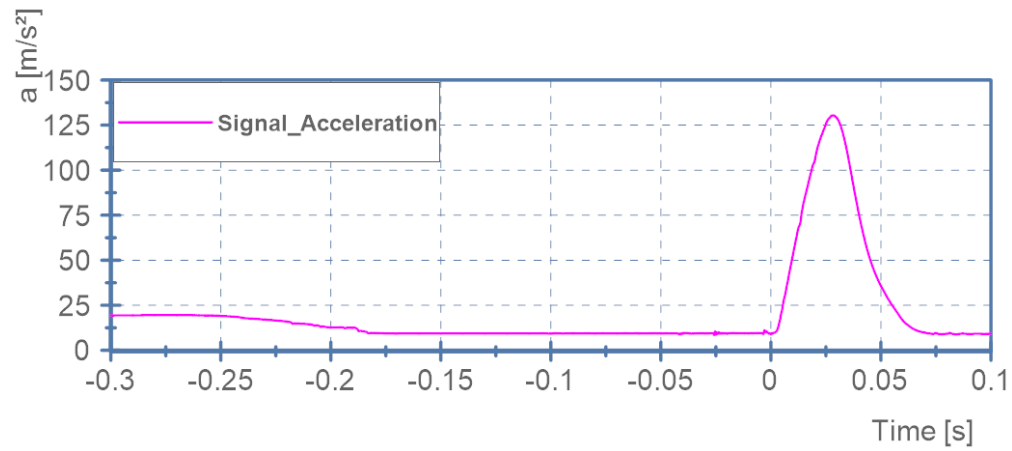

Figure 3- 16: Example of the adjusted diagram (offset, filter, units), head impactor acceleration

Figure 3-17 shows the final curves of acceleration and seat compression after adjustment as described above. The acceleration curve is blue and is named S01_acceleration, and the seat compression curve is red and is named as S01_deflection both curves stem from one single repetition of this impact test.

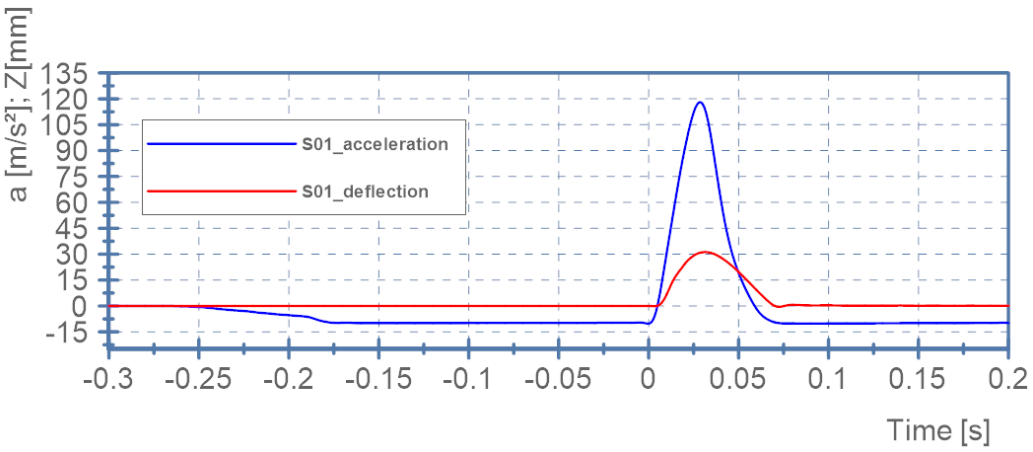

Figure 3- 17: Adjusted curves of acceleration of the impactor and the seat compression, S01T1

In the following, the test results of selected test configurations that were relevant for the comparison with corresponding simulation data are described. The remaining results are added in the appendix.

S01 - direct impact on poti: Acceleration head impactor (child), seat foam compression

In the test configuration the child head impactor is dropped directly onto the seat cushion above the potentiometer SP-R2_mi. Test 1 is the example with the scenario when the head impactor

child falls directly on the seat above the potentiometer SP-R2_mi. Figure 3-18 shows the setup of the configuration S01.

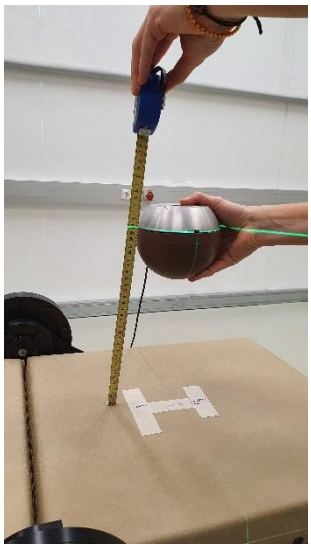

Figure 3-18: Freefall of the child head impactor

Figure 3-19 shows the diagram of test that consists of acceleration output data of three repetitions and one calculated mean curve. The mean curve is the arithmetic mean value from all three attempts for any sample. In the diagram it is represented as red curve under the name S01_mean. The attempts from the test are visualized as follow: first attempt under the name S01T01 as black dotted-dashed curve, second attempt under the name S01T02 as black solid curve, and third attempt under the name S01T03 as black dashed curve.

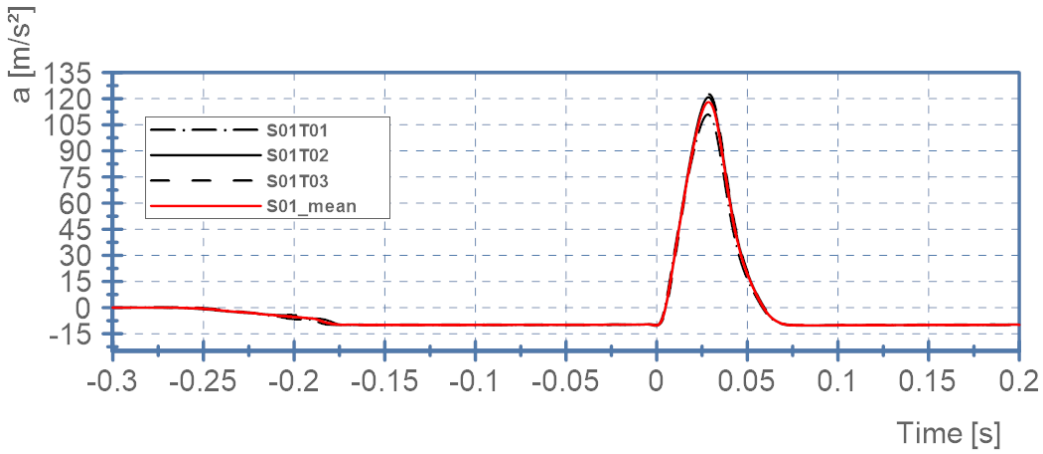

Figure 3-19: S01: Acceleration diagram example, three attempts with mean curve

Despite the relatively simple test execution, with the manual setting of falling height and the manual release of the impactor, a reasonable repeatability was achieved.

Analysing the other acceleration components, perpendicular to the fall direction, it could be checked if the impactor was not aligned properly with the vertical axis, due effects like a minor rotation, that could easily occur considering the manual release. It was checked if either the acceleration components but also the velocity components in x and y direction were small compared to the Z-component.

Figure 3-20 shows the velocity signal of the head impactor during the free fall and the impact, whereby again the curves of the three attempts as well as the mean curve are displayed.

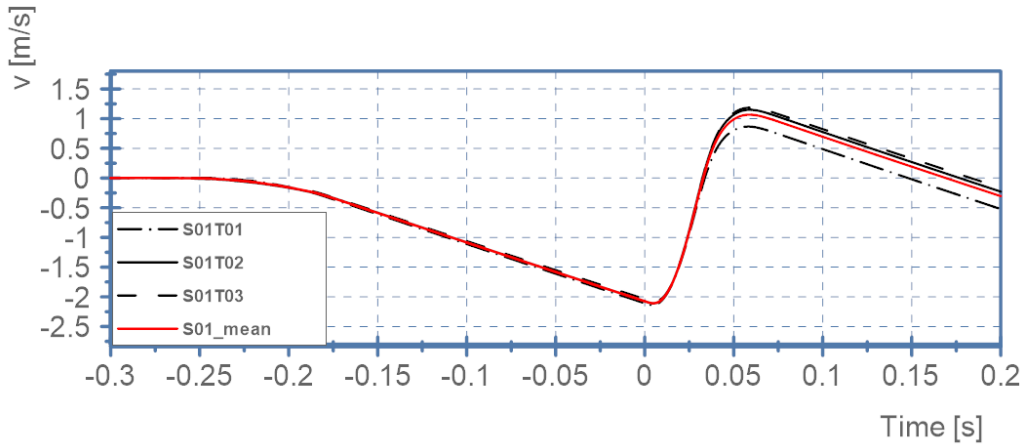

Figure 3-20: S01: Velocity diagram example, three attempts with mean curve

In figure 3-21 is the output signal of the compression of the seat foam at the potentiometer SP-R2_mi during the impact of the head impactor can be seen. This measure was used to validate the properties and material of seat foam and back seat foam in the FE model.

The diagram shows three attempts from the test and the calculated mean curve.

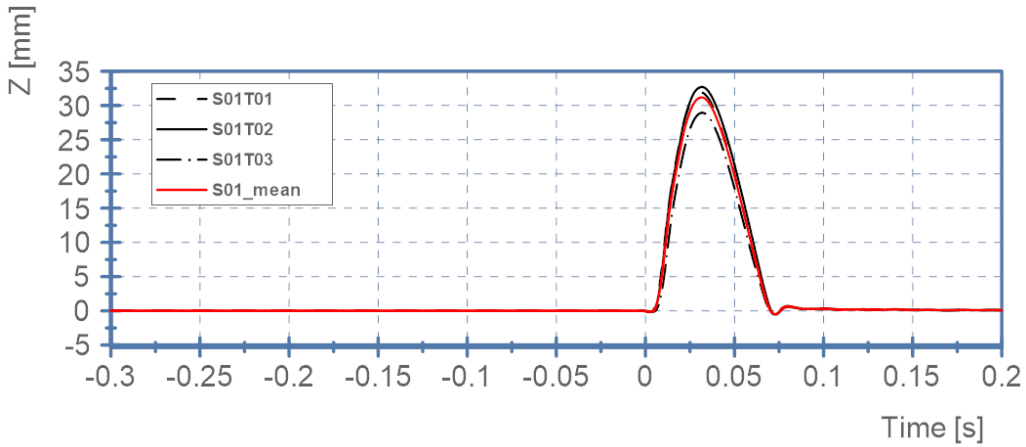

Figure 3- 21: S01: Seat compression diagram example, three attempts with mean curve

S02 - impact between two potis: Acceleration head impactor (child), seat foam compression

In the test series S02 the head impactor was dropped onto the seat cushion between the two potentiometers SP-R2_mi and SP-R3_mi (see figure 3-22).

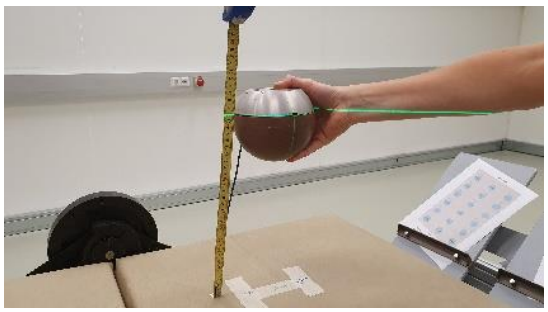

Figure 3- 22: Freefall child head impactor

In the acceleration and velocity diagrams, shown in figure 3-23 and figure 3-24 respectively, the signals are defined as follows. The mean curve is represented is displayed red with name S02_mean. The curves from three repetitions are a black dotted-dashed curve for S02T01, a solid black for S02T02, and black dashed for S02T03.

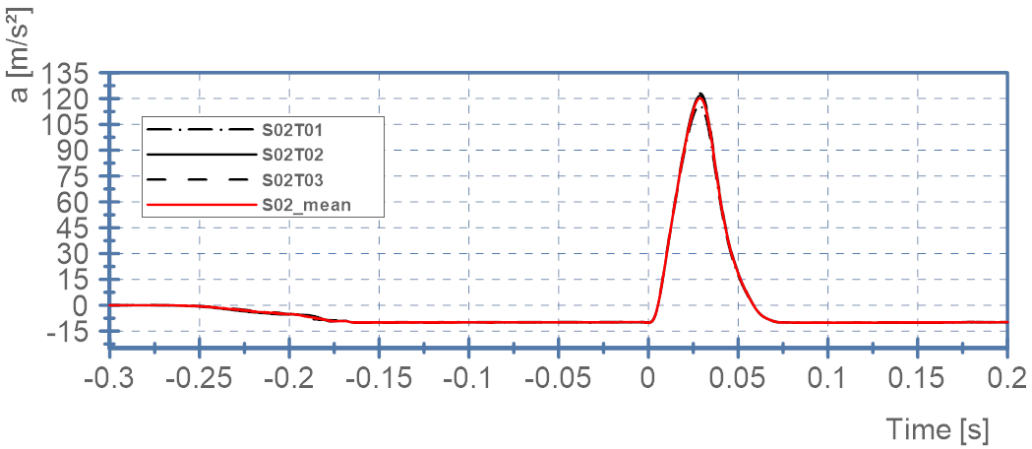

Figure 3- 23: S02: Acceleration diagram example, three attempts with mean curve

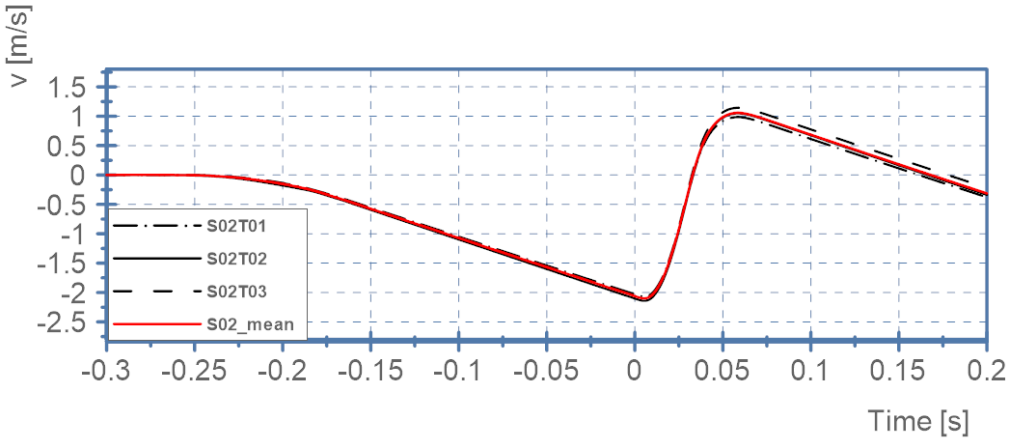

Figure 3- 24: S02: Velocity diagram example, three attempts with mean curve

The curves above are matching well with the curves shown for the series S01, where the same impact condition were tested, only the location was different.

Figure 3-25 shows the diagram with the data for the compression of the seat foam of three attempts and the mean curve. Theoretically, the compression signal of the two potentiometers SP-R2_mi and SP-R3_mi should be the same, but apparently in the experiment, the head impactor to did not fall exactly into the middle between the two potentiometers.

In figure 3-25, the signals of the seat compression from the test are represented as follow: The signals of the poti SP_R2_mi for the 3 repetitions are displayed in black coloured curves, the corresponding curves of the poti SP_R3_mi are displayed green. The mean curve of all 6 signals is shown in red.

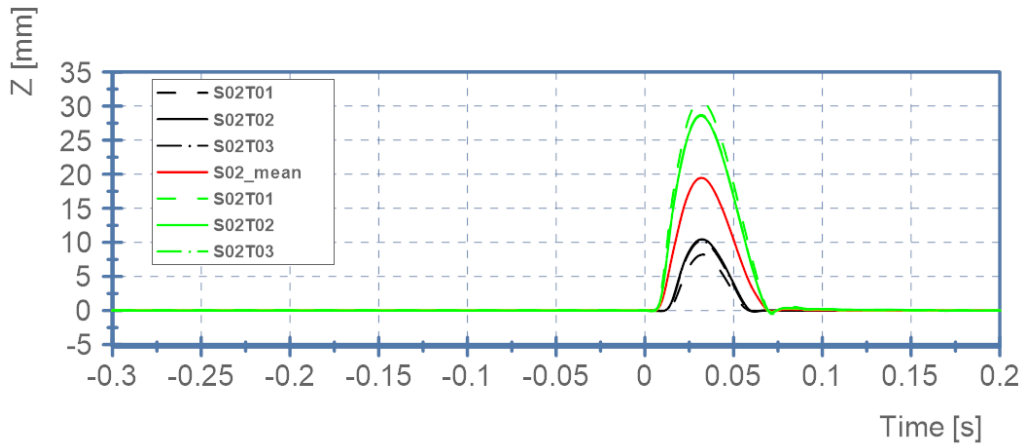

Figure 3- 25: S02: Seat compression diagram example, three attempts with mean curve

One possible reason for the deviation between the two potentiometer signals is a possibly not well hit target point. This could result from the manual release of the impactors, but also from a badly marked target point, not exactly in between the two potis.

In addition to the acceleration of the head impactor and the deflection of the seat foam, which was mainly used for the characterisation and validation of the seat foam material model, also the dynamic force response of the hexapod was analysed. Two exemplary configurations are described in the following:

The assumption is that the point between two potentiometers is not marked directly on the middle between two potentiometers. The second assumption is that the experiment setup also has leakages in settings.

The signals of the seat compression from the test are represented as follow. The compression signal from the potentiometer SP_R2_mi of the first attempt under the name S02T01 as black dotted-dashed curve, the compression signal from the potentiometer SP_R2_mi of the second attempt under the name S02T02 as black curve, the compression signal from the potentiometer SP_R2_mi of the third attempt under the name S02T03 black dashed curve, the compression signal from the potentiometer SP_R3_mi of the first attempt under the name S02T01 as green dotted-dashed curve, the compression signal from the potentiometer SP_R3_mi of the second attempt under the name S02T02 as green curve, the compression signal from the potentiometer SP_R3_mi of the third attempt under the name S02T03 as green dashed curve.

S01 - direct impact on poti: dynamic hexapod forces

The test configuration S01 was already described above. In the following figures 3-26 and 3-27 the curves of the resultant force results in the hexapod rods during the dynamic impact is shown. Each signal is named after the hexapod rod number on the test-rig and with different colour.

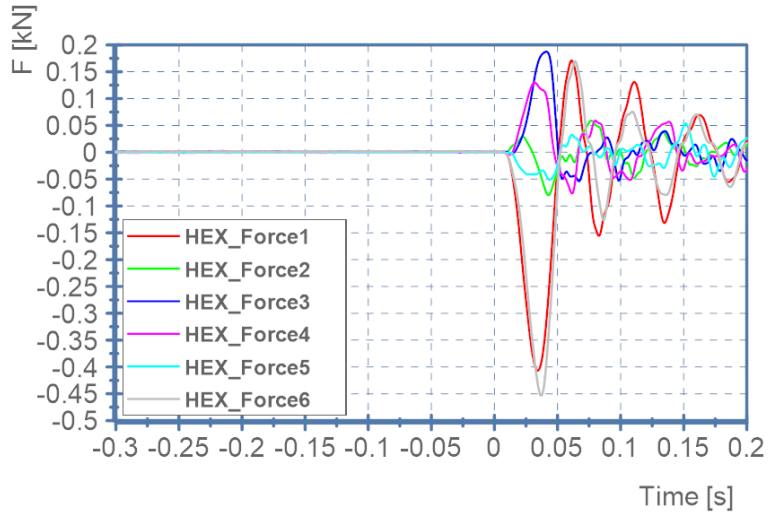

Figure 3- 26: S01: resultatnt forces on hexapod rods, child head impactor free fall, mean value

As can be seen above, and as already seen in the quasi-static seat load tests, the symmetric rods are in good correlation and giving the similar outputs. It is remarkable, that the magnitude of forces in the hexapod rods is comparable with the seat load test (centred), even though the mass of the impactor is only roughly 1/10 of the statically applied mass.

S05 - direct impact on poti, seatback: dynamic hexapod forces

Figure 3-27 shows the curves of the hexapod forces, that result from the free fall of the adult head impactor on the seatback right in between the potentiometers LP-R3-mi and LP-R4_mi.

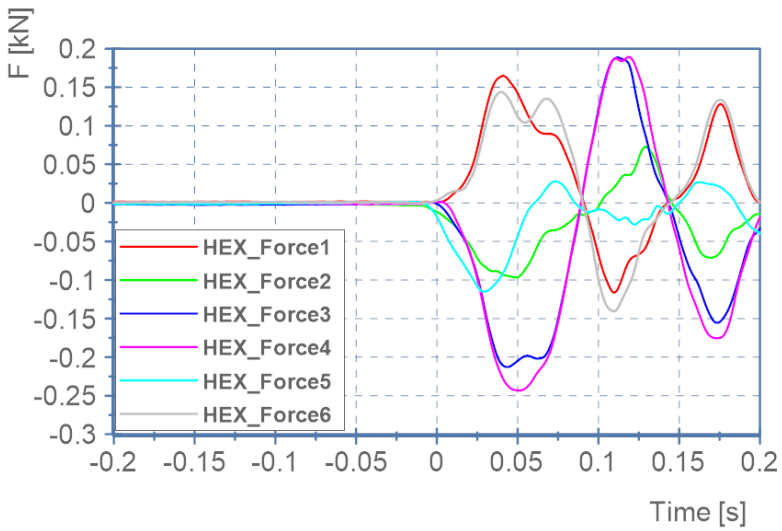

Figure 3- 27 S05: resultatnt forces on hexapod rods, adult head impactor free fall, mean value

From the results it can be seen, that the symmetric pairs of rods are giving similar outputs but during the impact. In comparison with the impact on the seat cushion, the oscillation following the initial impact shows higher amplitudes. In comparison to the results in figure 3-26, the outputs have the opposite direction, which is also in line with the quasi-static loading configuration with the ballast mass.

In table 3-1 the peak values of the acceleration of head impactors and the peak values of seat compressions in discrete locations are shown.

The child head impactor has an effective falling height of 194 mm compared to 44 mm for the adult head. Although the adult head impactor heavier than child the head impactor (see figure 2.6.2), the higher free fall distance and thereof resulting higher impact speed of the child head impactor causes more compression in the seat foam. This also causes higher acceleration values measured in the child head.

Table 3- 1: Table results – Head impact tests

Test	Test1	Test2	Test3	Test4	Test5
Name of the test	S01	S02	S03	S04	S05
Type of head impactor	Child	Child	Adult	Adult	Adult
Type of the teat	Seat	Seat	Seat	Seat	Back-Seat
Potentiometer	SP-R2_mi	SP-R2_mi <-> SP-R3_mi	SP-R2_mi	SP-R2_mi <-> SP-R3_mi	LP-R3_mi <-> LP-R4_mi
Height, mm	300	300	150	150	150
Effective Height, mm	194	194	44	44	44
Acceleration [m/s²]	118	120	38	36	37
Velocity [m/s]	0.46	0.47	0.19	0.18	0.18
Compression [mm]	32	19	22	12	12
Potential energy [J]	7	7	2	2	2

3.2 Simulation results

In this sub-section are represented selected simulations results are shown, beginning with the description of the steps done in the processing of the signals for analysis and concluding with the comparison with respective test data.

3.2.1 Simulation results with quasi-static loading condition – seat load test

In following sub-section the results of the simulations of ballasting the seat cushion and seatback with the steel plate on different positions is shown.

In order to compare the results with corresponding test data, some signal processing had to be carried out, which is described in the following:

The results of the experiments with the ballast plate is the delta value for resultant forces on the hexapod rods, considering the forces at the net weight of the test rig alone and the total forces, when the ballast plate is positioned on the seat.

To mimic this step in the analysis of the simulation results the output data of run without the ballast plate (see figure 3-30) has to be subtracted from the corresponding data of a simulation including the ballast plate (see figure 3-28).

In the following figures, each represents the simulation result of the resultant force of one hexapod rod. Each curve is named according to the respective hexapod rod and is shown in diagrams in different colours.

Figure 3-28 shows the simulation results without the ballast.

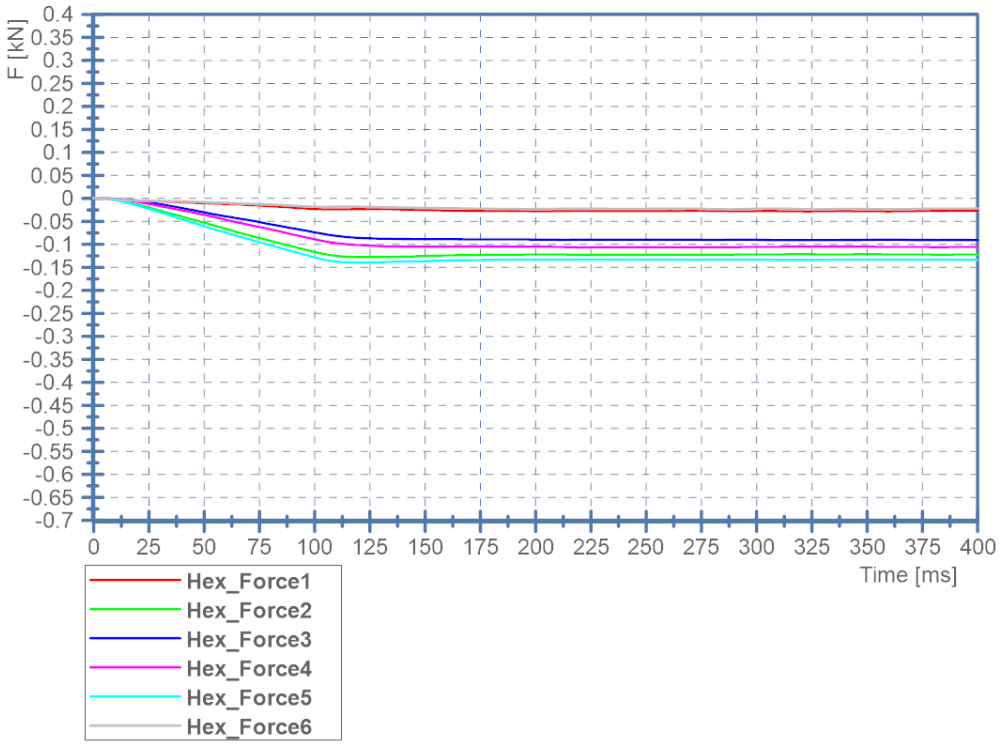

Figure 3-28: Simulation without the ballast plate

The simulation without ballasting plate (see figure 3-28) shows that signals, which should theoretically be the same, are in good correlation. Rods in symmetric relation are front hexapod rods 1 and 6, middle hexapod rods 2 and 5, and rear hexapod rods 3 and 4. In the signal, the defined ramping of the gravity in the first 100ms (see chapter 2.6.1) can be seen clearly.

The simulation of placing the ballast plate on the seat (see figure 3-29) – in this example centred on the seat cushion – shows that signals, which should theoretically be the same, are in good correlation. Moreover it can be seen, that the mass of the ballast has a significant influence on the resulting hexapod force levels.

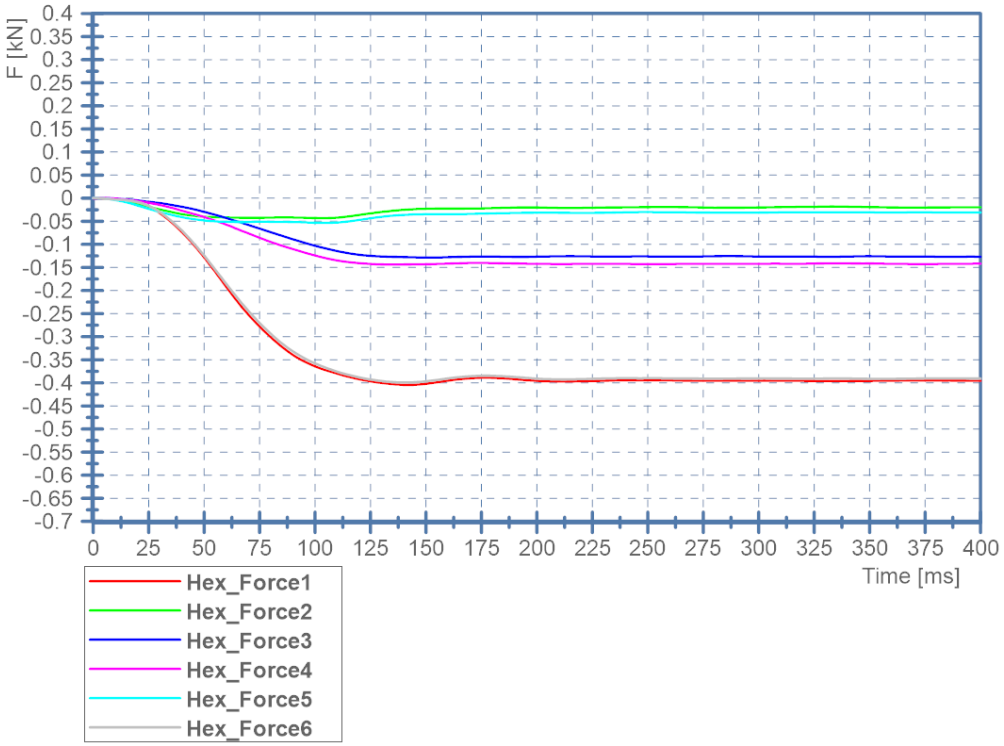

Figure 3-29: Simulation of the ballast plate in symmetrical position on the seat foam

Finally, by subtracting the respective curves, the net forces, resulting by the ballast mass only are derived, as shown in figure 3-30 for Test 1.

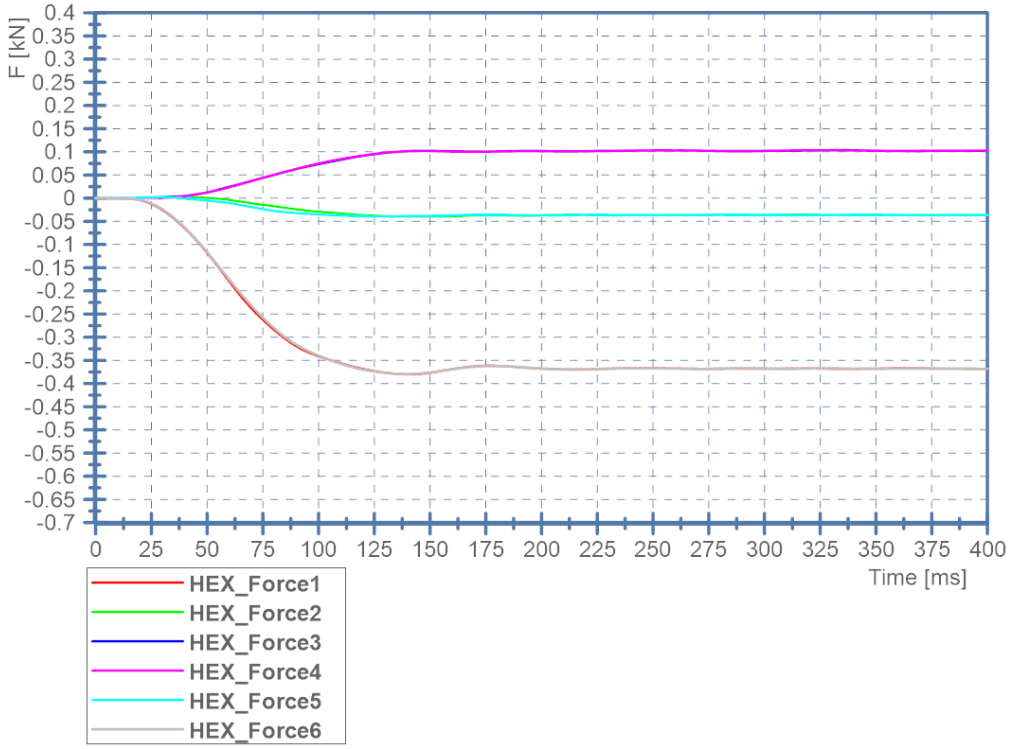

Figure 3-30: Test 1, symmetrical ballast, plate on the middle of the seat foam

These curves can later be used for comparing the simulation results with the experiments done.

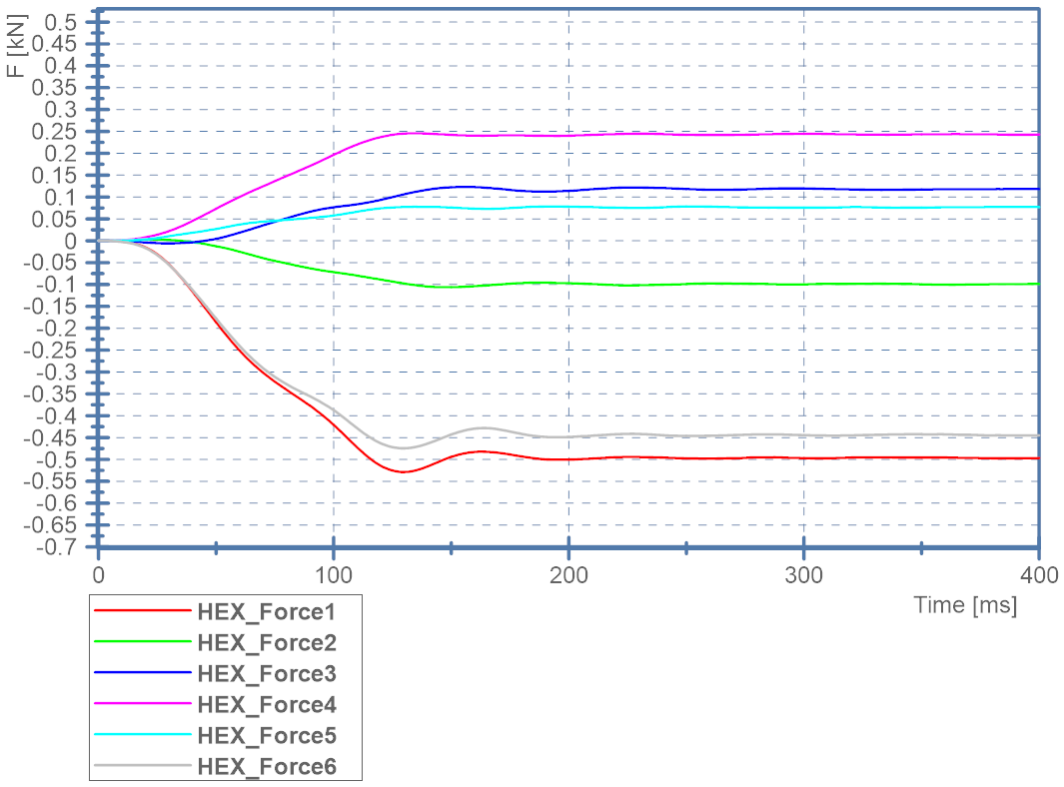

Figure 3-31: Test 4, symmetrical ballast, plate on the middle of the back seat foam

The simulation time of 400ms is shorter than the duration of an experiment of 45sec, therefore the offset correction of the simulation time channel was required for comparison of the simulations and experiment results.

In following figures, the curves of the simulation signals are represented with the full line and the respective signals from the experiment are represented as dot lines with the same colour. Each curve in diagrams are representing one signal of resultant force of one hexapod rod. Each curve is named after the hexapod rod and is named accordingly. For example, the signal for the resultant force on the hexapod 1 is named HEX_Force1, coloured in red and the solid line when refers to the simulation results, whereas the dot line when refers to the experimental data.

In the figure 3-32 and 3-33 the numerical and experimental results for the forces from Test 1 and Test 4 respectively, are compared.

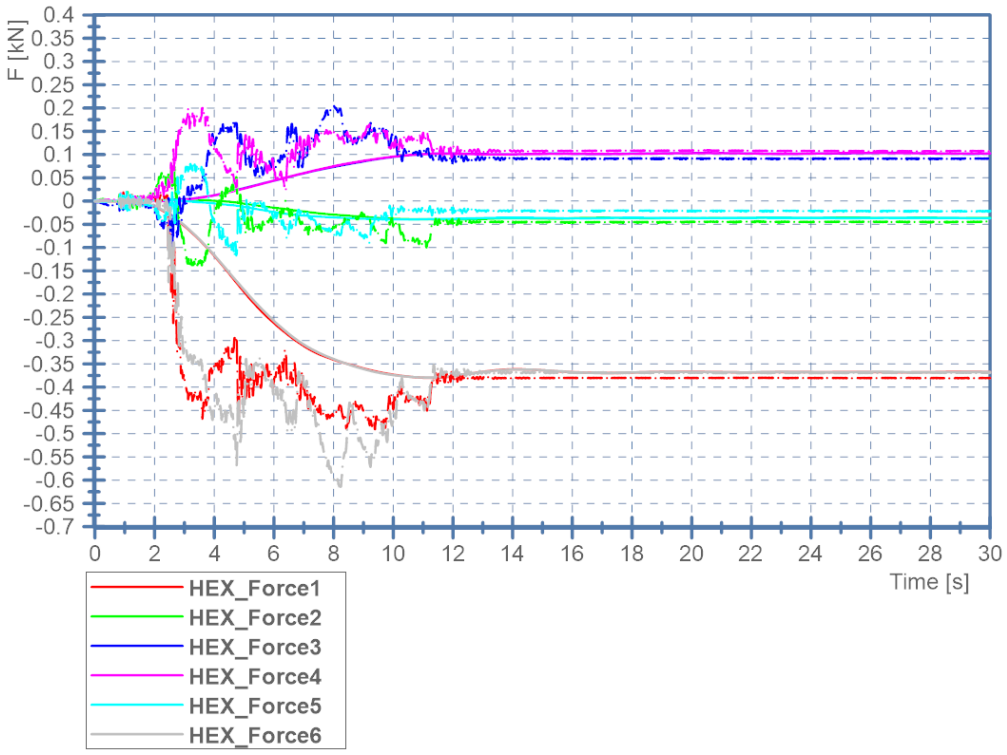

Figure 3-32: Test 1, ballast on the middle of the seat, symmetricity test

As the results shows, hexapod forces in the FE model are more symmetrical than the data from testbed. There are only minor deviations between simulation results and experiment results.

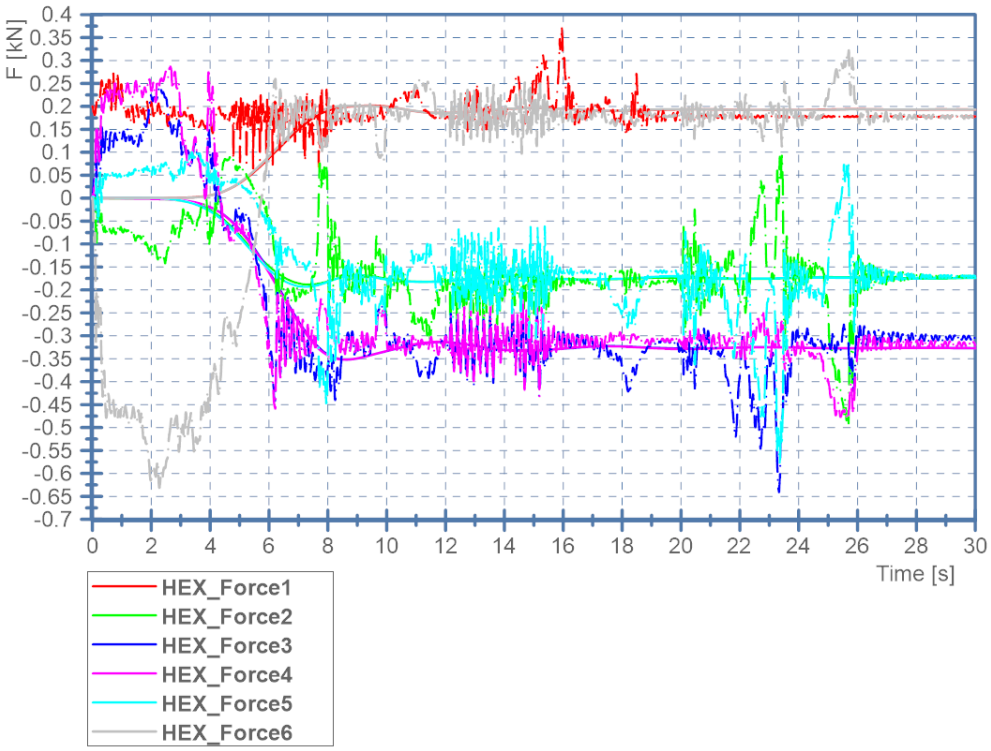

Figure 3- 33: Test 4, ballast on the middle of the backseat, symmetricity test

Same as for Test 1, the results from the experiments and the corresponding simulation is in very good agreement.

Following example diagrams are results of simulation model of Test 2 (figure 3-34), Test 3 (figure 3-35) and Test 5 (figure 3-36). In those three tests, the asymmetrical ballast on the seat has purpose to validate the FE model simulation.

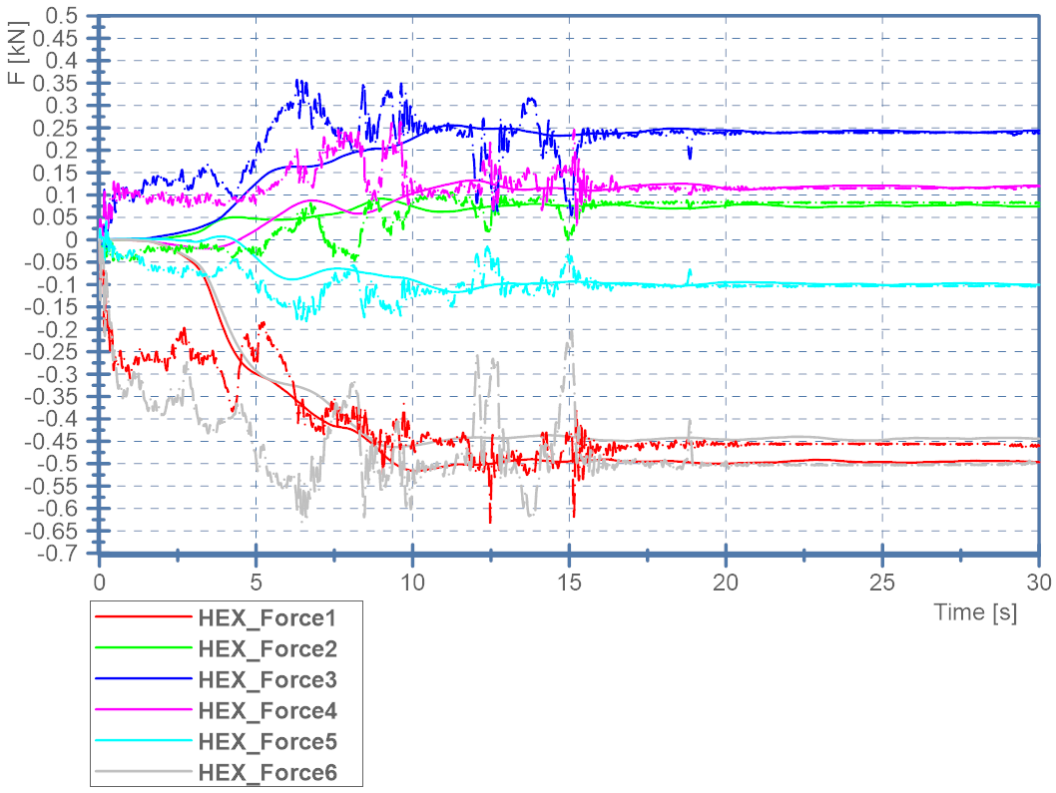

Figure 3-34: Test 2, ballast on the front left of the seat

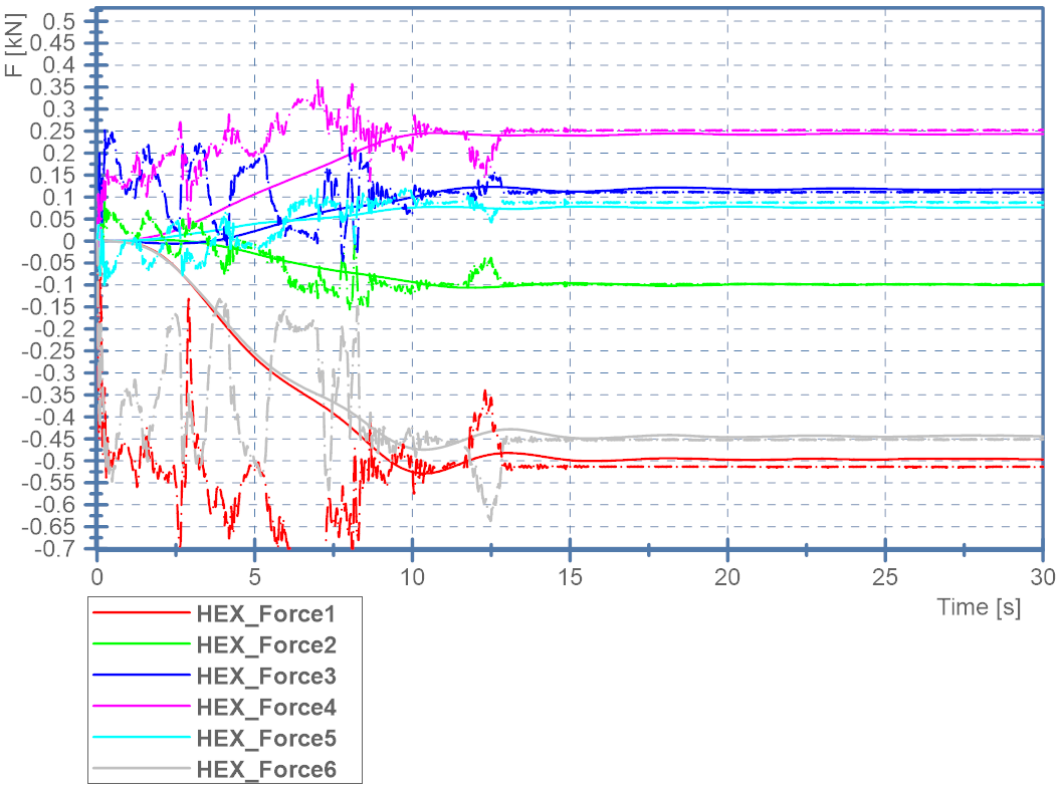

Figure 3-35: Test 3, ballast on the front right of the seat

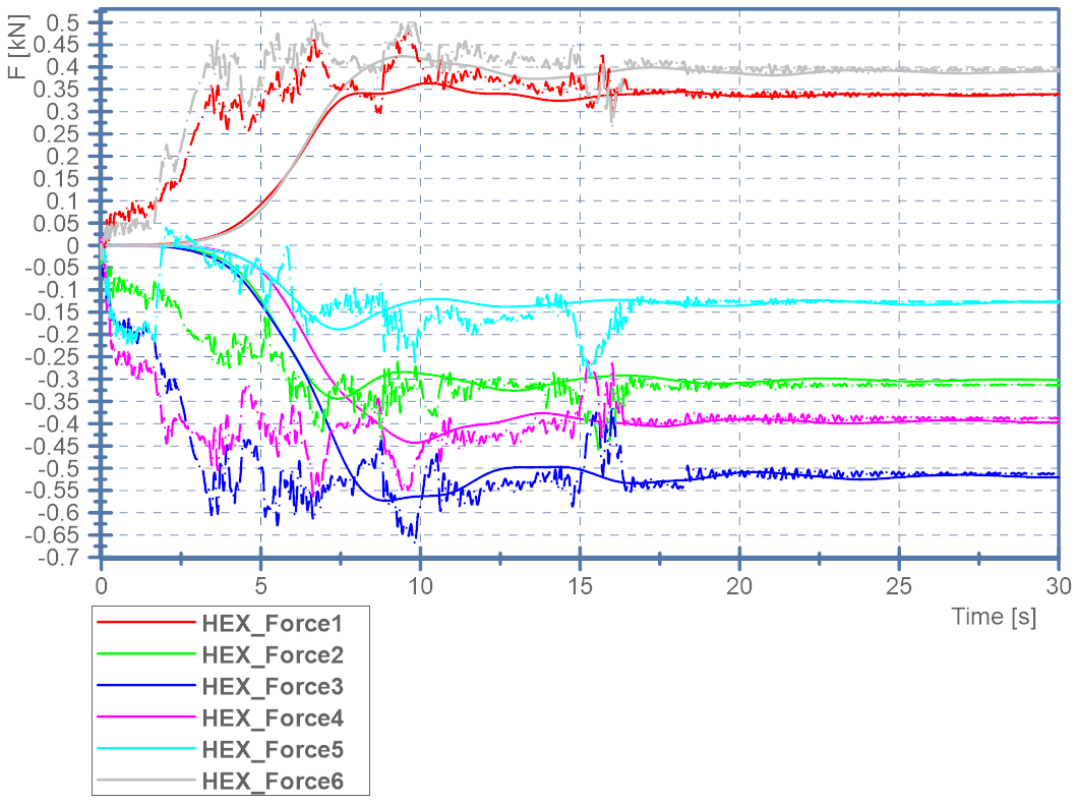

Figure 3-36: Test 5, ballast on the back right of the back seat

For any of the tested quasi-static loading configurations a very good correlation between the model output and the experimental data can be stated.

3.2.2 Simulation results with dynamic loading condition – head fall test

In following sub-section selected simulation results of the freefall of the head impactors on the seat foam and seatback foam are represented. Same as for the quasi-static simulation results, the goal is the validation of the simulation signals with the experiment data. To enable this comparison, some signal processing steps were done first

First step was to scale the simulation signals, as signals and metrics of this experiment are seat compression [mm], velocity [m/s], and acceleration [m/s²] of head impactors.

The time channel was scaled with 0.001 to convert the time unit of simulation from milliseconds into seconds. In addition the signals of acceleration, velocity and the compression of the seat foam needed to be inverted to match with the test data.

The time channel was offset to be the value of zero seconds at the point where the acceleration starts to increase in a positive direction which is at the time, where the head impactor first impacts the seat foam (see figure 3-37).

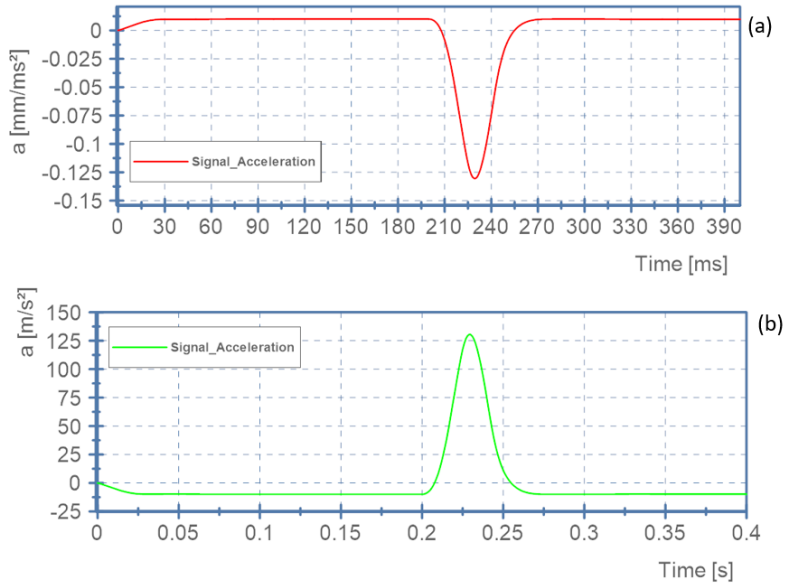

Figure 3- 37: Example of acceleration output data, simulation (a) original (b) scaled and offset

Subsequent to the analysis of the acceleration of the head impactor and the deformation of the seat foam, also the dynamic hexapod forces, resulting from the impact, are analysed. Also for this data, some processing needs to be done in order to enable a proper comparison:

In the figure 3-39 the diagram with the resultant forces on hexapod rods during the dynamic impact is shown. The actual area of interest in the shown diagram is the peak after approx. 200ms. Prior to that, the impact of the ramping gravity function and the settling of the forces to the static equilibrium are seen. In addition, the shown signals are not corrected with the time offset and the simulation time unit is still Milliseconds.

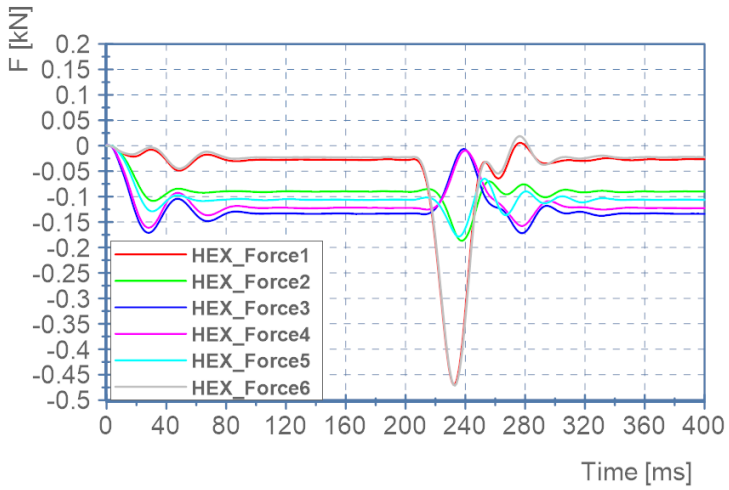

Figure 3- 38: Diagram with the simulation results, Test 1, head impactor child, resultant force on hexapod rods

Figure 3-39 is shows the diagram with the corrected signals regarding the force offset in order to of the hexapod rod in to enable the analysis of the delta forces caused by the dynamic impact of the head impactor.

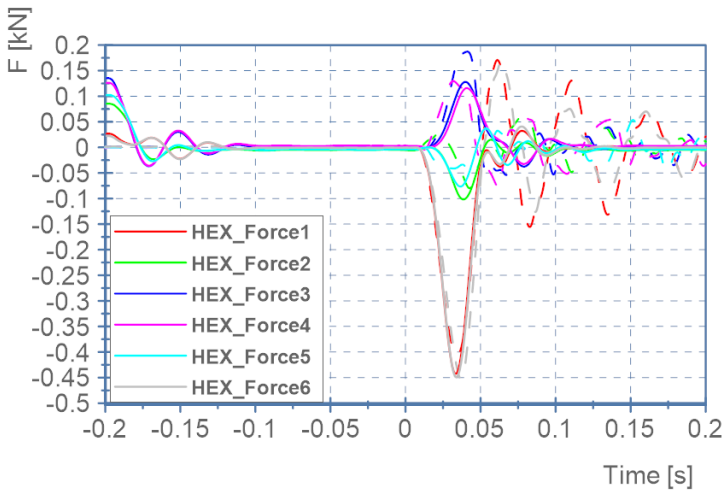

Figure 3-39: Diagram with the simulation results, Test 1, head impactor child, resultant force on hexapod rods

The main parameter for the creation of the FE model of the seat foam and seat back was the definition of the relation between stress and strain in material properties (see subsection 2.6.2). As the experiment proceeded with two types of head impactors, adult and child, the simulation also proceeded with two FE model types of head impactors.

As mentioned in section 2.2 the material model of the seat foam was carried over from another simulation model and by scaling the material properties, hereby in particular the stress vs. volumetric strain relation of the material, the results from simulation and test were aligned.

The approach followed was to vary the scaling of this relation for both setups (child head: lower mass, high impact velocity vs. adult head: higher mass, low impact velocity) and to identify a value that leads to an acceptable correlation on both. In this variation only the stress values were scaled, the strain values were not adjusted.

The following table gives an overview of the colour coding of the single variants in the figures below:

Table 3- 2: definition of signals in diagram in figure 3-39 and 3-40

Signal name	Stress Coefficient Value	colour
S03_SIM1	6.5	Red
S03_SIM2	7.0	Light green
S03_SIM3	7.3	Blue
S03_SIM4	8.0	Rosa
S03_SIM5	6.8	Black
S03_mean	/ (mean value, experiment)	Dark green

In the figure 3-40 the diagram with seat compression signals with different stress coefficients in stress-strain curve, from 6.5 to 8.0, for the simulation of Test 1, the child head impactor on the seat foam above the potentiometer SP-R2_mi is shown. A clear linear trends can be observed – increased stiffness of the foam leads to a reduction of the seat-foam deformation, which is as expected. The diagram shows that the correlation of test and simulation is best for a stress coefficient is 6.8.

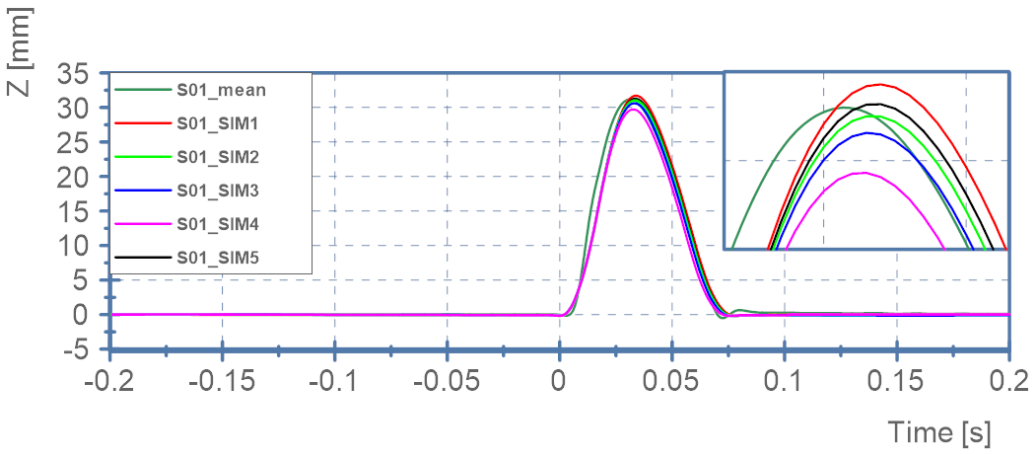

Figure 3- 40: Diagram Seat Compression, Test 1, example of mid value curve determination

The diagram in figure 3-41 shows the results of the simulations of Test 3, the freefall of the adult head impactor adult on the seat foam above the potentiometer SP-R2_mi.

Also here, any increasing the scaling factor for coefficient the stress, the seat compression stiffness increases, and the curve of the compression signal decreases. For a scaling factor of 7.3, the compression signal is nearest to the mean curve of the compression signal.

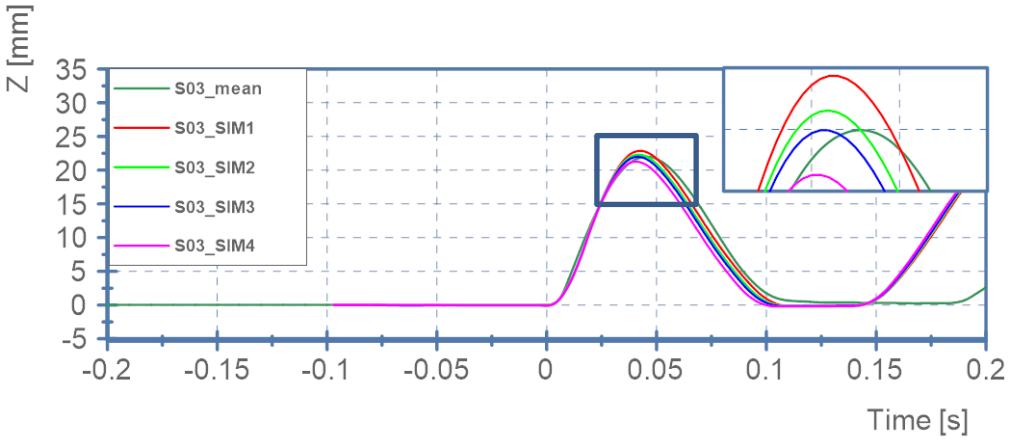

Figure 3-41: Diagram Seat Compression, Test 3, example of mid value curve determination

In summary, the scaling factors for the stress values of the seat foam stress-strain curve, that lead to the best correlation are 6.8 for the test with the child impactor, and 7.3 for the case with the adult head impactor. However, as for both tests the material is the, same also in the simulation model one common value has to be found. It was concluded, that the scaling factor of 7.0 is a good compromise for both configurations. Based on this, all further simulations were run with this setting and all results shown in the following are based on that seeing.

3.2.2.1 Head Fall Test with head impactor child

In this subsection, the simulation of the freefall of the child head impactor are shown. In the figures 3-42, 3-43 and 3-44 the output data for the case when the head impactor child falls on the point on the seat above the potentiometer SP-R2_mi. The mean curve of the three test repetitions in the experiment is represented as red curve S01_mean, and the respective simulation output is represented as blue curve with the name S01_SIM.

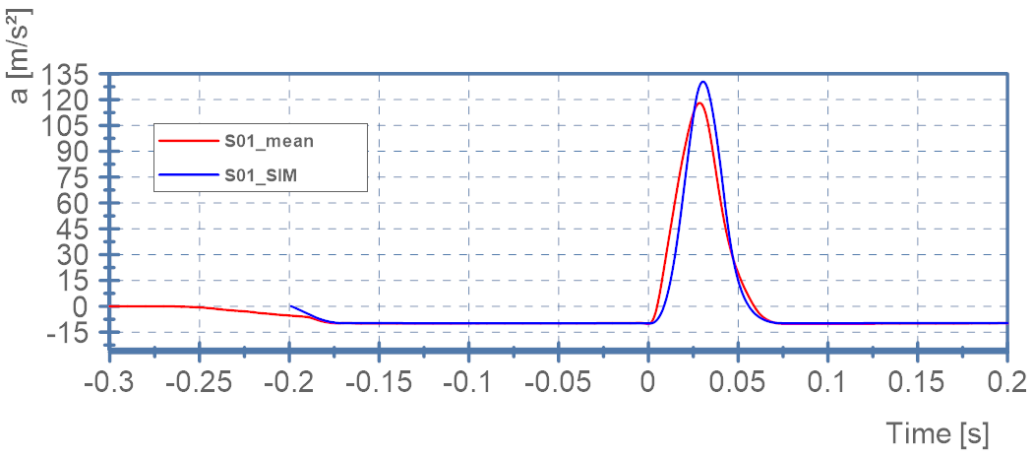

Figure 3- 42: Test 1, Head impactor Acceleration

Figure 3-42 shows the diagram with an output of the acceleration signal in comparison with the mean curve of the tests.

When the impactor is released, the mean curve signal and simulation signal reached values of approximately 9.81 m/s². In the impact on the seat foam, the curves are reaching different peak values, whereby the simulation signal is higher than the mean value signal.

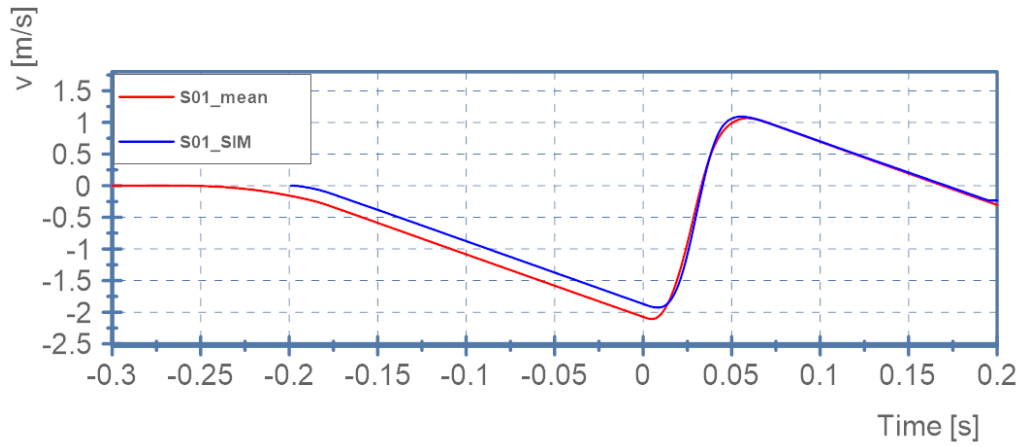

Figure 3- 43: Test 1, Head Impactor Velocity

In the velocity time chart in the figure above it can be observed that the initial release of the impactor is differing between test and simulation resulting in a slightly different impact speed.

Figure 3-44 shows the diagram with an output of the seat compression signal in comparison with the mean curve of the tests. Small deviations are apparent at the initial engagement of the foam. In general a very good match between the simulation and test results can be seen in this configuration.

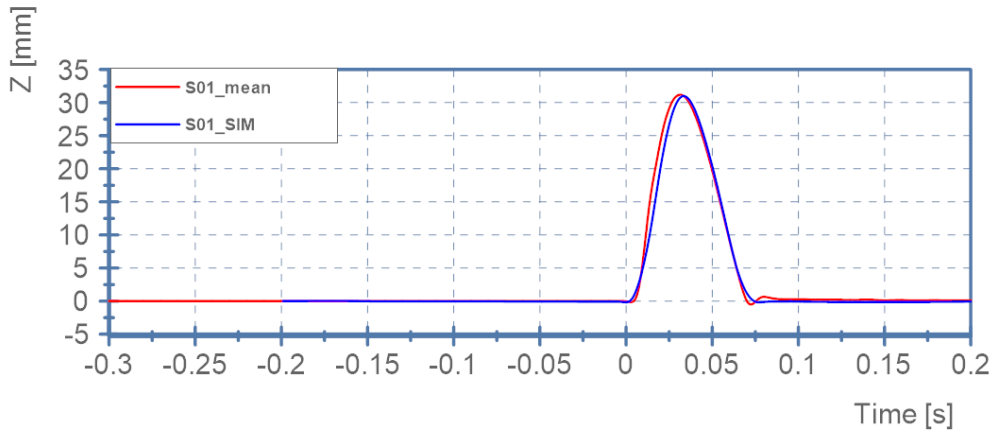

Figure 3- 44: Test 1, Seat compression

The figures 3-45, 3-46 and 3-47 are showing the diagrams with the output data for the Test 2, where the child head impactor is dropped right in between the potentiometers SP-R2_mi and SP-R3_mi approximately in the centre of the seat cushion.

The mean curve from the three experiments is represented as red curve S02_mean, and the simulation result is represented as blue curve with the name S02_SIM.

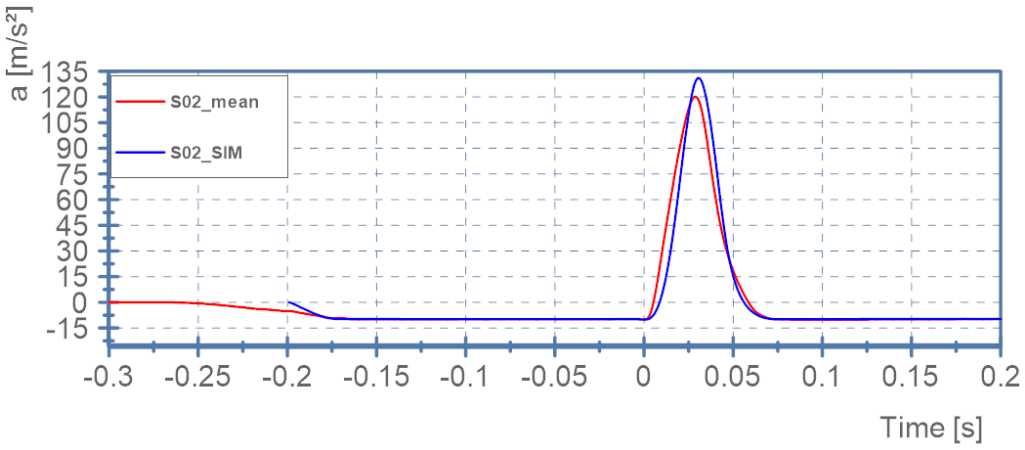

Figure 3- 45 : Test 2, acceleration

Figure 3-45 shows the diagram with an output of the acceleration signal in comparison with the mean signal.

Figure 3-46 shows the diagram with an output of the velocity signal in comparison with the mean signal.

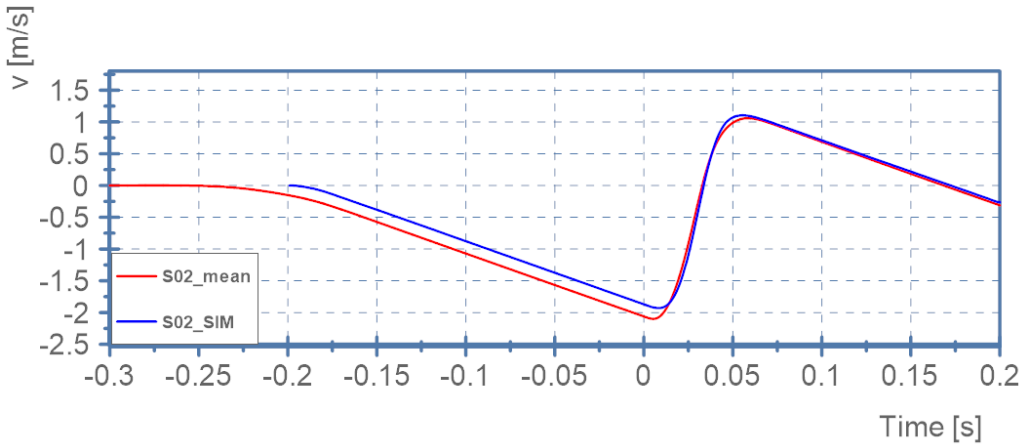

Figure 3-46: Test 2, velocity

Finally, figure 3-47 shows the diagram with an output of the compression signal in comparison with the mean value signal.

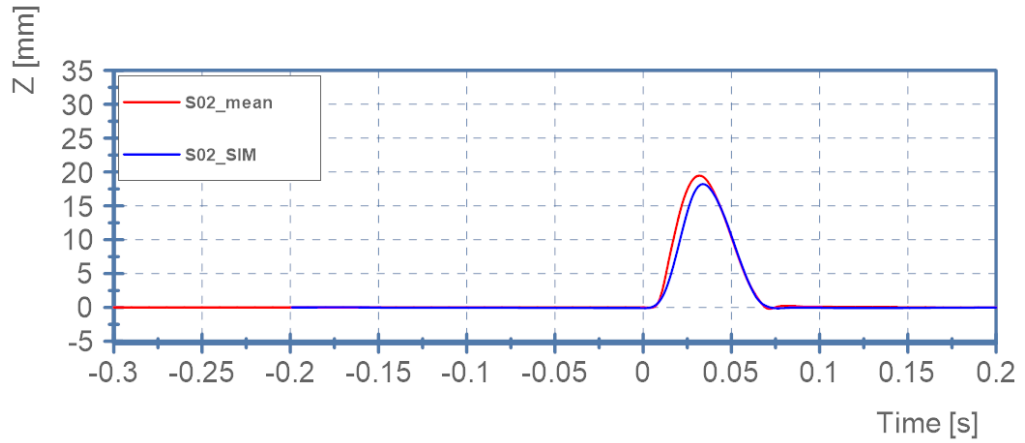

Figure 3-47: Test 2, seat compression

As for the configuration, where the impactor is dropped directly onto the potentiometer, also in this case a very good correlation is achieved. The simulation output matches well with the mean curve of the tests, even though there was a significant difference in the signals of the two potis, resulting from a bad alignment of the head during the tests.

In addition to the analysis of the acceleration in the head impactor and the compression of the seat foam, also the dynamic response of the hexapod forces was analysed. In figure 3-48, the diagram with the resultant forces on hexapod rods during the head impact onto the seat cushion (Test 1) is shown for test (here only results of a single test: S01T01) and simulation.

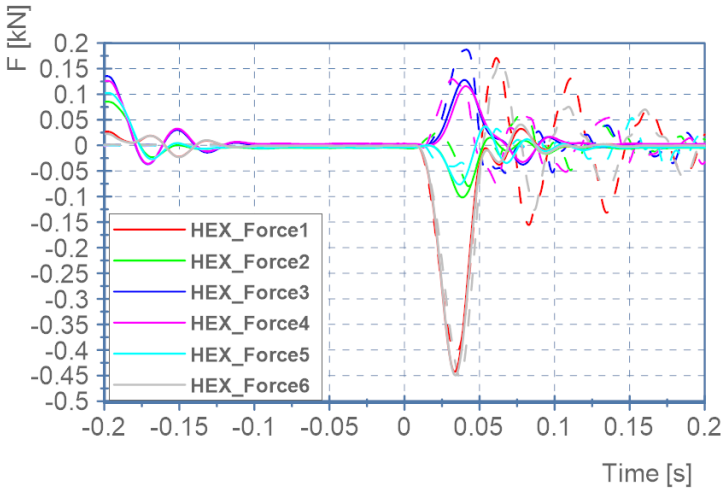

Figure 3- 48: Diagram with the experiment and simulation results, Test1, head impactor child, resultant force on hexapod rods

As can be seen, the simulation signals from front rods (HEX_Force1 and HEX_Force6), are in good corellation with the tests signals, where the mid rods (HEX_Force2 and HEX_Force5) have the approximately peak values but not the same time in comparison to the tests results. The rear rods (HEX_Force3 and HEX_Force4) are differing slightly, however also the test results are showing bigger deviations between the left and rear side.

The biggest discrepancy between the test and simulation data is actually the low frequency oscillation subsequent to the impact. In the test, a significant oscillation is present, whereas this effect can hardly be identified in the simulation result.

3.2.3 Head fall test with the head impactor adult

In this subsection selected examples of results of the FE model simulations of freefall with the adult head impactor are presented. In impact tests with the adult head were carried out at three different target points: In configuration S03, the impactor was dropped on the seat right ontop of potentiometer SP-R2_mi, in configuration S04, the impactor was dropped on the point on the seat between two potentiometers SP-R2_mi and SP-R3_mi, in the third configuration S05 the impactor was dropped on seatback between the two potentiometers LP-R3_mi and LP-R4_mi. The results for S03 and S05 are shown in the following. The data for S04 is added in the appendix.

In the following again only data that was achieved with a scaling factor of 7.0 for the stress characteristic of the seat foam is shown. The mean curve of three repetitions is represented as red curve S03_mean, and the simulation output is represented as blue curve with the name S03_SIM.

Figure 3-49 shows the diagram with an output of the acceleration signal in comparison with the mean curve from the experiments.

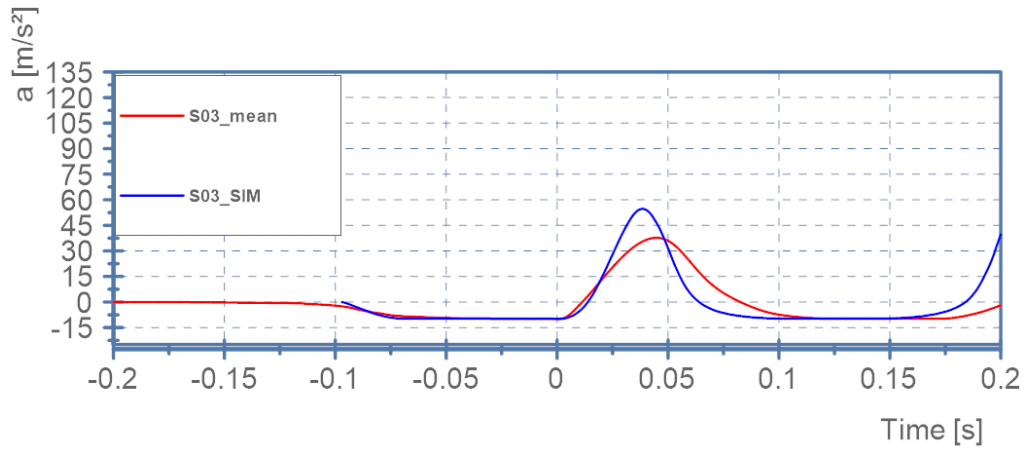

Figure 3-49: Test 3, Head Impactor Adult acceleration

The acceleration curve indicates a too stiff behaviour of the foam, resulting in a higher peak value compared with the test data.

Figure 3-50 shows the diagram with an output of the velocity signal in comparison with the mean value signal.

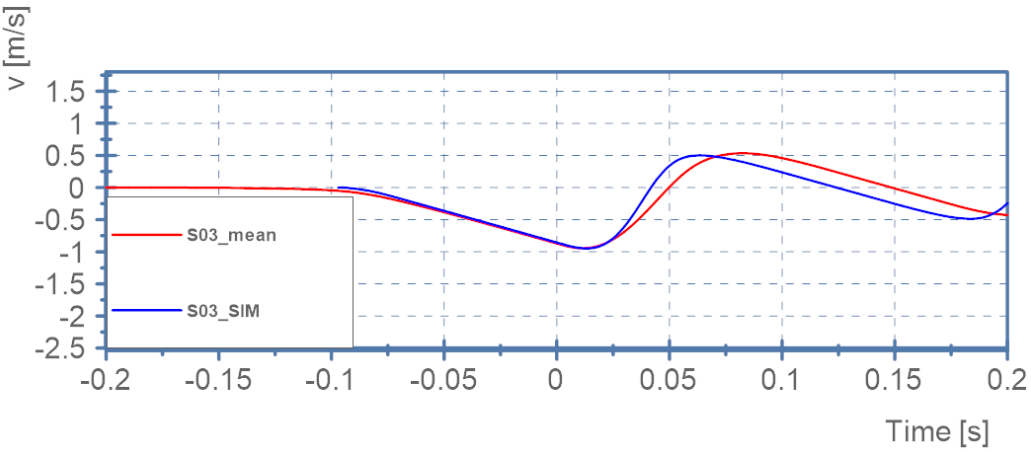

Figure 3-50: Test 3, Head Impactor Adult (a) velocity

During the freefall phase no relevant discrepancies are seen, between test and simulation resulting in a well matching impact speed. Figure 3-51 shows the diagram with output data of seat compression.

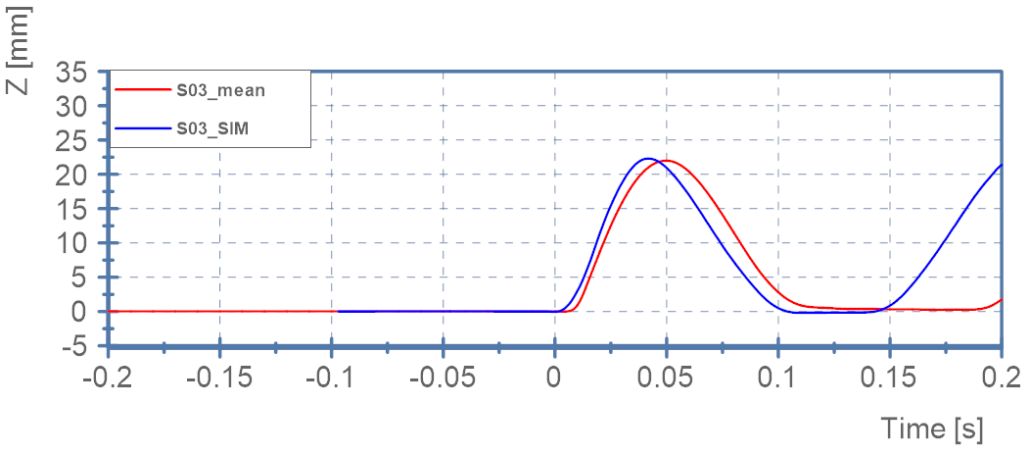

Figure 3-51: Test 3, Diagram, seat compression

Although the curves of the foam compression (see figure 3-51) are matching very closely and impactor speed (see figure 3-50) is the same for simulation and test, the acceleration (see figure 3-49) curve has some noticeable deviations. This could again indicate an induced rotation of the impactor in the course of the seat foam compression.

The figures 3-52, 3-53 and 3-54 are showing the diagrams with output data from the configuration S05, in which the adult head impactor was dropped on the centre of the back seat between the potentiometers LP-R4_mi and LP-R3_mi. The mean curve of the three repetitions in the experiment is represented as red curve S05_mean, the simulation data is represented as blue curve with the name S05_SIM.

Figure 3-52 shows the diagram with the acceleration signal in comparison with the mean curve of the tests.

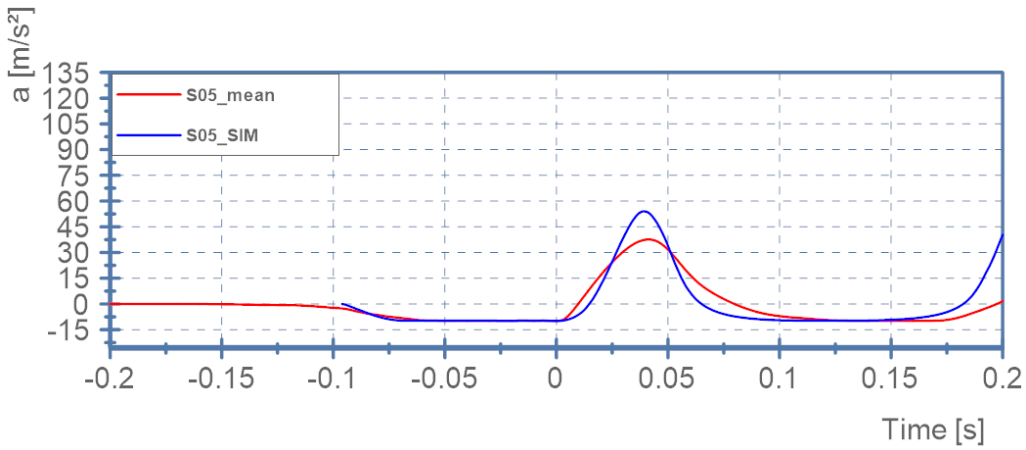

Figure 3-52: Test 5, Head Impactor Adult acceleration

It can be seen, that the peak acceleration of the adult head impactor as result of the simulation is exceeding the corresponding test result. In figure 3-53, the diagram with the velocity signal is shown in comparison with the test data.

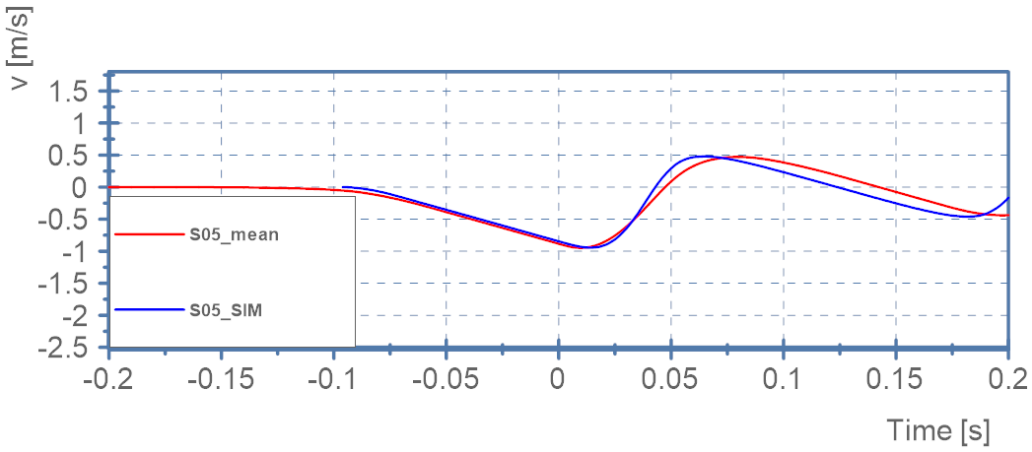

Figure 3- 53: Test 5, Head Impactor Adult velocity

Figure 3-54 shows the diagram with the output of the compression of the seat foam.

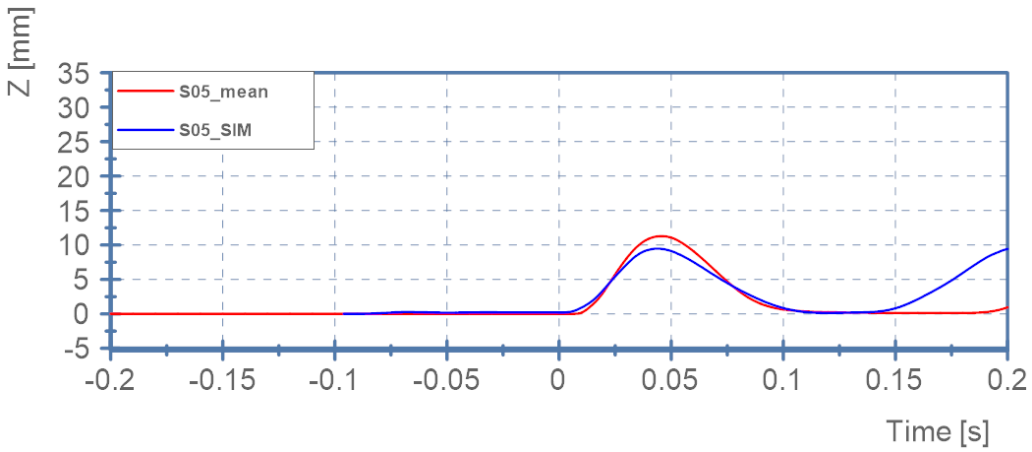

Figure 3- 54: Test 5, Seat compression

It can be observed, that the model underpredicts the compression of the seat foam, which is also in line with the too high accelerations. Apparently the foam model, that was tuned based on the deflection of the seat foam is not fully capable of predicting lower energy impacts in the same correlation.

In figure 3-55, the diagram with the resultant forces on hexapod rods during the from the impact of the adult head impactor is shown. The comparison of test and simulation results allows the

assesment of the correlation of the simulation results with the test data for the dynamic loading conditions.

As can be seen, the simulation signals, are in good corellation with the tests signals, in particular the initial onset and the peatk value of the force. As already seen at the results of the child head impact on the seat cushion, the dynamic behavior of the signals after the actual loading is differing significantly.

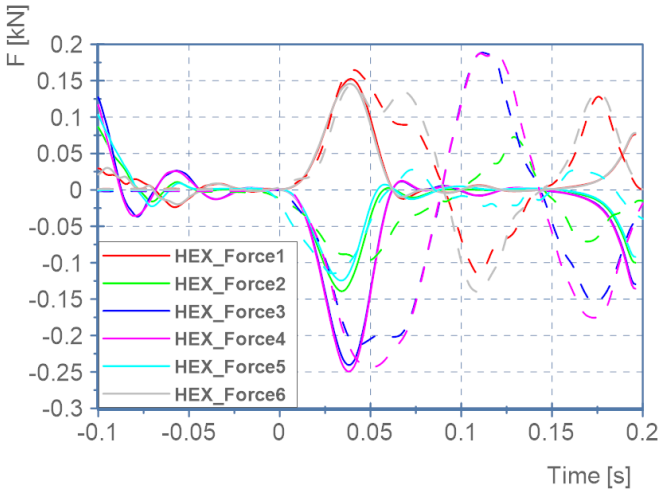

Figure 3-55: Diagram with the experiment and simulation results, Test 5, head impactor adult, resultant force on hexapod rods

Thereby particularly the front rods (HEX_Force1 and HEX_Force6) and rear rods (HEX_Force3 and HEX_Force4) show big oscillations, that are not present in the simulation data.

3.2.4 Results of the implementation of the HBM with the LowG Sled

In this subsection the result of the simulation with the implemented HBM on the FE model of the sled testbed is shown. The result is represented as sequence of pictures that display the kinematic of the testbed and the HBM. The goal was to verify, that the simulation model of the testbed is running stable with the THUMS v4 (passive) and v6 (active muscles) for the time required.

Figure 3-56 shows the start of the simulation, where the HBMs are positioned 1mm above the seat.

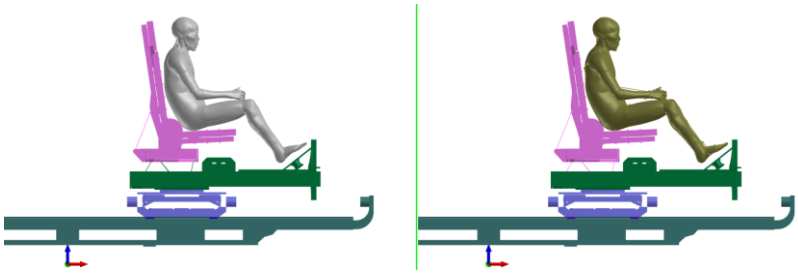

Figure 3-56: t=0.0 s; left: THUMS V4; right THUMS V6

Figure 3-57 shows the simulation at the 0.2 s, when the HBM falls on the seat because of the gravity. At that time, the z-motion of all nodes of the model (HBM + test bed) are set to zero to simulate a quasi-static equilibrium prior to the loading and subsequently the translation of the sled in the horizontal direction starts backwards (left) by accelerating the Y-sled with the seat assembly, the pedal assembly and the HBM.

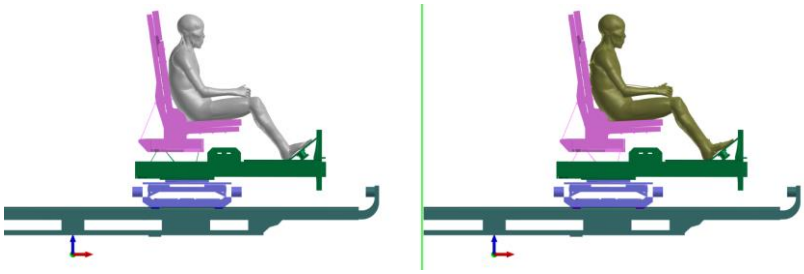

Figure 3-57: t=0.2 s; left: THUMS V4; right THUMS V6

Figure 3-58 displays the posture of the HBMs at approximately 0.8 and 0.9 s after start. At that time, the braking of the sled starts and the HBM reaches the maximum forward displacement. At this point a significant difference in the posture of the HBM can be seen.

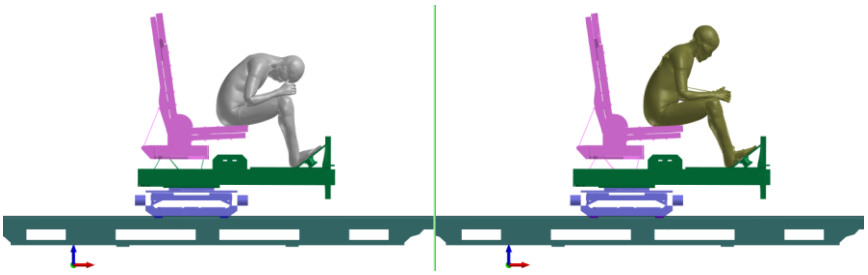

Figure 3-58: t=0.8 s; left: THUMS V4; right THUMS V6

The figure 3-59 displays a frame of the motion 1.2 s after start. The HBM is impacting the back seat and starts to compress the foam.

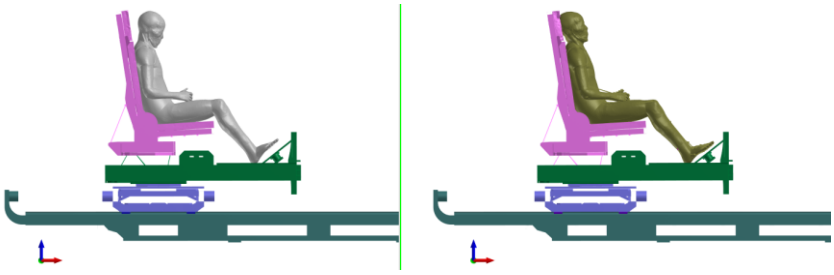

Figure 3- 59: t=1.2 s; left: THUMS V4; right THUMS V6

Based on this investigation it could be approved, that the developed simulation model of the LowG testbed is running numerically stable for the needed simulation time and is compatible with two exemplarily chosen HBMs.

4 DISCUSSION

The This chapter contains an the interpretation of simulation results, the analysis of the validity of the simulation models in the analysed load cases , as well a description of the limitations of the of the model.

4.1 Validation of model response in quasi-static loading condition – seat load tests

As shown in chapter 3.2.1, the simulation results are in good correlation with the corresponding test data. Moreover that plausibility of the test data as well as the model response could be approved based on the symmetric load cases.

However, the validation in quasi-static loading condition was performed in only one seat configuration. As the sled test-rig has possibility of multiple configuration cases (rotation about z-axis, different settings for seat back and seat angle, …), further experiments and simulations for model validation seen to be necessary.

The second limitation is the validation of the response to a loading with only one loading direction and loading type. Therefore, by using the gravity as the only load, stiffness of testbed in longitudinal or lateral direction could not assessed. Such tests and corresponding simulations are considered to be necessary.

The third limitation is the general output. This data is currently represented through the resultant axial forces of six hexapod rods. The transformation of these metrics into global forces and moments seems to be a useful next step to analyse the interaction of volunteers and the seat.

4.2 Validation of model response in dynamic loading condition – head fall test

The general finding of the FE model validation based on dynamic loading is a good correlation of the simulation with the experiment in following cases:

- with test data for head impactor acceleration
- with test data for dynamic forces
- with test data for seat foam compression

However, a relevant difference in the model response after the actual loading could be identified. The latter needs to be addressed by varying damping properties within the model. In the simulation model, a comparably high scaling factor of available foam model was necessary to achieve a proper correlation – and “ideal” scaling factors were determined to be different for child and adult head impactor. According to that, eventually a detailed foam characterisation would be better and improve remaining discrepancies between test and simulation.

5 CONCLUSION

The main goal of this work was to develop a detailed FE-model of the LowG testbed in order to be used in combination with numerical HBMs such as example the THUMS.

The implementation of the HBM in the simulation model with the FE model of the LowG was accomplished. The basis for further researches is the simulation model of the testbed with THUMS v6 runs stable for the required duration what will enable to investigate if the simplified version of the testbed would be sufficient.

The developed model was verified against a range of quality criteria and plausibility checks and the model response to defined loading conditions was approved in comparison with experimental data. The validation process was successfully accomplished with an open space for further improvements.

Following additional steps are proposed as follow up, to further improve the quality of the experiments, which are the base for the model validation as well as the quality of the model itself:

- Installing the stable frame for the experiment-setup with the head impactor to have identical start conditions (e.g. same height, position, straight movement in Z-direction) at the release of the impactor at each attempt
- Installing an additional measurement system on the seat and seat backrest to measure of the observed seat oscillations during the impact of the head impactor or for further experiments with dynamic impacts. Therefore, the FE model should also have the possibility to measure those oscillations.
- Selected parts are not fulfilling the quality criteria that were aimed for, which is degrading the quality of the results as well as the calculation time. It can be considered to replace single parts, with particularly high share of elements, not meeting the criteria. One possible idea could be a further simplification of parts with complex geometry.
- The simplified representation of the Item profile with the shell beams is considered to be as possibly too much simplified, as relevant effects as the stiffness of the sidewall of the profile are not captured. Likely an alternative approach for representing these structures could improve the model quality

The main motivation for the creation of this detailed model was the analysis of the impact of the test-rig deformation onto the kinematics of the occupant. The described model, considering the further recommended updates, is considered to be a proper, viable tool for addressing the above mentioned task.

6 REFERENCES

[1]C. Klug, E. Tomasch, Script Trauma Biomechanics, 2021

[2]Toyota Motor Corporation, Document TOTAL HUMAN MODEL FOR SAFETY (THUMS): REVOLUTIONIZING CRASH SIMULATION TO SUPPORT SAFE MOBILITY FOR ALL, 2021, 4

[3]Humanetics, Post ATD, https://www.humaneticsgroup.com/products/anthropomorphic-test-devices

[4]Kirchberger, Roland, Script Survey of CaX methods, 2021

[5]S. Ejima, Y. Zama, F. Satou, S. Holcombe, K. Ono, K. Kaneoka and I. Shiina, Prediction of the Physical Motion of the Human Body based on Muscle Activity during Pre-Impact Braking, *IRCOBI conference*, 2008, 13, Bernd, Switzerland

[6]D. Kato, Y. Nakahira, N. Atsumi, M. Iwamoto, Development of Human-Body Model THUMS Version 6 containing Muscle Controllers and Application to Injury Analysis in Frontal Collision after Brake Deceleration, *IRCOBI conference*, 2018, 17, Bernd, Switzerland

[7]N. Erlinger, D. Kofler, E. Heider, C. Klug, Effects of Boundary Conditions and Posture on Simulations with Human Body Models of Braking Events, *Proceedings of IRCOBI conference*, 2022, 25

[8]Resensys, Document Finite Element Method (FEM) Model Verification and Validation for Bridges, Buildings and other Structures, https://www.resensys.com/documents/Finite-Element-Method-Model-Verification-for-Structures.pdf, 2022, 6

[9]VSI, Script LowG Testbed, intern document, 2022, 8

[10]NASA, Article Standards Inform Comfortable Car Seats, https://spinoff.nasa.gov/Spinoff2013/t_4.html, 2013

[11]C. Klug, Joeressen, N. Erlinger, Weißenbacher, Ressi, G. Gstrein, Active Safety – Laboratory practical, Active Human Models SS, 2022; Vehicle Safety Institute, 68

[12] LS-DYNA® KEYWORD USER'S MANUAL VOLUME I, 2018, 3186

[13]Wikipedia, Text, https://en.wikipedia.org/wiki/LS-DYNA, 2018

[14]Wikipedia, Text, https://en.wikipedia.org/wiki/Altair_Engineering, 2022

[15]Calculation tool, https://www.item24.com/de-de/mb-systembaukasten/aluminiumprofile-und-zubehoer/

[16]graspengineering, Article Different Types of FEA Elements/How to Decide the Element Type, https://www.graspengineering.com/different-types-of-fea-elements-how-to-decide-the-element-type/, 2020

[17]J. Michalski, Forum Text What are the advantages and disadvantages of using beam elements instead of 2D plane stress elements to modes a thin beam attached to a wall that is an L – shape on Abaqus,https://www.quora.com/What-are-the-advantages-and-disadvantages-of-using-beam-elements-instead-of-2D-plane-stress-elements-to-model-a-thin-beam-attached-to-a-wall-that-is-an-L-shape-on-Abaqus, 2019

[18]NAC, Text post,http://www.nac.com.sg/2018/12/06/2d-elements-in-meshing-for-finite-element-analysis-fea/, 2018

[19]what-when-how, Text Post FEM for 3D Solids (Finite Element Method) Part 1, http://what-when-how.com/the-finite-element-method/fem-for-3d-solids-finite-element-method-part-1/, 2022

[20]Novotechnik, Post Potentiometers, https://www.novotechnik.de/en/products/sensor-technologies/potentiometers, 2022

[21]Spectromas, Document, http://spectromas.ro/wp-content/uploads/2018/10/S01265.pdf, 2022

[22]C. Hochenauer, Script Numerische Verfahren in der Energietechnik, 2021

[23]Altair, Manual HyperMesh Introduction, 2022, 456

[24]C. Klug, Script Contacts and Plausibility Checks, 2021, 11

[25]Euroncap, Text Post, https://www.euroncap.com/de/fuer-ingenieure/protocols/

[26]Measurement specialties, Document Model 1203 Accelerometer, 2012, 2

A APPENDIX

A.1 Experiment Head Fall Test

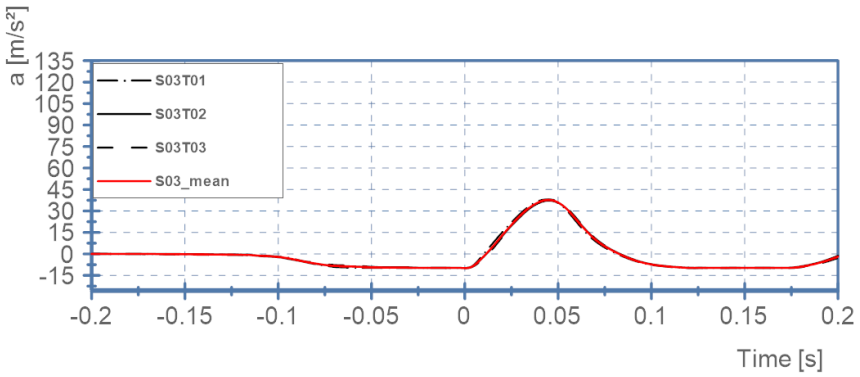

Figure A.1- 1: Test 3, Acceleration, Head Impactor Adult

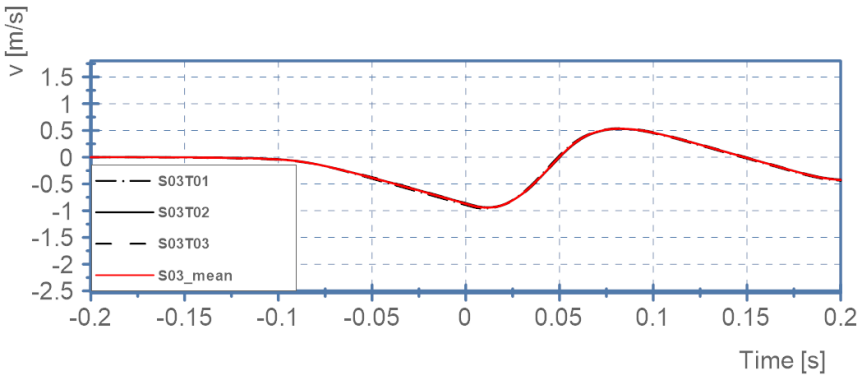

Figure A.1- 2: Test 3, Velocity, Head Impactor Adult

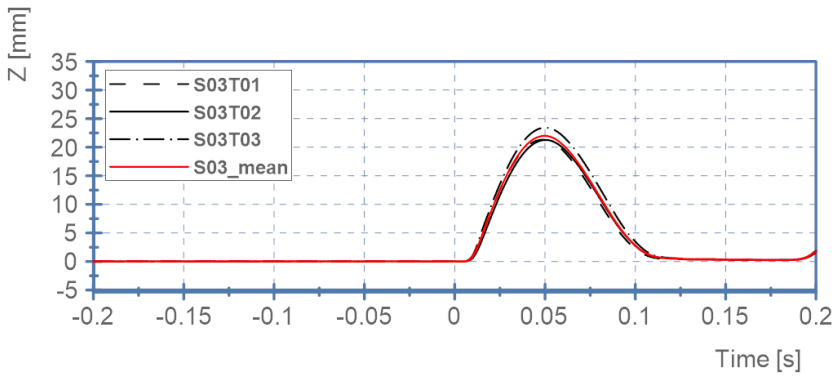

Figure A.1- 3: Test 3, Compression, Seat foam

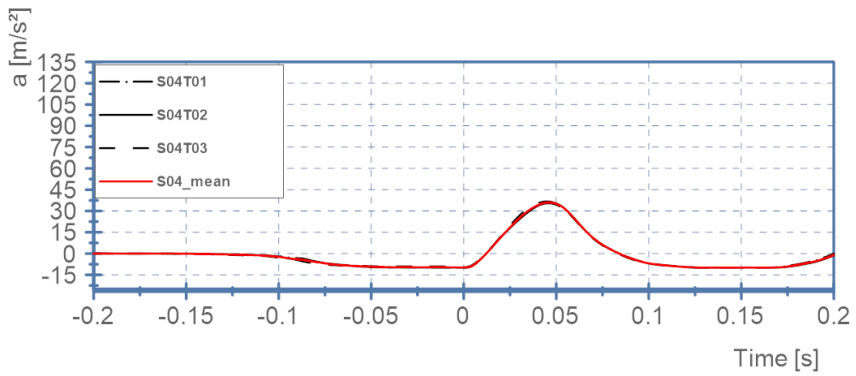

Figure A.1-4: Test 4, acceleration, Head Impactor Adult

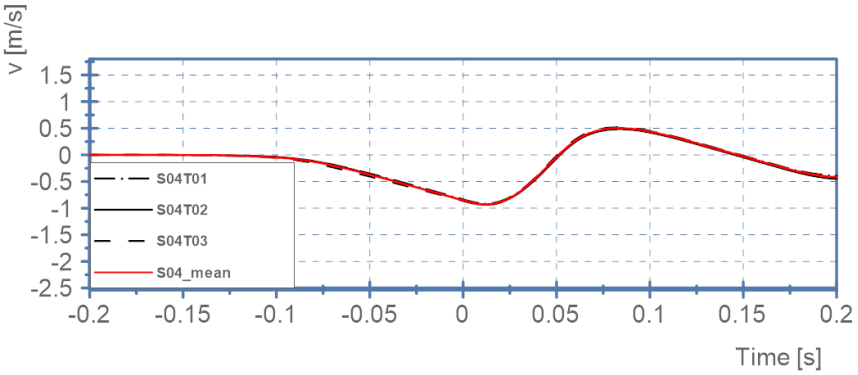

Figure A.1-5: Test 4, Velocity, Head Impactor Adult

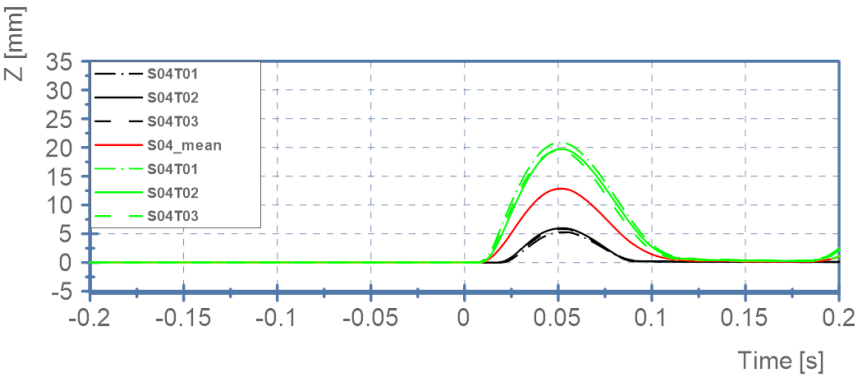

Figure A.1-6: Test 4, Compression, Seat foam

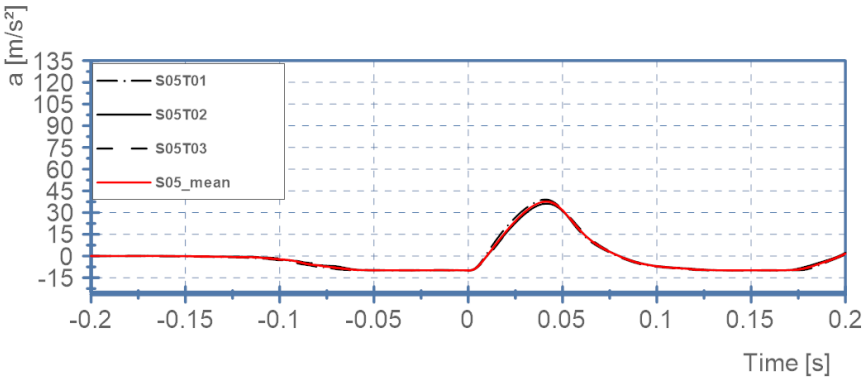

Figure A.1- 7: Test 5, Acceleration ,Head Impactor Adult

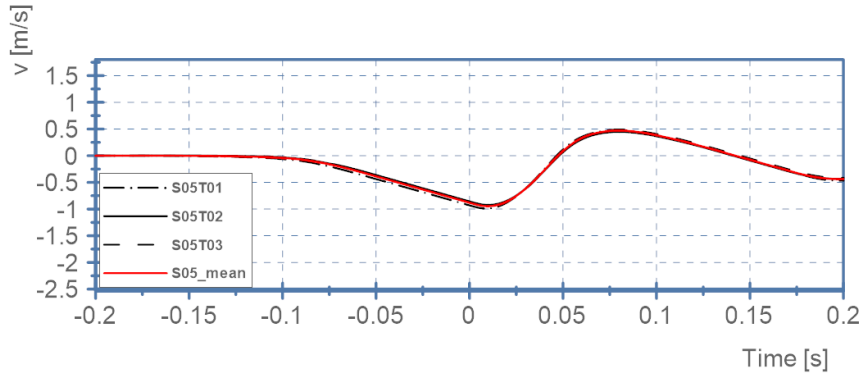

Figure A.1- 8: Test 5, Velocity, Head Impactor Adult

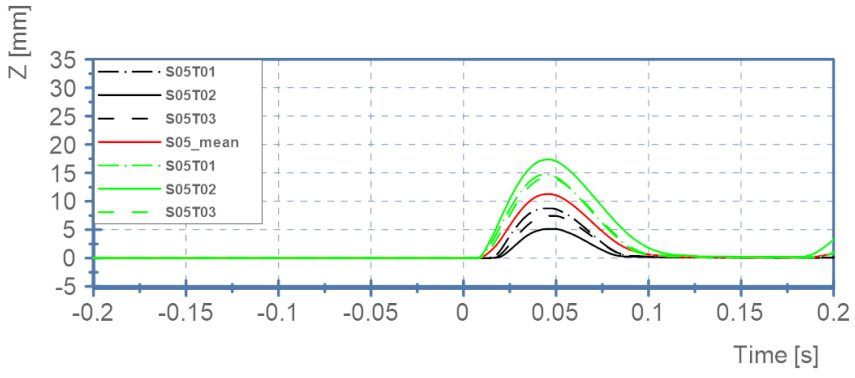

Figure A.1- 9: Test 5, Compression, Seat foam

A.2 Simulation Head Fall Test

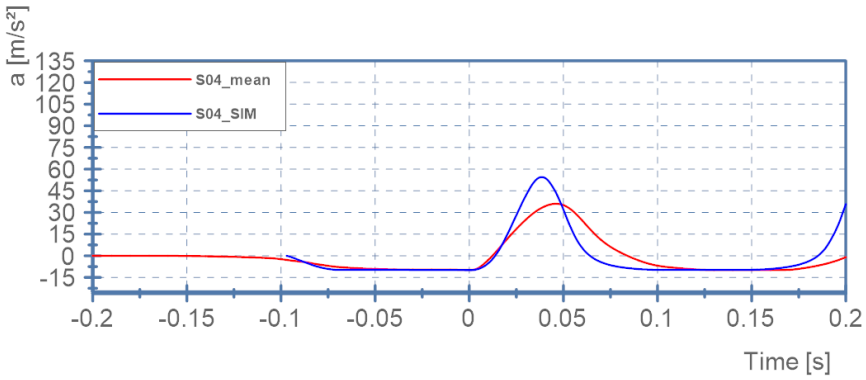

Figure A.2- 1: Test 4, Acceleration, Head Impactor Adult

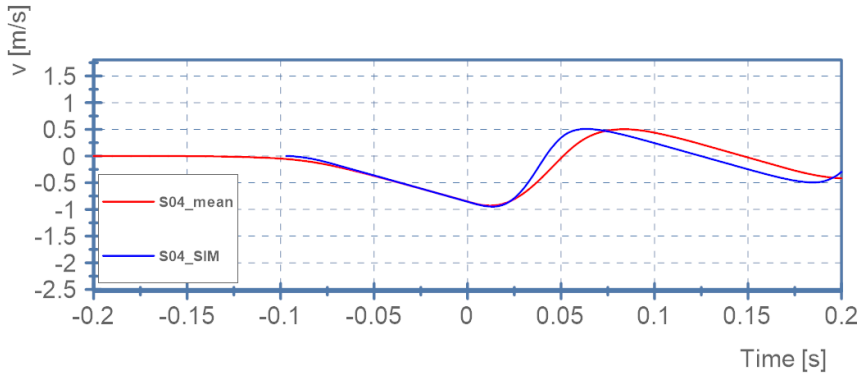

Figure A.2- 2: Test 4, Velocity, Head Impactor Adult

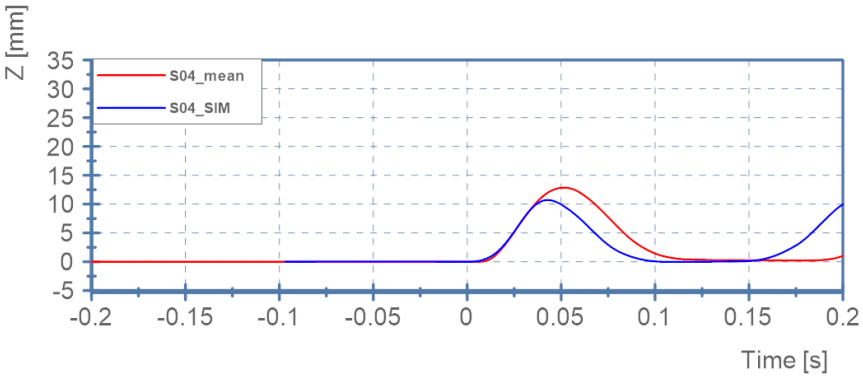

Figure A.2- 3: Test 4, Compression, Seat foam